Interactions of Semiconductor Nanoparticles with Environmentally Relevant Bacteria Model

A DISSERTATION SUBMITTED TO THE FACULTY OF THE GRADUATE SCHOOL OF THE UNIVERSITY OF MINNESOTA

BY

Sunipa Pramanik

IN PARTIAL FULFILMENT OF THE REQUIREMENTS FOR THE DEGREE OF DOCTOR OF PHILOSOPHY

Christy L. Haynes

Adviser

May 2019

Acknowledgements

I would like to acknowledge the help and support of all my colleagues, collaborators, friends and family whose support has made this dissertation possible.

I would like to thank my advisor, Prof. Christy Haynes, who has been a pillar of strength, and always encouraging. I would like to thank all my course work professors, who helped me build a solid scientific background. I have been part of two NSF-funded centers, the UMN MRSEC and CSN. While working as part of these two groups, I have had the wonderful opportunity to work with brilliant scientists from diverse fields. I am grateful to all past and present members of these groups for inspiring me and helping me learn better. I would like to thank Prof. Uwe Kortshagen and Prof. Eray Aydil,who are part of MRSEC, and Prof. Zeev Rosenzweig from CSN, as well as Jeslin Wu, Nancy Trejo, Samantha Ehrenberg and Denise Williams who have been my collaborators. I would also like to thank Prof. Robert Hamers and Prof. Joel Pedersen for their kind gesture of hosting me in their labs as part of the CSN lab exchange. I want to thank Prof. Vivian Feng, who has been always been a helpful presence. I am grateful for the National Science Foundation Center for Chemical Innovation (CCI) program Award CHE-1503408, and University of Minnesota MRSEC under Award Number DMR-1420013, that has funded my research during my PhD. I would like to thank the Haynes group for providing me with such a warm and positive lab atmosphere. I am grateful to all the past and present group members who I have had the good luck to work with. I would like to thank my best friends Anupama and Archi for always being there for me. I want to thank my boyfriend Dave, for all your love and support, and your belief in me. Lastly, I would like to thank my parents and dedicate

this dissertation to them, since I won't be where I am if it wasn't for your constant love and encouragement.

Table of Contents

List of Tables

Chapter 3

List of Figures

Chapter 1

Chapter 2

Chapter 3

Chapter 4

Chapter 5

List of Acronyms

AhR	Aryl hydrocarbon receptor
AQY	Absolute quantum yield
Cd	Cadmium
CdSe	Cadmium selenide
CdSe/ZnS	Cadmium selenide/zinc sulfide
CFU	Colony forming units
CIGS	Copper indium gallium selenide
CvME	Caveolae-mediated endocytosis
CZTS	Copper zinc tin sulfide
DCFDA	2′,7′-dichlorofluorescin diacetate
DHLA	Dihydrolipoic acid
DHR	Dihydrorhodamine 123
DLS	Dynamic light scattering
DPBS	Dulbecco's phosphate buffered saline
DPP	Diphenyl phosphine
EGFR	Epidermal growth factor receptor
EDS	Energy dispersive X-ray spectrometry
FWHM	Full width at half maximum
GO	Graphene oxide
GQD	Graphene QD
HDA	Hexadecylamine
HEPES	(4-(2-hydroxyethyl)-1-piperazineethanesulfonic acid
HSI	Hyperspectral imaging
HR-TEM	High resolution TEM
ICPMS	Inductively couple plasma mass spectrometry
In	Indium
LB	Luria-Bertani
LED	Light-emitting devices
LPS	Lipopolysaccharide

MDCK	Madin Darby Canine Kidney
MTT	(3-(4, 5-dimethylthiazolyl-2)-2, 5-diphenyltetrazolium bromide
NGQD	Nitrogen-doped GQD
NIR	Near infra-red
nCMFI	Normalized cell mean fluorescence intensity
OD	Optical density
ODE	1-octadecene
OA	Oleic acid
OLA	Oleylamine
PS	Polystyrene
PVP	Polyvinylprolidone
PAAc	Polyacrylic acid
PI	Propidium iodide
POPC	1-palmitoyl-2-oleoyl-sn-glycero-3-phosphocholine
POPG salt)	1-palmitoyl-2-oleoyl-sn-glycero-3-phospho-(1'-rac-glycerol) (sodium
QD	Quantum dots
QY	Quantum yield
RALN	Right auxiliary lymph node
ROS	Reactive oxygen species
SAM	Spectral angle mapper
Sccm	Standard cubic centimeter per minute
SiQD	Silicon quantum dots
SILAR	Successive ionic layer adsorption and reaction
SLG	Soda lime glass
SEM	Scanning electron microscope
SD	Standard deviation
TEM	Transmission electron microscopy
TOP	Trioctylphosphine

XRD	X-ray diffraction

Chapter 1

Biological and Environmental Interactions of Cadmium-free Quantum Dots

Adapted from manuscript in preparation "Biological and Environmental Interactions of Cadmium-free Quantum Dots" for *ACS Appl. Nano Mater.*

Overview

The growth in nanotechnology and the specific interest in the use of nanoscale quantum dots have increased recently. The environmental and health concerns over the use of cadmium (Cd) in quantum dots has led to research towards design and synthesis of Cd-free quantum dots. With the growth and synthesis of these alternative quantum dots, research is ongoing to understand their environmental and biological interactions and implications. In this review of current literature, we focus on four different types Cd-free QDs; graphene quantum dots, indium-based quantum dots, zinc-based quantum dots, and silicon-based quantum dots. This includes brief discussion about synthetic procedures and optical properties. The review assembles the data available on *in vivo* and *in vitro* experiments with these quantum dots and different model organisms or cell lines, with separate consideration of environmental models and biomedical models.

This chapter acts as a fitting introduction to the research work presented in the thesis which focuses on important semiconductor nanoparticles and QDs, and their environmental toxicity using bacteria as model organism.

1.1 Introduction

Quantum dots (QDs) are nanoscopic semiconductor particles that have size-dependent luminescent properties and can be used in biomedical imaging and electronics industries, among others.[1] Quantum dots exhibit quantum confinement effects where nanocrystals with diameters smaller than the Bohr radius ($a_0 \approx 5.29 \times 10^{-11}$ m) have quantized energy levels directly related to size.[2,3] QDs have certain advantages when compared to organic dyes for applications that require their luminescent properties. These attributes include high photostability, tunable photoluminescence, broad absorption range, and narrow emission range.[4] These unique properties make them very good candidates for a variety of applications, and thus the production of QDs has increased in recent years; in fact, the estimated yearly production of QDs was 0.6 tons (median value) in 2012.[5] This increase in production and use also leads to an increased probability that, at some point in their life cycle, these QDs may be released into the environment and interact with various organisms.[6] Thus, there are numerous studies that assess the biological and environmental implications of QDs.

Traditionally, QDs have been made from Cd-based compounds.[7,8] As such, there are many scientific articles about Cd-based QDs, their applications, as well as their effects on human cells, various organisms, and the environment.[9-14,8] The presence of Cd in traditional QDs has caused some concern regarding their usage, as well as their widespread applications. General cadmium toxicity is a well-known phenomenon that can result in liver and kidney injuries, skeletal deformations, neurological problems, and cancer.[15] Cd^{2+} ions are also known to generate reactive oxygen species (ROS) that can cause to oxidative damage to

cellular components, cause DNA damage, and inhibit DNA repair. In addition, there are reports of ROS generation by QDs themselves due to their bandgaps and ability to accept and donate electrons.[16] Since a major contributor to the toxicity of Cd-based QDs is the dissolution to Cd^{2+} ions, this has caused focus to shift to the design and synthesis of QDs made of benign and earth-abundant elements in hopes of producing less toxic, more environment-friendly materials. Studies are being conducted simultaneously to assess the effects of these new Cd-free QDs on various organisms and human cell lines. This review article critically assesses the present literature on Cd-free QDs, with a focus on how these nanomaterials fare in terms of both functionality and toxicity, in some cases by comparing them with their Cd-based counterparts. Based on frequency of use, this article will focus on the toxicity and biological interactions of graphene QDs, In-based QDs, Zn-based QDs, and Si-based QDs, pointing out some of the similarities/dissimilarities they have to their Cd-based counterparts and analyzing what is known about their *in vivo* and *in vitro* effects on various organisms and cell lines. The dosage of the quantum dots vary between the studies though generally they are observed to be in the range of 50-1000 μg/mL. Since the unique photoluminescence properties arise due to quantum confinement effects, the sizes of the quantum dots need to be smaller than the Bohr radius and are generally in the 3-8 nm diameter range. In each section, where possible, the environmental and biomedical toxicity studies will be presented separately.

1.2 Graphene-based QDs

Graphene QDs (GQD) are carbon-based nanomaterials that are made of small graphene lattices inside the dots, and they have excellent luminescent properties.[17,18] When compared

to other carbon-based nanomaterials, GQDs stand out because of their unique physical, electronic,[19,20,21] and optical properties,[22,23,24] due to the occurrence of edge effects and quantum confinement effects.[25] The synthesis of GQDs can be accomplished using a top-down approach,[26,27,28] where precursor materials like graphene, graphene oxide, graphite powder, or coal, are cut down to nanoscopic graphitic fragments. The other major synthetic route is a bottom-up approach[29,30] wherein organic substrates like benzene, glucose, or fullerene are assembled to form the GQDs. GQDs show photoluminescence due to a non-zero bandgap,[31] which can be influenced by particle size, functional groups, and defects. In one study by Sun et al., the quantum yield of nitrogen-doped GQDs reached 74%.[32]

GQDs have numerous potential applications such as sensing, bio-imaging, and nanomedicine.[33,34] Due to the vast potential of GQDs in biological applications, understanding the interactions of these particles with cell lines, living organisms, and the environment is of utmost importance.

1.2.1 Effect of GQDs on environmental models

In their 2015 paper, Wang et al. assessed the biodistribution and developmental toxicity of GQDs in zebrafish (*Dario rerio*) embryos.[35] Zebrafish is an important model for studying vertebrate biology (a much simpler model than commonly used mice). Their optical transparency allows for easy visual assessment of development in embryonic stage, and they are also good for assessment of genetic changes due to their short generation spans.[36] In general, they are considered to be good indicators of environment health. In this work, the embryonic stage was chosen since the zebrafish embryos are more sensitive to external factors than the adults. The GQDs in these experiments were synthesized by a previously

reported top-down procedure using graphene oxide (GO), ammonia solution, and hydrogen peroxide. In the time period of 4-96 hours post fertilization, the mortality of the embryos increased and the spontaneous movement and heartbeats decreased at GQD treatment concentrations of 50-200 μg/mL. There was also a significant decrease in hatching rate at 200 μg/mL GQD concentrations. Various malformations such as pericardial edema, vitelline cyst, bent tail, and bent spine were also observed in embryos treated with GQDs. Most of the GQDs were observed to accumulate in the heart and intestines. In a separate study done by Roy et al., the accumulation of GQDs were noticed to be mostly in the digestive tract, and not in the heart or the circulatory system.[37] This led to much less mortality in the embryos as compared to the controls, even at a GQD concentration of 2 mg/mL. Delayed hatching and deformations like pericardial edema and stunted growth were only observed at GQD concentrations of more than 2 mg/mL. In the latter study, the synthesis of the GQDs was done by hydrothermal treatment of neem leaf extract. Thus, GQDs synthesized through dissimilar routes resulted in completely different localization within the zebrafish embryos and toxic behavior towards the same organism. A recent study has investigated the effect of graphene oxide quantum dots (GOQDs, an oxidized form of the GQDs) on zebrafish embryos as well.[38] Hydrothermal treatment of graphene oxide obtained through the oxidation of graphite powder led to generation of the GOQDs used herein. In this work, at a GOQD concentration of 100 μg/mL, even though there was no effect on body length, hatching, or mortality, there was a decrease in heartbeats as well as occurrence of malformations. At concentrations less than 100 μg/mL, a dose-dependent upregulation of gene expression of the aryl hydrocarbon receptor (*AhR*) pathway was observed. The *AhR* pathways help in regulating the activities of foreign chemical

substances, regulation of cytochrome P450 enzymes, and also helps with physiological immunity. The effect of graphene-based materials on the *AhR* pathways is important to note due to the presence of aromatic hydrocarbon skeleton in the GOQDs.

The nematode *Caenorhabditis elegans* treated with GQDs at 5-100 μg/mL showed low lethality and neuronal damage when compared to graphite and graphene nanoplatelets.[39] *C. elegans* is a simple organism which can be found in soil and compost heaps and are therefore interesting to investigate from an ecological point of view. The *C. elegans* were exposed to various concentrations of GQDs in 24-well plates. The GQDs were observed to be dispersed in the *C. elegans* gut lumen, muscle, and visceral organs. In another study involving nitrogen-doped GQDs (NGQDs), at a concentration of 0.1–100 μg/mL NGQD exposure on *C. elegans* from larvae to adult state, there was no significant lethality or changes in function of targeted organs. There was no noticeable changes in physiological functions such as the brood size and locomotive behavior. No noticeable increase in gut ROS production was observed either.[40] Additionally, there were no adverse effects on the F1-progeny (first filial generation) of the NGQD-treated nematodes. Additionally, the NGQDs did not alter the expression of genes that are related to oxidative stress in nematodes, thus eliminating the possibility of toxicity route involving oxidative stress.

In contrast, GQDs synthesized by the breaking down of C-60 cages through a top-down procedure were reported to be specifically toxic to Gram-positive pathogenic *S. aureus* bacterial cells, while exhibiting no significant toxicity to Gram-positive *Bacillus subtilis* or Gram-negative *E. coli* and *Pseudomonas aeruginosa*.[41] Bacteria form the lowest trophic

level in the ecosystem, so any changes in their activity can translate up the food chain. In the case of pathogenic bacteria, many are also interested in the GQD potential for use as antibiotic agents. In this work, it was discovered that the main contributing factor to the toxicity towards *S. aureus* was the disruption of their cell membranes as observed from biological TEM imaging and a live/dead cell viability assay to assess membrane disruption. This specific association of the GQDs to the *S. aureus* cells was attributed to the surface gaussian curvature matching between the GQDs and the *S. aureus* cells, but not with the other bacterial species. In another study involving GQDs and the bacteria *S. aureus* and *E. coli*, toxicity was only observed when the bacteria were treated with a GQD solution (final treatment concentration 50-200 μg/mL) that had been photoexcited with blue light (465-475 nm).[42] AFM studies on the bacteria treated with photoexcited GQD solution exhibited surface roughness and increase in height of the cells, indicating cell membrane disruption. The reason for the toxicity of the irradiated GQD solution was proven to be the effect of reactive oxygen species (ROS) generation based on measurements of intracellular ROS using dihydrorhodamine 123 (DHR) when the cells were treated with photoexcited GQD. To summarize the results reported above, in the environmental models, the GQDs generally proved to be fairly non-toxic especially when compared to other kinds of graphene-based nanoparticles. In zebrafish embryos, toxicity was observed when there was accumulation in the heart, and not when there was accumulation only in the intestines. In the case of some bacteria models, like *S. aureus*, toxicity happened either due to the cell surface curvature matching with the GQDs leading to more association or the effect of ROS generated upon photoexcitation. Together, these suggest that both the initial design of the

GQDs (size and surface chemistry) will have a significant influence on eventual environmental toxicity.

1.2.2 Effect of GQDs on biomedical models

In the following examples, GQDs are explored for their potential applications in cellular imaging and other diagnostic applications where the GQDs must be internalized safely. While zebrafish, nematodes, and bacteria are good models to assess potential unintended environmental impacts of GQDs, localization and toxicity for biomedical applications are more likely to employ mammals and mammalian cell lines. For example, *in vivo* studies done on Balb/c nude mice bearing tumors treated with carboxylated GQDs (synthesized from carbon fiber using a top-down procedure) showed GQD-based fluorescence signals from the tumor 12 h post injection, but not from other organs such as heart and liver (Figure 1).[43] These results indicate that the GQDs can be an effective candidate for superficial tissue images that are required in skin cancer detection. However, the *ex vivo* images of different organs showed there was a distribution of the GQDs throughout the body in a time period of 12 h, including an accumulation in the heart and liver within 2 h and in the kidneys after 12 h. After 24 h, no fluorescence signal was observed *in vivo*, suggesting the excretion of the GQDs over time. According to the authors, lack of fluorescence signal could be due to either excretion or photobleaching over time. However, due to the accumulation of the QDs in the kidneys 12 h post injection, and the small size (5-nm-diameter) of the QDs that can pass the filtration barrier, it was hypothesized that excretion seems the more likely reason for decreased fluorescence signal. In another study employing the same Balb/c nude mice, a GQD-PEG tagged with NIR fluorescent *Cy*7 was used to

investigate the GQD biodistribution.[44] Similar results, including fluorescence signal from tumor, showed minimal accumulation in deep organs and quick excretion from kidneys. In a recent study done by Li et al., GQDs and various GQD derivatives such as GQD-NH_2, GQD-COOH and GOQD were systematically injected into mice via the tail vein.[45] The injected GQDs had cleared by 7-14 days, even though they were dispersed in certain organs like heart, liver, and kidneys right after injection. There were no other symptoms like weight loss or increase in white blood cell count observed, indicating the fairly non-toxic nature of the GQDs.

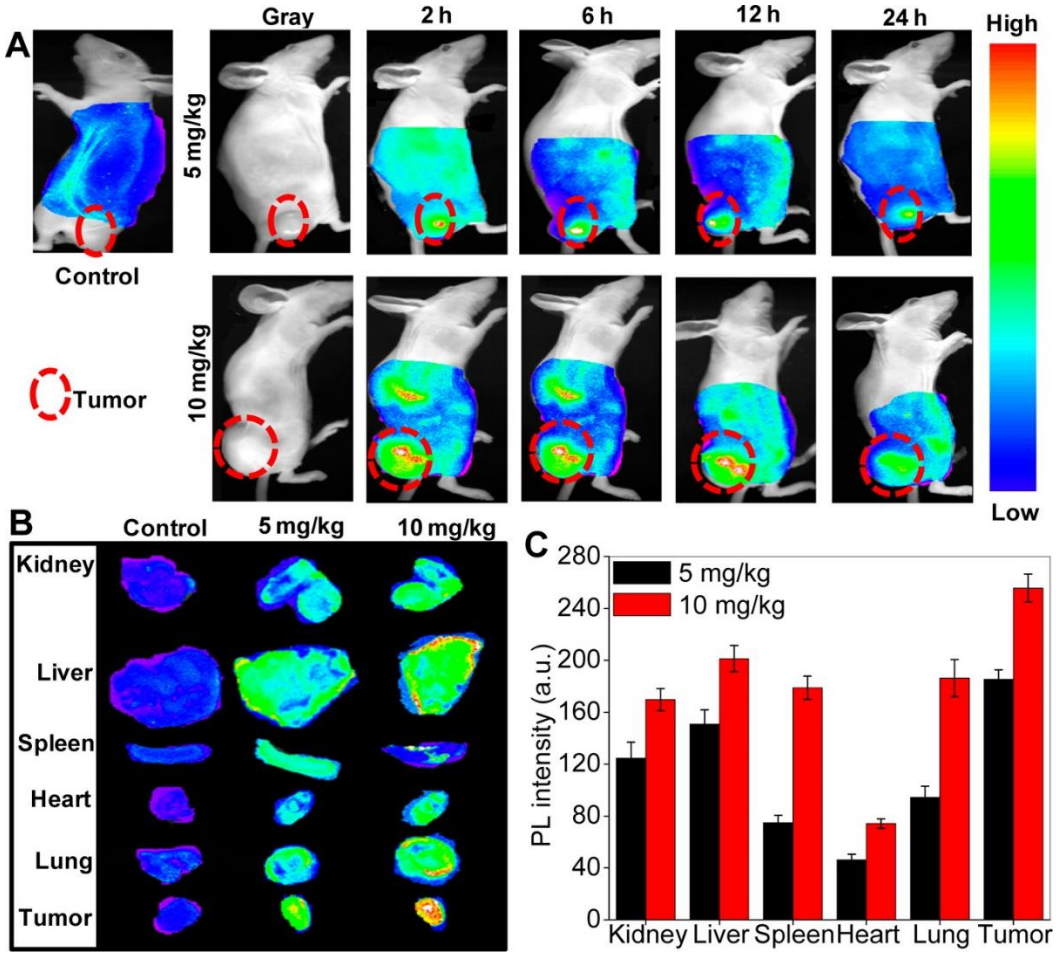

*Figure 1: Example of in vivo toxicity and biodistribution experiments (Reprinted with permission from ACS Nano **2013**, 7, 8, 6858-6867. Copyright © 2013 American Chemical Society.)*

In addition to studies using a whole mouse model, *in vitro* assessments have been done on various mammalian cells to test the efficiency of GQDs for nanoimaging and nanotherapeutics.[46] In a study with HeLa cells, a cancer model cell line, even though a significant decrease in normalized cell viability was observed for 0.5-1 mg/mL GQDs (obtained through a top-down synthetic procedure) at 4 h and 24 h incubation, the viability was still around 80% of the negative control even after 24 h. To assess the association of the GQDs (1 mg/mL) with the cells after treatment, normalized cell mean fluorescence intensity (nCMFI) was measured using flow cytometry. The nCMFI was higher than the autofluorescent level of the cells at both 4 h and 24 h after treatment. Fixed and stained HeLa cells treated with GQDs showed internalization of the QDs through fluorescence microscopy. To investigate the pathway of GQD uptake, the cells were first incubated in media with filipin (an inhibitor of the caveolae-mediated endocytosis pathway) for 30 min, and then the GQDs were introduced. Since the administration of filipin decreased the nCMFI significantly, it can be concluded that caveolae-mediated endocytosis (CvME) is a major pathway of uptake of the GQDs into the cells. The measurement was done after incubating the cells in media for 30 min with filipin, and then introducing the GQDs. Tian et al. studied the cytotoxic effect of hydroxyl-functionalized GQDs (commercially available) on the human lung carcinoma cell lines A549 and H1299.[47] Cell proliferation of A549 cells, 72 h after treatment with 50 μg/mL GQDs, was completely restrained, whereas

in case of the H1299 cells the process was significantly slowed down. ROS generation caused cell senescence, thus bringing the cell division cycle to a halt and potentially stopping the cell proliferation. Experiments done on human A549 lung carcinoma cells and human neural glioma C6 cells, using three kinds of GQDs with different modified groups (NH_2, COOH, and CO-$N(CH_3)_2$), showed a dose-dependent decrease in proliferation.[48] However, even at high GQD concentrations, the normalized cell viability (as obtained from an MTS assay) still remained at around 80%, showing minimal cytotoxicity of the GQDs. Studies done by Wu et al. compared the effect of GO and GQDs on human gastric cancer MGC-803 and breast cancer MCF-7 cells. Cell proliferation slowed down when treated with either GO or GQDs, but the effect was much more pronounced in the case of GO.[49] Also, more apoptosis was observed when cells were treated with the GO sheets. The reasoning behind the difference in cytotoxicity of GO and GQDs was explored as well. Under similar concentrations, GQDs were observed to produce less ROS and inflict less mitochondrial damage in the cells than GO, leading to its comparatively low toxicity. A more severe case of cell cycle arrest through autophagy was reported by Markovic et al. on the human glioblastoma cell line U251 in the presence of photo-excited GQDs.[50] In TEM images of cells treated with photoexcited GQDs, a vacuolization process was evident. These vesicles mostly encapsulated the GQDs, but some of them also contained cellular components, indicating a cellular self-digestion process known as autophagy. Significant ROS generation in cells can trigger the autophagic process to try and eliminate the severely damaged cell organelles.

Wang et al. did a study with a Madin Darby Canine Kidney (MDCK) cell monolayer and GQDs.[51] The viability of the cells was measured by the MTS assay (the amount of viable cells is measured by the quantification of a colored formazan dye that is formed from a tetrazolium compound in presence of viable cells) and the LDH assay (cell death is measured by quantifying the lactate dehydrogenase in the media, which is a soluble cytosolic enzyme in eukaryotic cells, and cell damage leads to its release into media). A decrease in cell viability and an increase in LDH release was observed at GQD concentration of more than 280 μg/mL at 6 h exposure time. This study also concluded that the smaller 3-nm-diameter sized GQDs had higher membrane permeability than their larger 12-nm-diameter counterparts and that lipid raft-mediated transcytosis was responsible for GQD uptake.

GQDs can also be used in targetable therapeutics as a vehicle for pharmaceutical agents. For the treatment of EGFR (epidermal growth factor receptor)-overexpressing breast cancer cells (MDA-MB-231), targeted GQDs with high cisplatin loading capacity were employed.[52] The GQDs were functionalized with a modified antibody (scFvB10) having high affinity for EGFR. The GQD- scFvB10 showed effective uptake into the cells via EGFR-mediated endocytosis. The cisplatin loaded GQD- scFvB10 also showed more targeted and effective killing of the MDA-MB-231 cells, than cisplatin-loaded GQDs. An important point to remember is that results from *in vitro* targeting studies don't always match results from *in vivo* targeting.

The last three studies presented herein examine the interaction of GQDs with various human cells and explore the causes that dictate association/internalization. Another study aimed at understanding how different cell permeabilities influence interaction with GQDs compared uptake of GQDs by monocytes, granulocytes, and lymphocytes. In fact, monocytes and granulocytes showed much higher uptake of GQDs, in comparison to the lymphocytes, following the expected trend since leukocytes have a permeability that is 4 times smaller than that of monocytes and granulocytes. Despite this enhanced uptake, the GQDs were proven non-toxic to the leukocytes.[53] Treatment of red blood cells with GO showed significantly more hemolysis and loss of ATP than when treated with nitrogen-doped GQDs.[54] To understand the mechanism of interaction of the materials with RBCs, lipid bilayer models were used. These lipid bilayer studies suggest strong hydrophobic interaction of GO with RBC membrane, while NGQDs caused only small changes in lipid conformations. Finally, studies on the effects of GQDs on human neural stem cells was done by Shang et al.[55] The uptake mechanism in this case was proven to be endocytosis, as low temperature and an ATP depleted environment that hinders endocytotic pathways caused a decrease in GQD incorporation.

In conclusion, as in the studies of GQDs interacting with environmental models, GQDs generally prove to be good alternatives to traditional Cd-based QDs in biomedical applications because they are low in toxicity to cells and organisms. Also, GQD precursors are earth-abundant in nature, which is good from a sustainability point of view. However, ROS generation is identified as a major pathway of toxicity in some cases, especially when the GQD undergo photochemical excitation. In an interesting study carried out by Chong

et al., GQDs exhibit antioxidant properties by scavenging free radicals.[56] In the same study, it is also shown that under blue light irradiation, singlet oxygen ROS species are produced by the GQDs leading to lipid peroxidation and cell death. Research is ongoing to mitigate the ROS generation from GQDs. One such study explores the embedding of the GQDs in a PEG matrix (PGQD).[57] On exposure to a high concentration of PGQDs at 4 mg/mL, the HeLa cells still maintained a 75% viability. This was due to a drastic decrease in intracellular ROS generation relative to the bare GQDs. The PGQDs were still incorporated into the cells and maintain fluorescence, thus making them great candidates for cell imaging.

1.3 Indium-based QDs

1.3.1 InP QDs

Despite their unique optical properties, Cd-based QDs have raised concerns over their toxic effects to living organisms as well as the environment. The lack of biocompatibility of Cd-based QDs has led researchers to look at QDs with more benign components. Indium is one such alternative option. One of the common methods used to synthesize InP QDs is to use indium chloride, stearic acid, zinc undecylenate, and hexadecylamine in octadecene and then introduce a solution of trimethylsilylphosphine in octadecene in a moisture- and oxygen-free atmosphere at high temperature.[58] The shelling process in done with a zinc precursor solution like zinc diethyldithiocarbamate.[59] InP QDs generally are not as photoluminescent as their Cd-based counterparts, but coating the core with a ZnS or ZnSe shell can increase the quantum yield up to 76%.[60] In contrast to Cd-based QDs, the InP QD biological and toxic effects have not been explored widely. In this review, we have

collected the data that are available to help us understand the presence or absence of toxicity in In-based QDs.

1.3.1.1 Effect of InP QDs on environmental models

To the best of our knowledge, there has only been one published study on the environmental toxicity of InP QDs, and this study used rare minnows as the model biological system. Rare minnows are known to be great model organisms for aquatic toxicity testing and chemical safety assessment. They can be used for genomic and proteomics studies to assess mechanistic pathways of toxicity.[61] Despite the hope that replacement of Cd by In would yield less toxic QDs, Chen et al. reported a high toxicity of InP/ZnS QDs on Chinese rare minnow (*Gobiocypris rarus*) embryos.[62] Developmental abnormalities such as pericardial edema, bent tail, and spinal curvature were observed at 72 hpf (hour post fertilization) after exposure to 200 nmol/L of QDs, as well as lower hatching rates were observed. At a higher exposure concentration of 800 nmol/L at 36 hpf, significant decrease in spontaneous movement rates were observed. A concentration-dependent increase in malformations and defects were observed in the minnow embryos. The mRNA expressions of *Hsp70*, *Wnt8α* and *Mstn* were significantly upregulated at InP concentrations of 200-800 nmol/L, indicating oxidative stress and teratogenic effects. However, the InP QDs did not show any significant genotoxicity or DNA damage as evidenced by the comet assay. Thus we can say that the InP QDs posed some developmental toxicity to the rare minnow embryos, as well as upregulation of certain enzymes, but did not show any DNA damage.

1.3.1.2 Effect of InP QDs on biomedical models

The literature reveals significantly more studies on the biomedical impacts of In-based QDs. For example, in their 2012 paper, Brunetti et al. explored the *in vivo* and *in vitro* toxicity of InP/ZnS QDs (core/shell) and compared it to CdSe/ZnS QDs.[63] Cell viability experiments carried out with epithelial cell line A549 (human lung carcinoma) and the neuronal cell line SH SY5Y (human neuroblastoma), showed the significant toxic effect presented by the CdSe/ZnS QDs to both the cell lines, though the effect was more pronounced in the SH SY5Y cells. The InP/ZnS QDs did not show any significant toxicity to either of the cell lines (<10% decrease in viability). An LDH assay (quantifying the lactate dehydrogenase in the media as an indicator of cell damage) was performed to assess any damage done to the cell membrane by the QDs, and CdSe/ZnS exhibited noticeable effects even at low concentrations of 1 pM. To assess the effects of ROS generation, qPCR experiments were performed to assess expression of *SOD1*, *SOD2*, *CAT*, and *Gpx* genes that are responsible for antioxidant and detoxifying effects. In the case of InP/ZnS QDs, no significant upregulation in gene expression was observed. The CdSe/ZnS QDs were responsible for inducing oxidative stress in the cells as indicated by the qPCR results, and once again greater effects were observed for the neuronal cells. For the *in vivo* toxicity assessment, *Drosophila* was chosen as the model organism, and toxicity assessments were performed after feeding them QD-enriched food. In case of the CdSe/ZnS QDs, an over-expression of *hsp70* and *hsp83* was measured by qPCR; *hsp70* and *hsp83* are proteins responsible for stress response as a result of ROS generation and systemic toxicity in the cells. Also, as overexpression of *p53* was observed, indicating genotoxic stress involving

DNA damage and hypoxia. In contrast, no significant upregulation of gene expression was observed for any of the genes following InP/ZnS QD treatment, proving their comparatively non-toxic nature for *Drosophila*. In another study done by Chibli et al, it was shown that the InP/ZnS QDs are non-toxic to various cell lines, including fibroblast NIG 3T3, KB, MDA and B16.[64] This was in agreement with complimentary results that showed no ROS generation, including the most damaging singlet oxygen, using spin-trap EPR.

Xie et al. studied the *in vitro, in vivo,* and *ex vivo* effects of core/shell/shell InAS/InP/ZnSe QDs on mice.[65] The RAW 264.7 mouse macrophage cells treated with a commercially available CdTe/ZnS QD showed higher cell uptake and retention when compared to the InAs/InP/ZnSe QDs. Also, an MTT assay (MTT (3-(4, 5-dimethylthiazolyl-2)-2, 5-diphenyltetrazolium bromide) indicates metabolically active cells) showed lower cytotoxicity of the In-based QDs. *In vivo* fluorescence microscopy showed much higher uptake of the Cd-based QDs in the liver, which was corroborated by *ex vivo* imaging of the mouse liver 24 h post injection. Higher signal of the In-based QD was obtained in the mouse kidneys as well as higher concentration in the urine, indicating the In-based QDs are cleared out from the body more quickly and more effectively than their Cd-based counterparts. Lin et al. performed experiments with BALB/c mice in the presence of InP/ZnS QDs at very high dose of 25 mg/kg.[66] No significant changes in body weight, eating and drinking patterns or physical characteristics were observed over 84 days of exposure. *Ex vivo* fluorescence imaging of various organs including heart, kidneys, liver, lungs, spleen and brain showed signal from only liver and spleen, indicating accumulation

of the In-based QDs in these organs. Elemental analysis through ICP-MS indicated the presence of In in other organs as well as the circulatory system, indicating some degradation of the QDs, though this concentration decreased over time. To assess if the QD accumulation in liver and spleen caused any changes in metabolic activity, blood pathology tests were done, including monitoring of red blood cell count, white blood cell count, platelet count, hematocrit and hemoglobin over the 84-day period. No significant change or abnormality was observed in these tests, indicating that the InP QDs are biocompatible and can be used for nanotheranostic applications. Similar biological experiments were done by Yaghini et al. on Lister Hooded rats using intravenous injections of In-based water soluble QDs at dosage of 12.5 mg/kg.[67] From the In concentrations, it was seen that even though there was a high concentration of the QDs in blood initially (5 min post injection), that decreased over time, with an increase in In concentration in the liver and spleen. However, the concentration in the spleen and liver stabilized after 4 h and decreased steadily to less than 15% (of the highest concentration observed) in 90 days. QD fluorescence was also observed in cryosectioned liver samples which reached its maximum in 4 h and then gradually declined, indicating QD dissolution. Blood pathology tests determining total protein, albumin, and bilirubin did not show significantly different trends when compared to the negative controls, denoting biocompatibility of the In-based QDs. Interestingly, even though the QDs used were bigger (12.2 nm) than the threshold for direct renal excretion, over time there was an increase in In concentration in kidneys, indicating intracellular QD degradation. Comparatively, in another study done by the group, where sub-cutaneous injection was administered in the paw of the rats, much slower and less accumulation of the QD was observed in the liver and spleen, reaching maximum in a

day.[67] However, the rate of elimination of the QDs from the liver and spleen over 90 day time period was comparable in both the cases (intravenous and subcutaneous injections).

In a paper by Chibli et al., they explore the phototoxicity of InP/ZnS QDs on NIH3T3 fibroblasts, KB cells, B16 murine melanoma cells, MDA-MB-231 breast adenocarcinoma cells, and PC12 pheochromocytoma cells.[59] Light irradiation of the InP/ZnS (with single ZnS shell) QDs with 2.5 mW, 440 nm LEDs caused significant increase in toxicity to all the cell lines when compared to the dark controls. EPR and ROS assays confirm the generation of superoxide and hydroxyl ions, which is causing oxidative damage and toxicity in the cells. Increasing the thickness of the ZnS shell to a double layer, can mitigate some of this toxicity. However, the toxicity observed for the InP/ZnS QDs were still significantly lower than the CdSe and CdTe QDs, and the absence of singlet oxygen formation is hypothesized to be the reason.

Indium is a rare metal and can be expensive; however, its excellent photoluminescence properties combined with relative lack of toxicity when compared to Cd-based QDs, makes it worthy of being considered as a potential replacement, especially for low volume biomedical applications. The toxicity of the InP QDs can vary depending on the target organism/cell lines, as well as their size and functionalization. Smaller QDs that can cross the renal filtration barrier, can be excreted easily, whereas larger nanoparticles are generally seen to accumulate in liver and spleen. QDs with positively charged functionalization can interact more with negatively charged lipids, proteins, amino acids

etc. and cause disruption of cells. Also, degradation of the QDs was observed *in vivo* evidenced by In accumulation in organs but loss of fluorescence over time. The degraded QDs can cause toxic effects in the organisms, but is not seen in the above case studies in case of In accumulation, possibly due to its excretion over time. III-V QDs are also known to be more robust than their II-VI counterparts,[66] which minimizes degradation, and release of heavy metals, thus making them generally lower in toxicity. Oxidative stress due to ROS generation can contribute to cytotoxicity seen in some of the cases.

1.3.2 $CuInS_2$ QDs

Another type of In-based QDs that are being studied are $CuInS_2$ nanomaterials. These QDs can be used as light absorber material in solar cells, and their highly fluorescent counterpart $CuInS_2$/ZnS have applications in biological imaging and LEDs. $CuInS_2$ can be synthesized using a "one-pot synthesis" in which indium acetate, copper iodide, dodecanethiol and octadecene are degassed and oleic acid is added at 80°C, and the shelling can be done using a zinc precursor like zinc stearate.[68] As with other QD systems, the QY can be improved by adding a shell to passivate the surface defects. In one study, the QY was increased from 1.4 to 48% with the addition of a ZnS shell.[69]

1.3.2.1 Effect of $CuInS_2$ QDs on environmental models

In vivo studies with *C. elegans* were performed which showed the gradual transport of the $CuInS_2$ QDs from the organism's pharynx to their intestines to their reproductive organs. At that point the QDs were still fluorescent, proving their stability inside the body after 96 h. In a recent study done on rare minnow (*Gobiocypris rarus*) embryos exposed to

$CuInS_2$/ZnS QDs, developmental toxicity was observed as evidenced by pericardial edema, bent spines, lower heart rates, decreased hatching rates and survival rates.[70] The mRNA expressions of *Wnt8α* and *Mstn* were upregulated which can lead to bent tails and spine curvatures. Increased *SOD* activity and altered expression of *Hsp70* as obtained experimentally indicates oxidative stress and ROS generation. Thus, in contrast to the other studies that are reported here, $CuInS_2$/ZnS QDs posed significant toxicity to the rare minnow embryos.

1.3.2.2 Effect of $CuInS_2$ QDs on biomedical models

In a study done by Pons et al., biological imaging capability of lymph nodes as well as the cytotoxicity of NIR-emitting $CuInS_2$/ZnS QDs are assessed.[71] After a subcutaneous injection of the QDs into the right anterior paw of a mouse, the two right auxiliary lymph nodes could be visualized using NIR fluorescence imaging (Figure 2A). On injecting a 10 pmol solution CdTeSe/CdZnS QDs, inflammation is observed in the nearby lymph nodes, whereas the same level of inflammation is reached at 100 pmol for $CuInS_2$/ZnS QDs, suggesting comparatively lower acute toxicity. Histological sections of the right auxiliary lymph nodes treated with $CuInS_2$/ZnS QDs did not show significant difference from the controls (Figure 2B), whereas for the CdTeSe/CdZnS QDs there were clear signs of inflammation and damage as evidenced by the presence of histiocytes, and vesicles showing signs of autophagy. Thus, the $CuInS_2$/ZnS QDs can potentially be used for imaging purposes without significant toxic effects. In another study, $CuInS_2$/ZnS QDs conjugated to an anti-Ki-67 monoclonal antibody were employed to detect Ki-67 expression in human breast cancer MDA-MB-231 cells.[72] These QDs showed high

colloidal stability in aqueous media, and MTT cell viability assay on the QD treated MDA-MB-231 cells showed slight toxic effects. Toxicities of three hydrophilic $CuInS_2$/ZnS QDs with different PEG content and surface charge were investigated by Speranskaya et al. MA-104 (embryonic rhesus monkey kidney) cells treated with the three QDs showed only a slight decrease in cell viability which was similar, if a little less than the toxicity shown by the polymer itself.[73] The three QDs did not show any hemotoxicity on the red blood cells or platelets, as there were no morphological changes or changes in size distribution and global cell counts. There was however a change in leucocyte size distribution which is attributed to increased toxicity due to phagocytotic nature of the cells. These QDs have high quantum yields (QY) and photostability, which along with their relatively low cytotoxicity and no hemotoxicity, makes them attractive candidates for cellular imaging. In a study done by Chen et al., toxicities of $CuInS_2$ and $CuInS_2$/ZnS QDs functionalized with a modified chitosan ligand were tested on two cancer cell lines HeLa and $OECM^{-1}$.[69] The viability of the cells remained at 90% at 72 h exposure time. Overall, the toxicity data on $CuInS_2$/ZnS QDs are limited right now, and further investigations into their effect on organisms, especially with chronic exposures, need to be done.

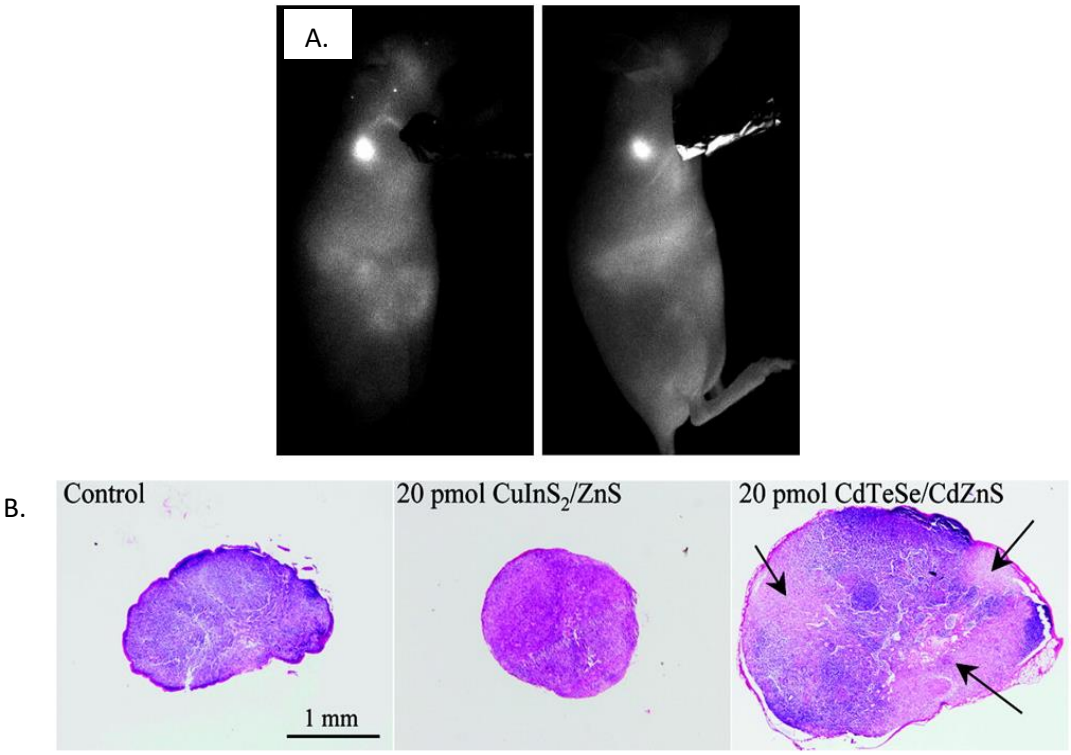

Figure 2: A. NIR Fluorescence image of mice right auxiliary lymph nodes after injected with QDs. B. Histology images of RALNs. (Adapted with permission from ACS Nano ***2010****, 4, 5, 2531-2538. Copyright © 2010 American Chemical Society.)*

1.4 Zn-based QDs

Zn-based QDs such as ZnS, ZnSe, ZnSe/ZnS and ZnO are II-VI QDs like the Cd-based ones, but consist of more benign and earth-abundant Zn; these nanomaterials are known to exhibit size-dependent photoluminescence properties and are attractive alternatives for sensing and imaging applications. In addition, Mn-doped ZnS QDs show room-temperature phosphorescence and are being explored as novel optical sensors. ZnS QDs can be synthesized by the reaction of $ZnSO_4$ and Na_2S solutions. The Mn-ZnS QDs can be

made in a similar fashion, except instead of just zinc sulfate, a solution of zinc sulfate and $MnCl_2$ are used as initial precursors.[74] ZnO QDs can be obtained by the dropwise addition of KOH (potassium hydroxide) solution to $Zn(Ac)_2$ (zinc acetate).[75] ZnS QDs on their own can be poorly luminescent, but in presence of Mn^{2+} can show dopant-enabled emission.[76]

1.4.1 Effect of Zn-based QDs on environmental models

In a recent study by Williams et al., a comparative analysis of the toxicities of Zn-based QDs (ZnSe and ZnSe/ZnS) and Cd-based QDs (CdSe and CdSe/ZnS) was done, and the Zn-based QDs were demonstrated to be non-toxic to bacteria *Shewanella oneidensis*.[77] Analogous studies were also done in presence of liposomes to assess QD association. In the case of both the liposomes and the bacteria, more membrane disruption was caused by the Cd-based QDs compared to the Zn-based QDs. In the viability studies with the bacteria, the difference in the membrane disruption was correlated directly with the lower toxic effect of the Zn-based QDs. In another study, antibacterial effects of ZnO QDs were assessed with two bacterial strains *Escherichia coli* MG1655 and *Cupriavidus metallidurans* CH34 modified to exhibit constitutive luminescent phenotype.[78] A decrease in the luminescence was observed in case of toxic effect of the QDs. *E. coli* cells were more susceptible to the ZnO QDs and $ZnCl_2$ solution of equivalent total Zn as the QDs than the *C. metallidurans*. Since the experiments were done in the dark, any toxicity observed is proposed to be due to dissolved ions rather than photochemical effects. In the case of *E. coli*, the toxicity posed by the ZnO QDs and the $ZnCl_2$ solution were comparable, which suggested full dissolution of the QDs, but the $ZnCl_2$ solution showed more toxicity than the ZnO QDs to *C. metallidurans*, suggesting incomplete dissolution. It was also

hypothesized that the bacteria had some role in the dissolution pattern of the QDs. In a study done by Jin et al., the antibacterial effects of ZnO QD powder, ZnO-polystyrene (PS) nanocomposite films, and ZnO QDs suspended in a polyvinylprolidone (PVP) gel were assessed against three bacterial pathogens: *Listeria monocytogenes, Escherichia coli,* and *Salmonella enterica serovar*.[79] The ZnO QD powder and ZnO-PVP proved to be more toxic than the ZnO-PS film to all three bacteria. The non-toxicity of the ZnO-PS film suggests minimal release of QDs from the film. ZnO-PVP showed a dose-dependent toxicity to the three bacteria. In the case of the ZnO QD powder, sedimentation of the QDs was observed in media, which is potentially responsible for the lower toxicity of the QD powder when compared to the ZnO-PVP, which stays in solution. Also, PVP alone did not pose any toxicity to the bacteria, attributing the toxicity to the ZnO QDs completely. *E. coli* bacteria treated with a protein-stabilized Mn-doped ZnS QDs showed a dose-dependent uptake of the QDs into the cytoplasm, but only when the cell membrane was weakened temporarily by a $CaCl_2$ treatment. The presence of the QDs in the cytoplasm generated oxidative stress only when present in high concentrations. The internalized QDs stay stable when the cells are in PBS media, as indicated by their fluorescence properties, but the fluorescence gradually decreases in LB media where the cells rapidly replicate. Thus, we can see from the reported studies, ZnS QDs were generally non-toxic, ZnO QDs exhibited some antimicrobial properties, and the Mn-ZnS QDs posed oxidative stress only at high concentrations.

1.4.2 Effect of Zn-based QDs on biomedical models

In the context of considering biomedical applications of Zn-based QDs, PANC-1 cells (a human pancreatic cancer cell line) were treated with chitosan-coated ZnS and Mn-ZnS.[80] Fluorescence imaging revealed that the QDs were largely incorporated into the cytoplasm of the cells. Despite their presence, 80% of the cells' metabolic activity was retained after being treated with 200 μg/mL of the QDs, and even at a much higher concentration of 1000 μg/mL, more than 70% of the metabolic activity was conserved, indicating a very low cytotoxicity for the ZnS QDs.

Yang et al. studied the toxicity and biodistribution of PEG-functionalized ZnS and ZnO QDs in male Kunming mice as well as human RBCs.[75] Even at a very high concentration of 1600 μg/mL, no significant hemolysis was observed in human RBCs treated with the PEG-QDs. Atomic absorption spectroscopy was used to assess the amount of Zn in various organs of mice, and it was observed that a bulk of the Zn was accumulated in the liver and lungs. Also, at a high QD dose, the ZnO QDs were cleared out quicker than the ZnS QDs from the liver and spleen. Interestingly, the excretion of the QDs through urine and feces decreased with increasing dose of QDs. Also, no significant differences in daily activities like eating and drinking, and functions of organs like liver, lungs and kidneys were observed.

Toxicity assessment of Mn–ZnS QDs on rat liver derived cell line (BRL 3A) showed a significant increase in lethality in comparison to their undoped counterparts.[81] Further investigations were done to determine the mechanisms of toxicity for the doped ZnS QDs. The Mn-ZnS QDs generated 86 % of the ROS generated by the positive control, whereas the undoped QDs produced 26%. DNA fragmentation in the cells due to the doped QDs

was significantly higher than the undoped QDs when compared to the negative control. Also, the introduction of an antioxidant (Trolox) reduced the DNA fragmentation, indicating the genotoxic effect of the ROS. Mn-ZnSe/ZnS QDs conjugated with biocompatible fluorine-doped hydroxyapatite exhibited lower toxicity and higher biocompatibility towards HeLa and HepG2 cells as reported by Zhou et al (Figure 3).[82] The cells treated with the QDs showed increased fluorescence intensities signifying QD uptake. Macropinocytosis and caveolae-mediated endocytosis were the uptake pathways in HepG2 cells, as treatment of the cells with inhibitors amiloride and genistein decreased the QD uptake. In HeLa cells caveolae-mediated endocytosis is solely responsible for the QD uptake. Biocompatibility of the QDs was proven by cell viability tests which did not show any cytotoxicity. Yang et al. introduced Mn-ZnS QDs and Mn-ZnS QD-PEG into mice which did not pose any significant changes to daily habits or body weights of the mice at time points of 24 h and 28 days post injection.[83] No changes in activity of serum aminotransferases were observed 28 days after treatment, signifying absence of hepatotoxicity. Additionally, there were no changes in antioxidant enzyme activities in liver, thus indicating an absence of oxidative stress. In conclusion, it can be said that the ZnS and ZnO QDs showed minimal toxicity on biomedical models, whereas the Mn-ZnS QDs showed different levels of toxicity and ROS generation depending on their coating and functionalization, on the type of cells and organisms considered.

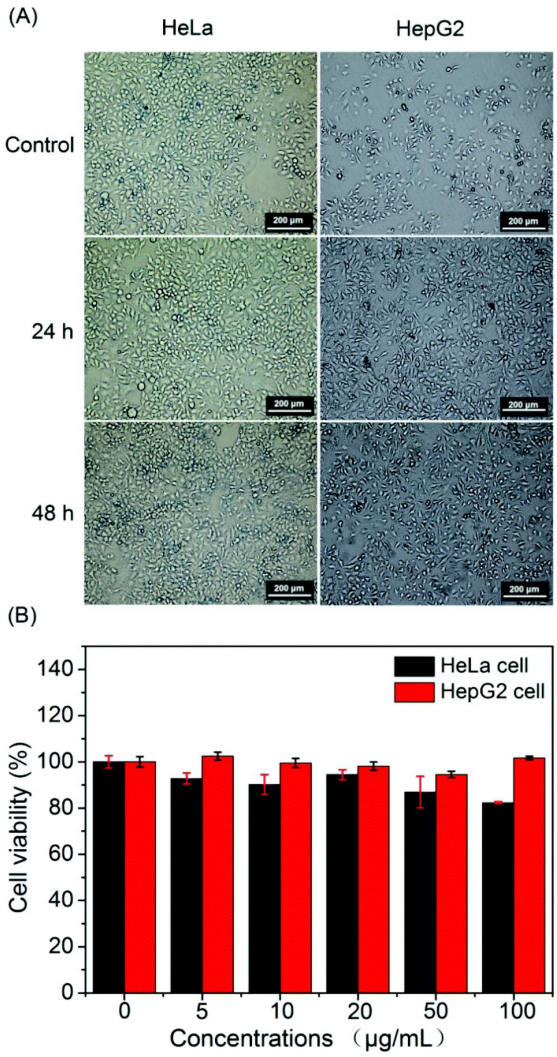

Figure 3: In vitro toxicity assessment of HeLa and HEPG2 cells with Mn-ZnSe/ZnS QDs conjugated with hydroxyapatite ligand. (Reproduced with permission of RSC Pub in the format Thesis/Dissertation via Copyright Clearance Center.)

1.5 Silicon-based QDs

Nanoscale silicon shows quantum confinement effects, and can have all the properties of Cd-based QDs. In addition, silicon as an element is abundant, non-toxic, and has a limited environmental footprint. Si QDs can be synthesized through various routes such as in inverse micelles,[84] oxidation of metal silicide,[85] and reduction of silicon tetrahalides.[86] There are also reports of plasma-based synthesis of Si QDs, which is a cheaper route to synthesis as well as a method that results in less agglomeration of the particles.[87] Quantum yields have been improved over time with quantum yields around 60-75% reported regularly.[88,89] All this makes silicon an excellent option to use for future QD applications. While there is a relatively small amount of data available assessing Si QD toxicity, the work done to date will be presented here.

1.5.1 Effect of Si QDs on environmental models

Liver damage in Gibel carp (*Carassius gibelio*) in the presence of Si/SiO_2 QD QDs was assessed by Stanca et al.[90] The experimental group was injected with a dose of 2mg/kg QDs per body weight. Gibel carp is a good model to assess the oxidative stress effects induced by QDs, since they have excellent antioxidant defense mechanisms.[91] Histology of liver tissue showed the production of macrophages which could be a response to nutritional imbalances and starvation. Abnormalities of the liver parenchyma was noticed as well. Oxidative stress caused damage to important enzymes which could lead to toxic effects. The effects were more pronounced with increasing concentrations and accumulation of the QDs in liver cells. Fan et al. performed *in vivo* studies with zebrafish embryos and Si QDs which induced abnormalities like yolk-sac edema, head edema, and

tail truncation at very high concentrations, but overall due to their low cytotoxicity, good photoluminescence and high photostability they can be considered as good candidates for biological applications.[92] Si QDs stabilized with hydrocarbons (C_4H_9, C_6H_5), a fluorocarbon (C_4F_9), or N-heterocyclic carbene radicals were synthesized by Kustov et al., and their cytotoxicities were analyzed using swollen river mussels *Anodonta anatina* and zebrafish *Dario rerio* embryos.[93] The authors were interested in investigating whether the toxicity observed in due to the Si QDs or most of the toxicity was due to the attached ligands. Treatment of the mussels with 3.3-nm-diameter C_4F_9-Si QDs induced significant bradycardia in the mussels, and 50% mortality was reached in 28 h. The Si content in the liver and gills of the mussels was much higher than the controls. Si QDs functionalized with C_4H_9 and C_6H_5 did not show any toxicity under the experimental conditions, whereas the carbene radical-functionalized one showed significantly less toxicity than the C_4F_9-Si QDs. Similar toxicity trends were also observed in the zebrafish embryos. The presence of the perfluorobutyl ligand with the Si QDs proved to be toxic, even though perfluorocarbon ligands are generally biocompatible; the toxic effect could be due to some synergistic interaction of the Si QD and the ligand. Thus, in this work shows some toxic effects of the Si QDs on gibel carp through the generation of ROS, but no toxicity was observed in zebrafish. Differently functionalized Si QDs varied in their toxicity properties depending on the ligands attached to them.

1.5.2 Effect of Si QDs on biomedical models

To assess the biocompatibility of Si QDs, QD uptake in monocytes was explored by Fan et al. using fluorescence microscopy and flow cytometry.[92] Internalization of the QDs in

the monocyte cells was observed but an LDH assay revealed that cell membrane damage was minimal. A Si/SiO_2 QD was reported to produce inflammation in MRC-5 human lung fibroblasts indicated by an increase in the interleukin-6 and interleukin-8 protein expressions.[94] A dose-dependent increase in the release of LDH form the cells was observed, signifying cell membrane damage and cytotoxicity. There was an increase in lysosome formation (measured by staining with LysoTracker Green) and autophagosomes (measured by staining with monodansylcadaverine). It is hypothesized that oxidative stress caused by the Si QDs can lead to the formation of autophagosomes. Also, the association of the QDs with cell organelles can trigger further autophagy as the QDs can be perceived as damaged proteins that need to be digested. Depending on the concentration of QDs in the cytoplasm, an uncontrolled autophagy might occur, leading to cell death. In another study that assessed the effect of Si QDs on human osteoblast-like cell line SAOS-2, a decrease in the cell metabolic activities was observed at high concentrations of 250-500 μg/mL.[95] Treatment with lower than 200 μg/mL of QDs was deemed to be safe. Poly-acrylic acid (PAAc)-coated Si QDs were proven to be biocompatible through *in vitro* cytotoxicity tests on mammalian cells HHL5, HepG2 and 3T3-L1.[96] There was cellular uptake of the QDs as evidenced by fluorescence imaging and flow cytometry. The cells did not show any difference in viability, proliferation, or morphology on treatment with the QDs, along with no significant DNA damage.

In vivo studies of Si QDs in mice and monkeys (rhesus macaques) were done by Liu et al. In mice most of the QDs accumulated in liver, spleen, lung, kidneys, and lymph to begin with.[97] After 14 weeks the lymph and kidneys cleared out, but Si QDs were still retained

in significant amount of the liver and spleen. The mice stayed outwardly healthy through the time of the exposure with no decrease in body weight and no changes in their daily activities such as eating, drinking or excretion. Elevated white cell count in blood is generally an indicator of body's defense mechanism against inflammation or toxicity. However, the blood tests did not show any significant changes in white blood cell and red blood cell counts. Though there were no obvious toxic effect observed in the time period of the experiments, the histology of liver showed slight signs of inflammation and necrosis. Longer term experiments might be necessary to assess if these signs get worse over time and lead to observable toxic effects. On treatment with the Si QDs, the monkeys remained healthy and did not show signs of any toxic effect. Blood tests were normal and comparable to controls. Histology of lung, kidney, liver, spleen, renal tubule, intestine, lymph nodes, and skin of the rhesus macaques showed no signs of damage that can be associated with the QDs. Thus, it can be concluded that the Si QDs showed no toxic effect on the monkeys under the experimental conditions. The potential for the use of these QDs in human biological applications and their possible toxic effects is inferred to be more related to the response in the monkeys, who relate to humans more closely physiologically than the mice.

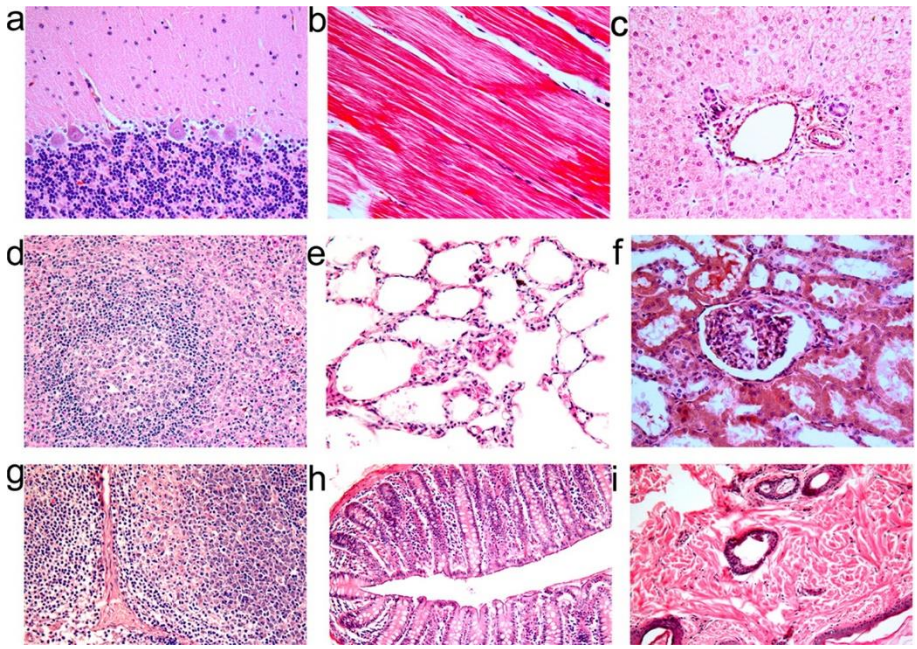

Figure 4: Histology images of various organs of monkey after treatment with Si QDs. (Reprinted with permission from ACS Nano 2013, 7, 8, 7303-7310. *Copyright © 2013 American Chemical Society.)*

From the studies so far, Si QDs seem generally non-toxic and benign to biomedical models. However, oxidative stress generation was hypothesized as the cause of certain toxicities that were observed.

1.6 Conclusion

Cd-free QDs present the opportunity to explore the unique and advantageous properties related to QDs, without the use of toxic element Cd. The optical and luminescence properties of these QDs have undergone improvements in recent years, and can be competitively used as substitutes for Cd-based QDs in various applications and commercial

products. Most importantly, as showcased in this review, a vast majority of these Cd-free QDs have proven to be biocompatible with low cytotoxicity and appear to be a more sustainable option than their Cd-based counterparts.

Chapter 2

Comparative Toxicity Assessment of Novel Si Quantum Dots and their Traditional Cd-based Counterparts using Bacteria Models *Shewanella oneidensis* and *Bacillus subtilis*

This work was completed with the assistance of Samantha K. E. Hill, Bo Zhi, Natalie V. Hudson Smith, Jeslin Wu, Eileen A. McIntire, Amani Lee, Prof. Uwe Kortshagen and Prof. Christy L. Haynes

Adapted with permission from Pramanik et al. *Environ. Sci.: Nano*, 2018, **5**, 1890-1901

. (*Reproduced with permission of RSC Pub in the format Thesis/Dissertation via Copyright Clearance Center.)*

Overview

Quantum dots are crystalline semiconductor nanoparticles with unique optical properties due to quantum confinement effects. They have several advantages compared to traditional organic fluorescent dyes, such as high fluorescent brightness, photostability, and tunable emission wavelengths, dependent upon particle size. Their unique optical properties have led to an increased use in a variety of devices, including diode lasers and television displays, as well as in biomedical research. The most commonly used quantum dots (QDs) are made of cadmium selenide (CdSe) and have a cadmium selenide core with a zinc sulfide shell (CdSe/ZnS), containing inherently toxic cadmium. This work focuses on comparison of the toxic effects of conventional CdSe and CdSe/ZnS quantum dots and silicon quantum dots, which are emerging as a potentially benign alternative, using bacteria as a model organism. The bacteria models used for our studies are *Shewanella oneidensis* MR-1, a Gram-negative bacterium, and *Bacillus subtilis* SB 491, a Gram-positive bacterium. This research assesses changes in cell viability, respiration pattern, and cell membrane integrity in the presence of the nanoparticles using colony counting, respirometry and membrane integrity assays, respectively. The association of the QDs with bacterial cell membranes was investigated using transmission electron microscopy (TEM). Results indicate that the silicon QDs are benign to the bacteria considered, and they do not associate with the cell membranes. The CdSe cores exhibit significant toxicity to the bacterial cells, whereas the CdSe/ZnS QDs are comparatively less toxic.

Environmental significance statement

QDs are presently used in electronic displays because of their electronic and optical properties that can improve the color gamut and brightness, and even reduce power

consumption. Cd-based QDs have been primarily used for these applications based on their high quantum efficiencies. However, the presence of toxic cadmium metal in these QDs makes them a potential risk to the environment as their use increases and products reach end of life. The work herein focuses on a silicon-based alternative QD and compares the interactions between the different kinds of QDs (silicon and Cd-based) and bacterial cells. The interaction of QDs with environmentally beneficial bacteria are an indicator of how these QDs may behave once released into the environment. Because the silicon-based QDs are less toxic to the bacterial cells than the Cd-based QDs, as well as made of an earth-abundant element, the silicon-based QDs offer a sustainable and environmentally friendly alternative to Cd-based QDs for commercial products. The Cd-based QDs have been preferred in commercial products due to their superior performance and luminescence properties. Even though the Si-based QDs have high quantum yields, further scientific research is ongoing to improve their properties, so they can be viewed as a lucrative alternative option not only from a sustainability point of view, but also from a performance point of view.

2.1 Introduction

An enormous growth in the use of nanotechnology-based products in the last ten years means that there is an increased risk of human and environmental exposure to engineered nanomaterials. It is thus important to investigate the behavior of industrially relevant engineered nanomaterials in the environment, as well as their toxicity towards living organisms. Based on their unique electronic and optical properties, there has been considerable interest in the synthesis and application of semiconductor nanocrystals in recent years.[1-3] Quantum dots (QDs) are crystalline semiconducting nanomaterials that display quantum confinement effects, a property exhibited by nanocrystals smaller in size than the Bohr radius, and have been traditionally synthesized from toxic and rare metals, such as cadmium. [2,3] The result is a size-dependent band gap and thus, extraordinary optical properties.[4,5] QDs were first discovered entrapped in a silicate glass matrix by A. I. Ekimov and A. A. Onushchenko in 1981[6] and have since become the subject of intensive research[7-16] based on their advantages over traditional organic fluorescent dyes, such as high luminescent brightness, good photostability, and tunable size-dependent emission wavelengths. The unique optical properties of QDs have led to their increased use in a variety of devices, including light-emitting diodes for electronic displays as well as in biomedical research. The total market impact of QDs is projected to reach around $3.4 billion by 2021, with the electronics sector totaling around $1.1 billion and the optoelectronics sector just over $1.8 billion, according to a study done by BCC Research titled “Quantum Dots: Global Market Growth and Future Commercial Prospects,” published in September 2016. Leading electronic companies such as Philips and Samsung have QD-based LCD displays in their devices currently on the market.[17]

The increasing use of QDs in commercial products has led to concerns regarding their environmental impact. 41.8 million tons of e-waste was generated in 2014 globally, of which only 6.5 million tons were collected and treated by respective national electronic take-back systems.[18] Only 12% of the e-waste generated in United States and Canada is collected by designated organizations and sent to facilities to remove toxic materials before being disposed of in landfills or incinerators. A majority of the e-waste that is discarded as regular mixed waste directly ends up in landfills without any prior treatment and can be hazardous to the environment. Although there has been extensive research about the toxicity of QDs to mammalian cells as a model for potential implications on human health,[19,20] the effect of quantum dots on the various trophic levels of the ecosystem are not as well characterized. Previous studies have identified the leaching of toxic ions, such as Cd, from QDs and generation of reactive oxygen species (ROS) as the main contributing factors to QD toxicity.[21,22,23] CdTe QDs have been reported to inflict oxidative damage on *Escherichia coli* cells.[24] Growth inhibition and lipid peroxidation have been observed in the microalgae *Phaeodactylum tricornutum* in the presence of CdSe/ZnS QDs due to ROS generation.[25] Biomagnification and accumulation of QDs have also been observed in certain freshwater and seawater species.[26] As the dissolution to Cd ions is one of the major pathways of quantum dot toxicity, some researchers have been focusing on the synthesis of Cd-free quantum dots (as discussed in chapter 1) or the inclusion of other design elements that block Cd release.[27] For example, the incorporation of a ZnS shell around the Cd-based core is a common strategy used to mitigate QD toxicity.

This work focuses on Cd-free quantum dots using the earth-abundant and potentially more benign element silicon to make silicon quantum dots (SiQDs) and presents a detailed comparison of the optical properties and environmental toxicity of the SiQDs to the more traditional CdSe and CdSe/ZnS QDs. The luminescent SiQDs used in this study were synthesized in a low-pressure, non-thermal plasma and subsequently treated with an atmospheric pressure microplasma to make them dispersible in water due to formation of a silica shell.[28] SiQDs tend to exhibit broad luminescence peaks, unlike more conventionally used QDs. Most of the semiconducting materials used to make QDs are direct band gap materials, whereas Si is an indirect band gap materials, thus leading to its unusual optical profiles.[29] There are mixed outcomes within the limited examples investigating the nanotoxicity of silicon-based QDs in the literature. SiQDs have been shown to induce inflammation in MRC-5 human lung fibroblasts by causing cell membrane damage, affecting the actin filaments, as well as disturbing the function of matrix metalloproteinase enzymes.[30] Another study shows the accumulation and oxidative stress inflicted by SiQDs in gibel carp liver.[31] Herein, bacteria was chosen as the model microorganism for the nanotoxicity experiments, as they are at the base of the food web, ubiquitous in the ecosystem, and have important roles in decomposition, nutrient cycling, and bioremediation. *Shewanella oneidensis* MR-1, a Gram-negative bacterium, and *Bacillus subtilis* SB491, a Gram-positive bacterium, are the two environmentally-beneficial representative bacteria species employed in this work. *S. oneidensis* has shown significant resistance to the effect of engineered nanoparticles in previous studies, thus making it a robust bacteria model to screen the QDs for any possible toxic effects under extreme conditions.[32] Even though the facultative anaerobic *S. oneidensis* is a known

dissimilatory metal reducing bacteria, this strain is chosen since it is unlikely to respire by assimilating metals in the Cd-based QDs in aerobic conditions,[33-35] as used in the following studies. Additionally, there are no reports of *S. oneidensis* being able to reduce silicon in either aerobic or anaerobic conditions. *B. subtilis* is not a metal-reducing bacteria, and thus our studies provide an interesting aspect of comparison with *S. oneidensis*. One Gram-negative and one Gram-positive bacterium were chosen because they present distinct surface chemistry during QD exposure. Gram-negative bacteria exhibit a double-membrane system, with two lipid membranes (outer and inner cytoplasmic), which are separated by a thin peptidoglycan layer. Lipopolysaccharide molecules are present on the outside of the outer membrane. The cell wall of a Gram-positive bacterium comprises a single cytoplasmic lipid membrane with a thick exterior layer of peptidoglycan. Teichoic and lipoteichoic acids are embedded within the peptidoglycan layer. By assessing QD interaction with both Gram-negative and Gram-positive bacteria, this work moves towards generalization of QD impacts based on bacterial membrane characteristics.

Briefly, this work demonstrates the effects of two Cd-containing QDs and SiQDs on the viability of the Gram-negative bacteria *Shewanella oneidensis* MR-1 and the Gram-positive bacteria *Bacillus subtilis* SB 491 using techniques such as colony counting, respirometry, and a membrane integrity assay. This work also investigates the association of the QDs with the bacterial cells using biological transmission electron microscopy (TEM). The CdSe QDs exhibit significant toxicity towards the bacteria cells, but CdSe/ZnS and SiQDs are largely benign, presenting two promising proactive design

strategies for current and future technological applications. A previous study where rhesus macaques were treated with CdSe/CdS/ZnS QDs did not show any evidence of toxicity, but showed the presence of Cd in organs even 90 days after the initial treatment.[36] Similar studies on mice and monkeys using SiQDs displayed no toxic effects, but there was Si accumulation in liver and spleen of the animals 3 months post-treatment.[37] So, it's worth pointing out that the CdSe/ZnS QDs may exhibit delayed toxic effects due to oxidation and dissolution of the ZnS shell and release of Cd^{2+}, and the limited time exposure we have carried out with bacteria and QDs, may not be enough to rule out their toxicity. The benignness of SiQDs even at high dosage as used in our studies, to some extent rules out the negative effect of accumulated higher concentration of SiQDs In the future SiQDs can prove an extremely important alternative to all the Cd-based QDs, not only due to their benign nature but also because theyuse only earth-abundant elements, as opposed to Cd-based QDs.

2.2 Methods

2.2.1 Materials: The SiQDs were synthesized as described below, while the CdSe QDs and CdSe/ZnS core-shell QDs were purchased from NN-Labs. The CdSe/ZnS QD surfaces are functionalized with a carboxylic acid ligand (listed in the catalog as item CZW), and the CdSe QDs were custom-made by NN Labs, stabilizing them with the same carboxylic acid ligand.

2.2.2 Synthesis of SiQDs: SiQDs were synthesized in a low pressure, non-thermal plasma driven by a 13.56 MHz RF power source, nominally set to 60W. Silane (SiH_4) presented

at 5% by volume in helium was used as the silicon precursor at 14 sccm, while 10 sccm of argon acted as the ionizing carrier gas. Both gases flew the entire length of a 9.5 mm outer diameter borosilicate glass tube which expands to 25.6 mm outer diameter roughly 4 mm downstream of the powered electrode.[38] Hydrogen was injected in this expanded afterglow region at a flow rate of 100 standard cubic centimeter per minute (sccm) to initially passivate the surface. The plasma pressure was maintained at ~1.6 Torr via an orifice, after which particles were collected via inertial impaction. These as-produced particles were then wetted with 0.2 mL of ethanol per 10 mg of silicon nanocrystals via sonication and subsequently diluted in an additional 1.8 mL of deionized water and shaken. The solutions were then treated by an atmospheric pressure, non-thermal microplasma jet to improve the dispersion of the hydrophobic particles in water.[28] The radiofrequency driven microplasma used argon at a flow rate of 750 sccm was operated at an average power of 2.5W. The nozzle of the jet was placed 3.5 mm above the water surface so that the plasma plume touched the liquid surface. The volume of water was adjusted every 15 minutes to counter evaporation, and the total treatment time was 1 hour. After treatment, the particles gain an oxide shell that improves the hydrophilicity.[28]

2.2.3 Characterization of QDs:

The QDs were characterized using a combination of transmission electron microscopy (TEM), UV-vis extinction spectroscopy, dynamic light scattering (DLS), and fluorescence spectroscopy. TEM samples were prepared by dropcasting a small amount of the QD solution on a TEM grid, drying the samples in ambient conditions, and images were acquired using an FEI Tecnai T12 TEM. SiQD samples were prepared for cryogenic TEM by administering 5 μL onto a lacey carbon grid, which was immediately dried and plunge

frozen with a FEI Mark IV Vitrobot. Samples were either deposited on hydrophobic grids or lacey carbon grids that were made hydrophilic via glow discharge. Cryogenic TEM images were acquired on a Tecnai G2 Spirit Biotwin. The hydrodynamic diameter of the SiQDs was determined via DLS on a Brookhaven ZetaPALS instrument. This experiment was performed to assess the stability of the QDs in bacterial media used for toxicity experiments. The fluorescence properties, including excitation/emission spectra as well as quantum yield (QY) of the QDs, were assessed using a calibrated integrating sphere paired with an Ocean Optics USB2000 spectrometer.

2.2.4 Bacterial culture: Shewanella oneidensis MR-1 stock was a gift from the lab of Jeff Gralnick at the University of Minnesota. *Bacillus subtilis* strain SB 491 was purchased from Bacillus Genetic Stock Center (Columbus, OH). The bacteria were stored at -80 °C before being inoculated onto LB broth agar plates, which were incubated at 30 °C for *S. oneidensis* and 37 °C for *B. subtilis*.

2.2.5 Colony counting assays (Drop-plate and Pour-plate assays): Colony counting experiments were performed to assess the dose-dependent effect of the various QDs on both bacteria at 50 mg/L, 100 mg/L, and 200 mg/L QD concentrations. Bacteria liquid cultures were grown in Luria Broth media (Difco LB Broth, Miller) for 4 h at 30 °C to mid-log phase from colony inoculants on solid agar plates. Bacterial cells were harvested by centrifugation for 10 min at 2000xg, washed in Dulbecco's phosphate-buffered saline (D-PBS) buffer, and suspended in a HEPES buffer (2 mM HEPES and 25 mM NaCl, at pH 7.4). The cultures were then diluted to OD 0.2 at 600 nm (OD600) to achieve a cell

density of approximately 2 x 10^8 colony-forming units (CFUs)/mL. Serial 10-fold dilutions of this bacterial suspension were performed at this stage to achieve a cell concentration of 10^4 CFUs/mL in HEPES buffer. The resultant diluted bacteria suspension was then treated with QDs at various concentrations (50 mg/L, 100 mg/L and 200 mg/L) and incubated for 15 min. An adapted drop-plate method was used for the *S. oneidensis* cells, where six 10 µL droplets of the exposed bacterial suspensions as well as untreated negative controls were dropped on an LB-agar plate, which had been pre-sterilized under UV-illumination for 20 min. The droplets were dried under air flow in a biological cabinet and were incubated at 30 °C for 20 hours before colonies were counted using a Bantex Colony Counter 920A. The viability of cells from each treatment was reported as a ratio to the control samples. Due to the high motility and swarming mobility of *B. subtilis* cells, the pour plate method of colony counting was employed instead of the typical drop plate method. In this method, 60 µL of QD-incubated bacterial cell suspension was placed in each well of a 12-well plate, and 1 mL of melted LB-agar solution at 45 °C (1.5% agar) was poured and mixed well. The well plates were incubated at 37 °C for 20 hours, and the colonies in each well were counted. The viability of cells from each treatment was reported as a ratio of number of colonies counted to the control samples. The experiments were done using three different batches of SiQDs, and two different batches of Cd-based QDs, and repeated three times (three biological replicates) for each batch of QDs.

2.2.6 Respirometry: Aqueous minimal media (buffered with 10 mM HEPES and containing 11.6 mM NaCl, 4.0 mM KCl, 1.4 mM $MgCl_2.6H_2O$, 2.8 mM Na_2SO_4, 2.8 mM NH_4Cl, 0.088 mM Na_2HPO_4, 0.051 mM $CaCl_2$, and 100 mM sodium lactate for *S.*

oneidensis or 10 mM dextrose for *B. subtilis*) was used to culture bacteria for 24 h. The concentration of the cell suspension was modified to OD 0.2 at 600 nm (OD600) to achieve a cell density of approximately 2 x 10^8 CFUs/mL, and then further diluted 10-fold in minimal media. Aliquots of this diluted cell suspension were pipetted into 125 mL respirometry glass bottles containing removable rubber septa, and QD samples were introduced to achieve the desired QD exposure concentrations of 50 mg/L, 100 mg/L and 200 mg/L in a final exposure volume of 100 mL. As aerobic respiration entails consumption of O_2(g) and generation of CO_2(g), KOH(aq.) inserts were placed into the headspace above the culture, to remove the resulting CO_2. The glass bottles were placed in a water bath maintained at 30 °C for *S. oneidensis* and 37 °C for *B. subtilis*, and the suspensions were stirred continuously at 500 rpm. A small gauge needle was placed through each septum, and tubing (Tygon® 4040-A) linked each bottle to a respirometer system (Respirometer Systems and Applications, Inc., Springdale, AK) that monitored cellular $O_{2(g)}$ consumption over 24 h. As the cell population size increases over time, total aerobic respiratory activity also should increase. Aerobic respiration decreases the total $O_{2(g)}$ pressure in the headspace of the sealed bottles, and $O_{2(g)}$ was supplied as needed at 10 min intervals to maintain a constant pressure. The total mass of $O_{2(g)}$ delivered to each vessel was recorded at 10 min intervals over 24 h.

2.2.7 Membrane integrity assay (Live-Dead assay kit): In parallel to the colony counting and respirometry measurements, the integrity of bacterial cell membranes was also monitored. A fluorescent LIVE/DEAD™ *Bac*Light Bacterial Viability Kit containing two nucleic acid stains, propidium iodide (PI) and SYTO9, was used to evaluate the "live:dead ratio" which is the ratio of cells with intact cell membranes to cells with compromised cell

membranes. SYTO9 is a cell permeant, intercalating nucleic acid stain that can stain all the bacterial cells in suspension, whereas PI is a cell impermeant nucleic acid stain that only associates with cells that have damaged cell membranes. For this experiment, bacteria (either *S. oneidensis* or *B. subtilis*) were incubated in LB broth overnight, and diluted to OD 0.2 at 600 nm (OD600) to achieve a cell density of approximately 2 x 10^8 CFUs/mL in HEPES after a washing step with DPBS. The diluted bacteria were incubated with QDs at 50 mg/L, 100 mg/L, or 200 mg/L resultant concentrations for time periods of 1 h or 6 h. 100 µL of bacteria samples were aliquoted into a 96-well plate, then mixed with the 100 µL of dye mixture containing both SYTO9 and PI, and fluorescence measurements were collected in a Synergy 2 Multi-Mode Microplate Reader (BioTek, VT). The sample mixture was excited at 485 nm, and emission data was collected at 528 nm for SYTO9 and 635 nm for PI. The emission data for both SYTO9 (indicating "live" cells) and PI (indicating "dead" cells) were normalized to their respective negative controls, and the ratio of these normalized data indicate the "live:dead ratio".

2.2.8 Biological TEM analysis: Bacteria were cultured in LB broth overnight, then diluted to an OD of 0.8 at 600 nm in HEPES. The diluted bacterial suspension was centrifuged down to a pellet, washed thrice with 0.1 M cacodylate buffer solution, then resuspended in a fixation buffer of 2.5% glutaraldehyde in 0.1 M sodium cacodylate buffer and fixed for 50 minutes. The pellet was washed with sodium cacodylate buffer, and dehydrated stepwise with increasing concentration of ethanol (30, 50, 70, 80, 90, 95, and 100% ethanol in water). After removing the last ethanol rinse, the pellet was washed with propylene oxide three times, and the infiltration steps were carried out. The pellet was

soaked for 2 h in a 2:1 propylene oxide:epoxy resin mixture. This was replaced with a 1:1 propylene oxide: epoxy resin mixture, and the pellet was incubated in this mixture overnight. After this, the pellet was incubated in a fresh batch of 1:1 propylene oxide: epoxy resin mixture for 6 h, and finally placed in a pure resin mixture and infiltrated overnight. The resin sample was then cured in a 40 °C oven for one day and then 60 °C oven for two days. Ultrathin sections (65 nm) were sectioned by using Leica UC6 microtome and Diatome diamond knife, then stained with uranyl acetate and lead citrate. These sections were placed on copper TEM grids (Ted Pella Inc.), and imaging was done using an FEI Tecnai T12 TEM.

2.3 Results and discussion

2.3.1 Characterization of QDs

2.3.1.1 Physical characterization: Figure 1 shows the TEM images of the three QDs compared herein: CdSe, CdSe/ZnS and SiQDs. The approximate diameter of the CdSe QDs, as provided by the manufacturer, is 4.6 nm, and that of the CdSe/ZnS QDs is roughly 9 nm total with a 4.5 nm core. It was difficult to assess the exact size of the SiQDs using TEM images due to the extensive aggregation; hence, cryogenic TEM images were acquired to observe SiQDs in vitrified water. When SiQDs were deposited on hydrophilic grids, particles had an average diameter of 3.8 ± 0.04 nm (n=400, mean ± std. error). Larger aggregates were observed on both hydrophobic and hydrophilic grids with average diameters of 19.2 ± 0.2 nm (n=300, mean ± std. error). DLS experiments were performed to evaluate the hydrodynamic diameters of the SiQD aggregates both in water and HEPES buffer (the media used for biological exposures). The measurements were done at SiQD concentrations of 50 mg/L, 100 mg/L, and 200 mg/L to monitor not only the effect of the

incubating media, but also QD concentration on aggregate size. These results are shown in Figure 2. In the DLS data, the SiQDs exhibit very large aggregate formation in both Milli-Q water and HEPES (4-(2-hydroxyethyl)-1-piperazineethanesulfonic acid) media. However, no significant difference in aggregate size was observed when comparing the data in Milli-Q water and HEPES or at the different concentrations. The zeta potential of the SiQDs was measured to be - 13.2 ± 0.3 mV. This low magnitude zeta potential likely contributes to the colloidal instability of the SiQDs in dispersion.[39]

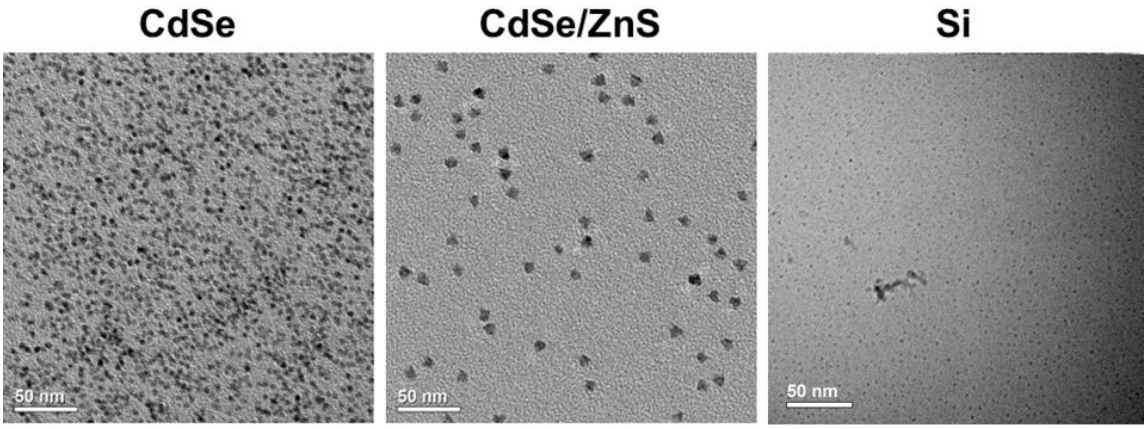

Figure 1: Representative transmission electron micrographs of CdSe, CdSe/ZnS and cryogenic transmission electron micrographs of SiQDs

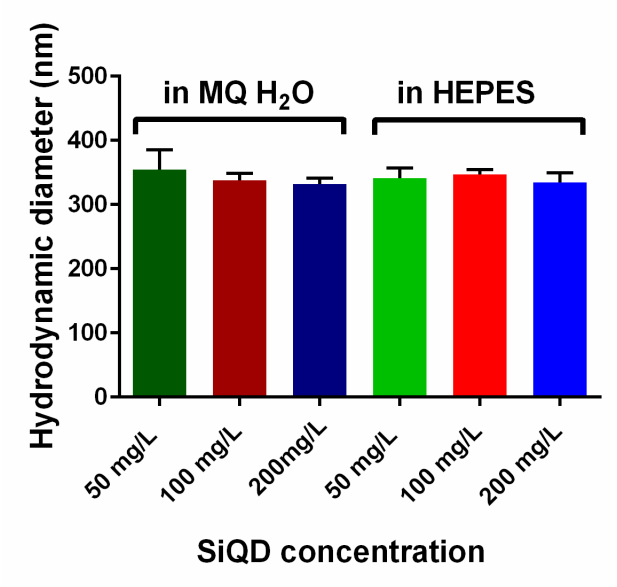

Figure 2: Hydrodynamic diameter of the SiQDs in MQ H_2O and HEPES buffer obtained by dynamic light scattering. No significant difference in hydrodynamic diameter is observed for the two media or among different nanoparticle concentrations used. The error bars indicate standard deviation using three measurements.

2.3.1.2 Optical characterization: To investigate the optical properties of the QDs, UV-vis extinction, steady-state emission, and absolute quantum yield (AQY) measurements were completed. The emission spectra and AQY were measured using a calibrated integrating sphere paired with an Ocean Optics USB2000 spectrometer. The measurement methods are described by Mangolini et al.[40] with excitation provided by a 395 nm LED. The CdSe cores exhibited observable absorption signals at 500 nm and 590 nm, similar to the CdSe/ZnS QDs absorption in Figure 3A. However, as the surface defects were not passivated by a protective shell, namely the ZnS layer, the photoluminescence of CdSe QDs were quenched significantly.[41] Therefore, the CdSe QDs did not exhibit bright enough emission to be detected by our spectrometer. The CdS/ZnS QDs exhibited an emission peak at 630 nm (Figure 3A) and their AQY was 47%, whereas SiQDs exhibited an emission peak near 830 nm (Figure 3B), and their AQY was measured to be 25%. Because of the near infrared (NIR) limitations of our spectrometer, it is possible the broad SiQD emission actually extends further to NIR. If so, the AQY would be greater than measured and the reported value can be considered a lower bound. The peak emission of

the CdSe/ZnS at 630 nm corresponds to a red-orange color, while the peak of the SiQDs at 830 nm is in the near infrared, rather than the visible. However, the SiQDs emit a red-orange color, which is redder than the CdSe/ZnS QDs. The SiQDs synthesized in a plasma reactor can provide an inexpensive and potentially environment-friendly alternative to Cd-based QDs, though further optimization needs to be done to reach quantum yields that match their Cd-containing counterparts.

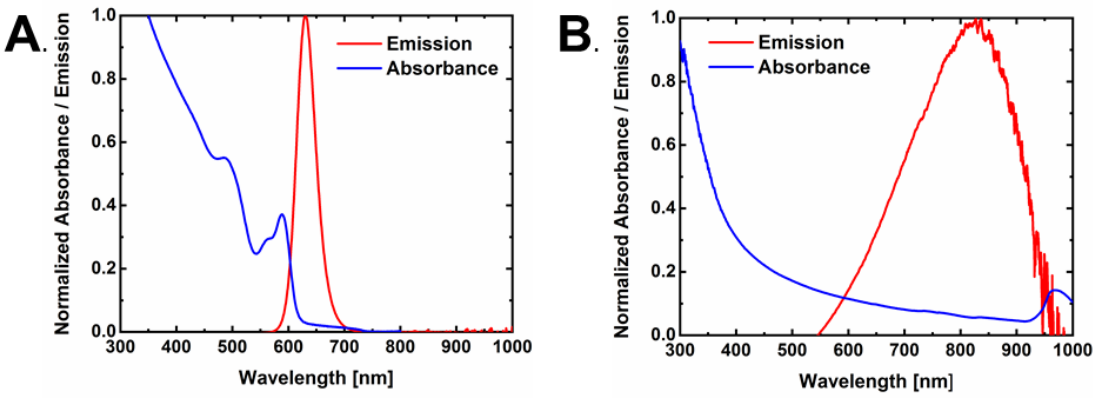

Figure 3: A) Optical properties (UV-vis absorption and emission) of CdSe/ZnS QDs and (B) optical properties (UV-vis absorption, and emission) of SiQDs.

2.3.2 Comparative toxicity assessment of QDs:

2.3.2.1 Colony counting assays (Drop-plate and Pour-plate assays):

Colony counting assays have been considered a gold standard in bacterial cell enumeration in microbiology. In this work, colony counting assays were used to determine the number of viable bacteria cells in a solution after they had been treated with the different QDs (CdSe, CdSe/ZnS, or Si). The bacteria solution was diluted to obtain discrete and non-overlapping colonies on the LB-agar plate. The diluted bacterial suspension was exposed

to increasing QD concentration to assess the dose-dependent nature of any toxicity that the QDs exhibit. These solutions were plated on LB-agar plates and incubated for 18-20 h so that countable colonies were discernible. The number of colonies formed on the LB-agar plate indicate the number of viable cells present in the exposure solution. Thus, any decrease in the number of colonies compared to the negative control was attributed to toxic effects exhibited by the QDs. The drop plate colony counting method was used for the Gram-negative bacteria *Shewanella oneidensis* MR-1, and the pour plate colony counting method was employed for the Gram-positive bacteria *Bacillus subtilis* SB491.

The results of the drop plate colony counting assays with *Shewanella oneidensis* following exposure to QD concentrations of 50 mg/L, 100 mg/L, or 200 mg/L are shown in Figure 4. The results for parallel pour plate colony counting assays with *Bacillus subtilis* are shown in Figure 5. Statistical analysis was performed using one-way ANOVA, followed by post-hoc Tukey's multiple comparisons tests (GraphPad Prism software, La Jolla, CA). All values plotted are the mean ± standard deviation (SD), and statistical significance is indicated using asterisks (p values < 0.0001 indicated by ****, 0.0001 to 0.001 indicated by ***, 0.001 to 0.01 indicated by **, and 0.01 to 0.05 indicated by *).

The SiQDs did not have any significant toxic impact on either *S. oneidensis* or *B. subtilis* cells at any of the tested concentrations. The CdSe QDs were significantly more toxic to the bacteria cells, when compared to the SiQDs or the CdSe/ZnS QDs. At a concentration of 200 mg/L, the CdSe QDs killed about 95% of the cells in case of *S. oneidensis* and 75% cells in case of *B. subtilis*. The CdSe/ZnS QDs were not toxic to *S. oneidensis* cells at any

of the concentrations considered, but showed mild toxicity to the *B. subtilis* cells at 200 mg/L. Cd-based QDs can exhibit toxicity due the effect of dissolved toxic Cd(II) ions,[42,43] as well as the generation of reactive oxygen species (ROS).[44,45,24] ROS is known to induce growth defects in bacteria, inactivate mononuclear iron proteins, cause DNA damage, oxidize cysteine proteins, and peroxidize lipids, amongst other effects.[46] Reactive oxygen species (ROS) produced in cells by heavy metal stresses are known to damage iron-containing proteins in *S. oneidensis*.[47] Cd(II) ions can impact biological systems in several ways: (1) by inhibiting DNA repair mechanisms by impairing the damage recognition step,[48] (2) by causing oxidative stress in cells through ROS generation, and subsequent damage to cell membranes,[49] and (3) by incorporating into Gram-negative cells through the Mg(II) uptake system or Gram-positive cells by the Mn(II) uptake system.[50] The ZnS shell on the CdSe core can mitigate some of the toxicity of the cores[42] by protecting the cores from weathering and oxidation and eventual dissolution to Cd(II) ions.[2] Despite the protective shell, some toxic effect was observed for the *B. subtilis* cells when treated with 200 mg/L CdSe/ZnS QDs. Gram-positive bacteria, like *B. subtilis*, can be more susceptible to toxicity posed by nanoparticles than Gram-negative bacteria, like *S. oneidensis*, because they lack an outer cell membrane with lipopolysaccharide (LPS) chains that play a protective role.[51]

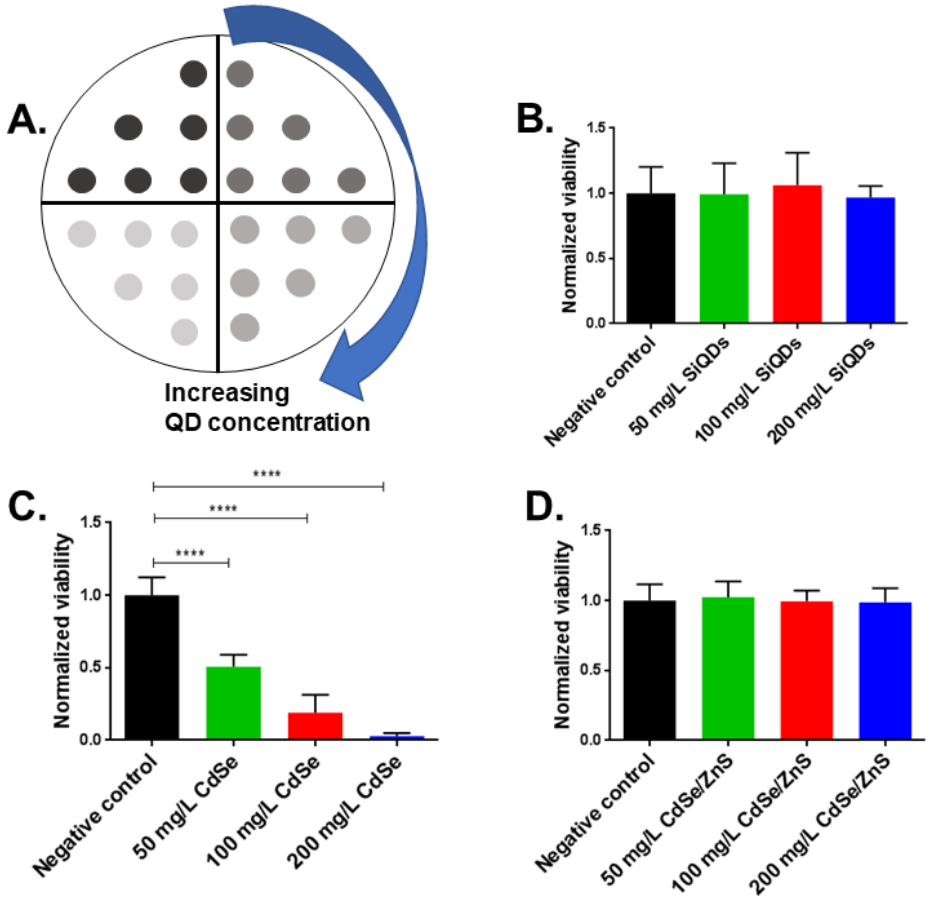

*Figure 4: Bacterial viability of S. oneidensis assessed using drop plate colony counting. A. The template of an LB-agar plate for drop plate assay B. No observable effect on bacterial viability with treatment with SiQDs C. Significant dose-dependent toxic effect when treated with CdSe QDs D. No effect on bacterial viability upon exposure to CdSe/ZnS QDs. The error bars denote the standard deviation between three biological replicates. p values < 0.0001 indicated by ****.*

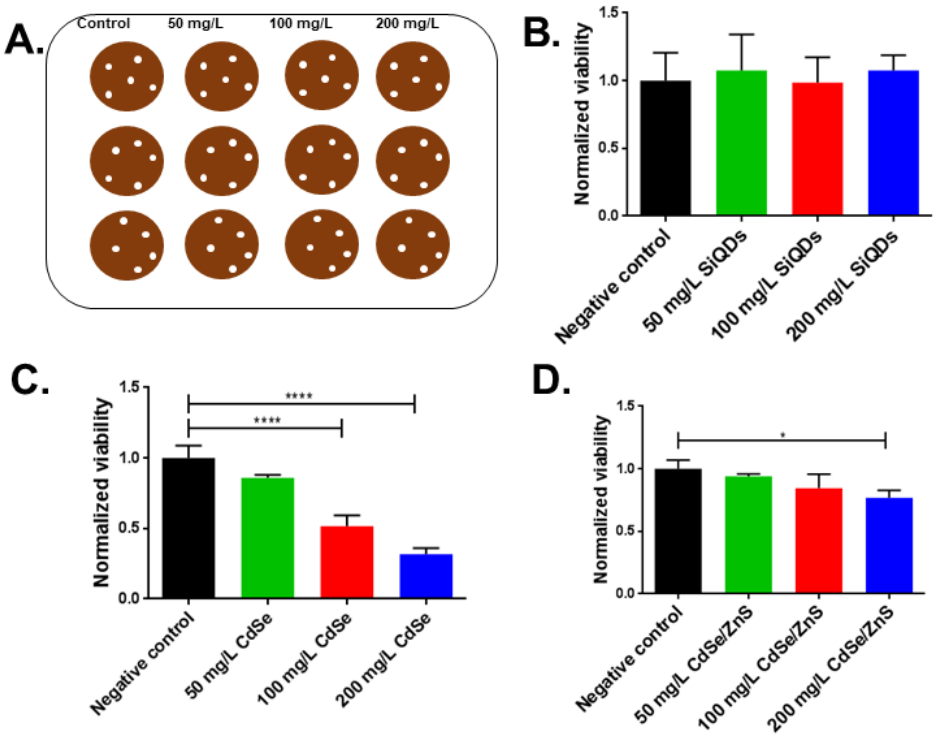

*Figure 5: Bacterial viability of B. subtilis assessed using pour plate colony counting. A. The template of a 12-well plate for pour plate assay B. No observable bactericidal effect on treatment with SiQDs C. Significant dose-dependent toxic effect when treated with CdSe QDs D. Small effects on bacterial viability upon exposure to CdSe/ZnS QDs. The error bars denote the standard deviation between three biological replicates. p values < 0.0001 indicated by ****, and 0.01 to 0.05 indicated by **

2.3.2.2 Biological TEM analysis:

Biological TEM imaging provides qualitative insight into the spatial interactions between bacterial cells and QDs after the cells have been incubated with the QDs. Figure 6 shows the results obtained from imaging *S. oneidensis* samples exposed to the three different QDs at 200 mg/L for 15 minutes. The CdSe-treated *S. oneidensis* cells show significantly damaged cell membrane structures, and many polyp-like globules of disintegrated cell membranes far from their original location (Figure 6A). One interesting feature present in

the CdSe-exposed *S.oneidensis* samples was the abnormal elongation of the bacterial cells (Figure 6B). Similar results have been observed previously with *S. oneidensis* cells incubated with CdTe QDs.[52] This abnormal elongation is a known phenomenon in bacteria cells called filamentation. This occurs when a cell continues to elongate but does not undergo cell division due to inhibition of chromosome replication caused by DNA damage.[53] The presence of filamentous cells in the sample suggests DNA damage and genotoxicity to *S. oneidensis* cells in the presence of CdSe QDs. This can be directly correlated with the cell viability data obtained from the colony-counting assay. Neither the CdSe nor the CdSe/ZnS QDs were observed near any of the *S. oneidensis* cells.

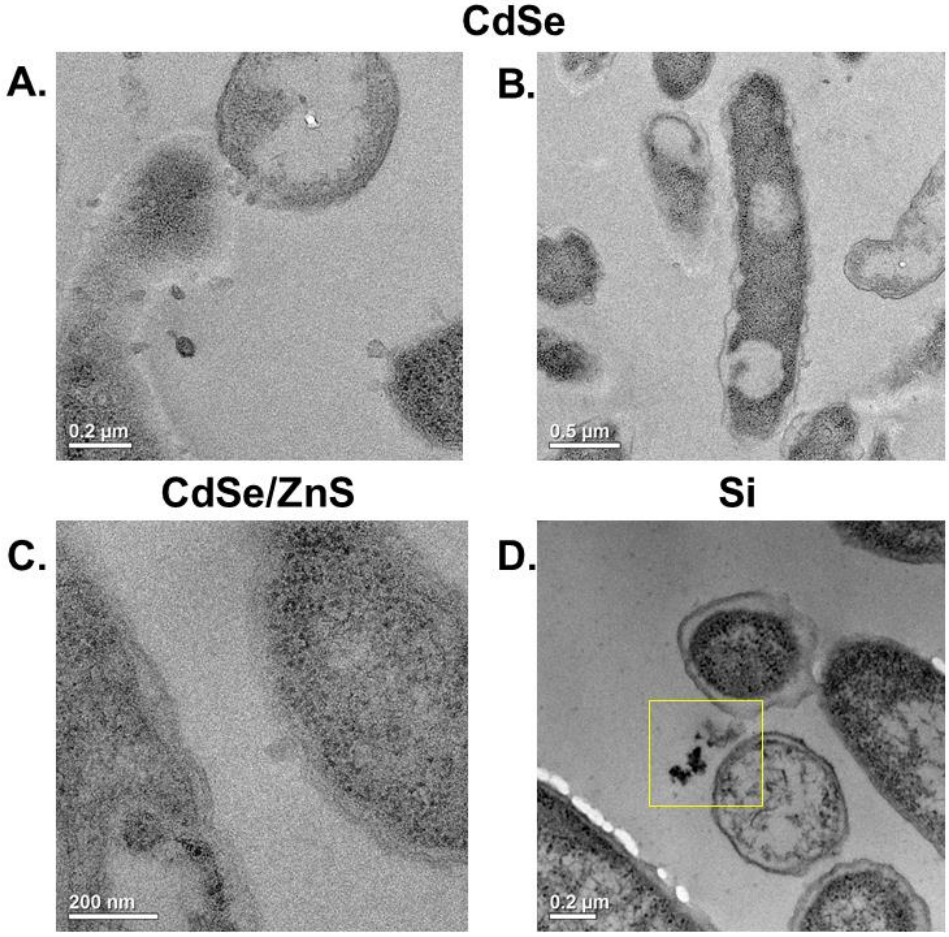

Figure 6: Biological transmission electron micrographs for S. oneidensis after treatment with QDs. A. & B. TEM images of S. oneidensis treated with CdSe QDs. Indicate the cell

membrane damage and filamentation of bacterial cells following exposure to CdSe QDs. C. TEM images of S. oneidensis treated with CdSe/ZnS QDs. Indicates no association of CdSe/ZnS QDs with bacterial cells. D. TEM images of S. oneidensis treated with SiQDs. Indicates no association of SiQDs with bacterial cells although the presence of SiQD aggregates is apparent (indicated by yellow box).

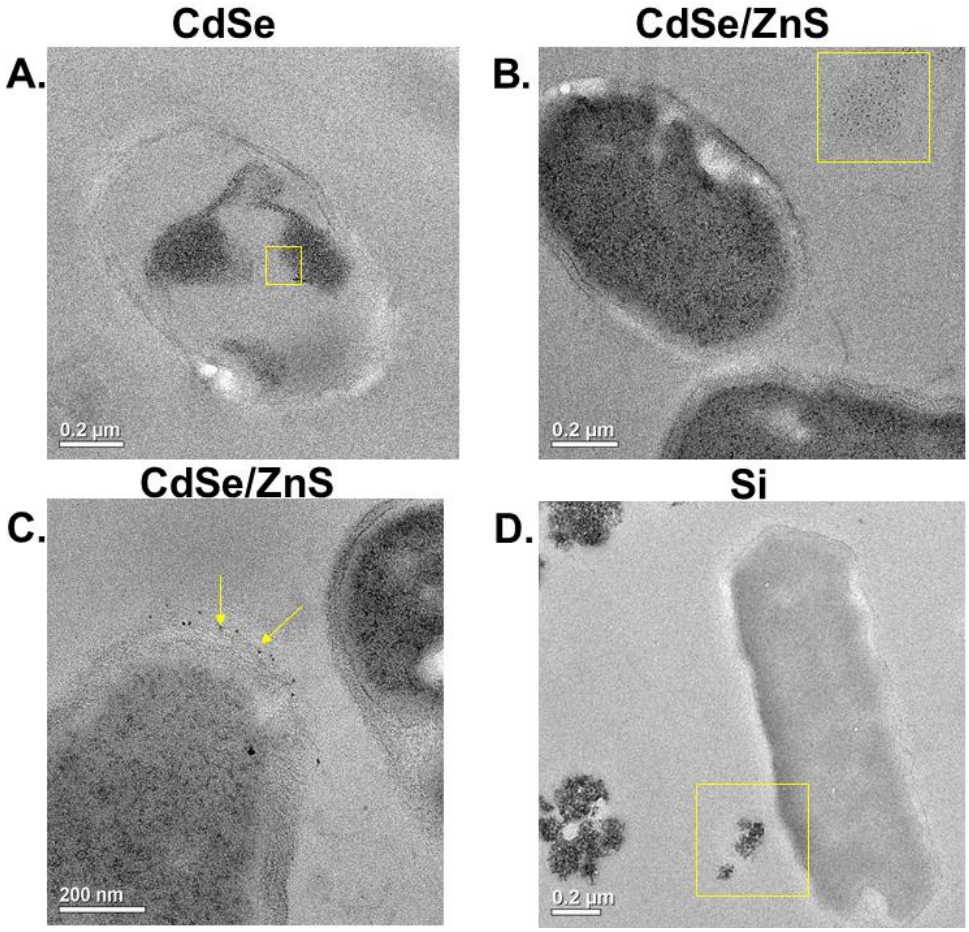

Figure 7: Biological TEM for B. subtilis after treatment with QDs. A TEM images of B. subtilis treated with CdSe QDs. Indicate the cell membrane damage of bacterial cells following exposure to CdSe QDs. The yellow box indicates CdSe QDs associated with cellular material. B. & C. TEM images of B. subtilis treated with CdSe/ZnS QDs. No association of CdSe/ZnS QDs with the majority of bacterial cells. Cell membrane damage and association observed in some cells as denoted by yellow arrows in 7C. D. TEM images of B. subtilis treated with SiQDs. No association of SiQDs with bacterial cells as denoted by SiQD aggregates in the box in 7D.

Neither the CdSe/ZnS nor the SiQDs exhibited any noticeable qualitative association with or impact on the *S. oneidensis* cells. For the sample containing the SiQDs, the QDs were aggregated near the cells, but no direct contact between the QDs and the cells were observed after visualizing a minimum of 20 bacterial cells across 2 TEM grids. For the *B. subtilis* cells, cell membrane damage was observed following treatment with CdSe QDs. A majority of the cells treated with CdSe/ZnS QDs appear intact, with no association with the QDs (Figure 7B); however, a few cells showed localized cell membrane damage, with QDs dotted along the compromised cell wall (Figure 7C). No interaction between the SiQDs and *B. subtilis* cells was noted. (Figure 7D)

2.3.2.3 Further toxicity assessment of SiQDs: Due to the novel nature of the SiQDs used in this study, and the lack of previous studies on toxicity assessment of Si-based QDs, further experiments were performed to probe any possible sub-lethal effects of the SiQDs on the two model bacteria, *S. oneidensis* and *B. subtilis*. The effect of the SiQDs on bacterial respiration and oxygen uptake was assessed using respirometry, and the membrane integrity in presence of the SiQDs was monitored using the Live-Dead *Bac*Light assay kit.

2.*3.2.4 Respirometry:* The oxygen consumption of bacterial cells over time was examined using a respirometer. Any sub-lethal impact due to the QDs, such as delayed onset of growth, can be assessed from the oxygen uptake curve. The oxygen uptake curve generally follows a sigmoidal shape, like the bacterial growth curve, since the population growth

and oxygen uptake are proportional to one another. With one biological replicate for each of the two materials replicates, neither the 50 nor 100 mg/L SiQDs had significant effects on the respiration of either *S. oneidensis* or *B. subtilis* cells (Figure 8).

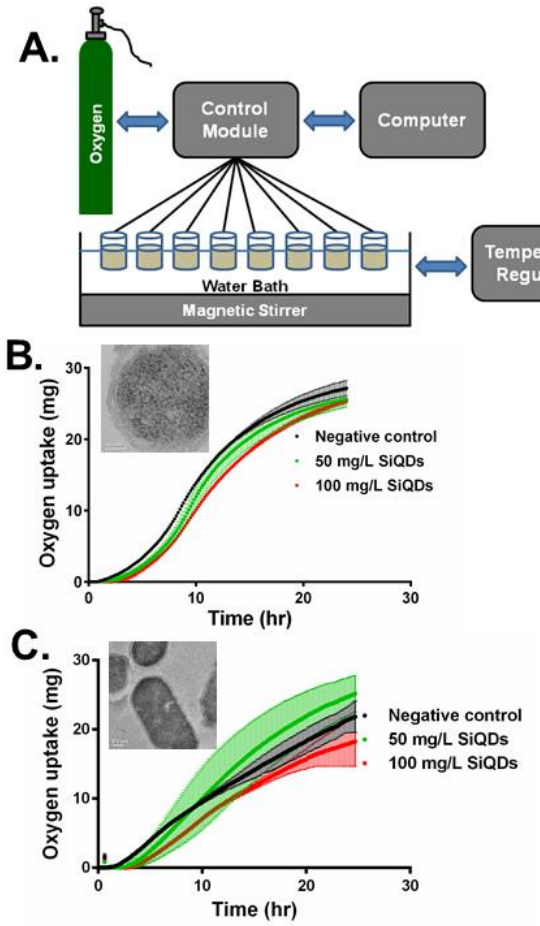

Figure 8: A. Schematic of the respirometer setup. B. Representative respirometry data for S. oneidensis and C. B. subtilis. Both the negative control and SiQD-exposures to 50 and 100 mg/L are shown.

2.3.2.5 Membrane integrity assay (Live-Dead assay kit): The membrane integrity assay using the Live-Dead *Bac*Light assay kit employs two nucleic acid stains: green fluorescing SYTO-9, which stains all cells, and red fluorescing propidium iodide, which penetrates and stains cells with compromised membranes. A decreased green/red fluorescence ratio indicates a more permeable membrane. The experiment was done by treating the bacteria

cells with QDs for 1 h or 6 h time periods, introducing the dye mixture, and then measuring the fluorescence data. The results show minimal effect of the SiQDs on the cell membrane integrity for both bacteria species. Even at an extended exposure time of 6 h, there was no significant change in the "live:dead ratio" compared to the negative control. Thus, it can be concluded that the SiQDs do not damage the cell membrane of the bacteria.

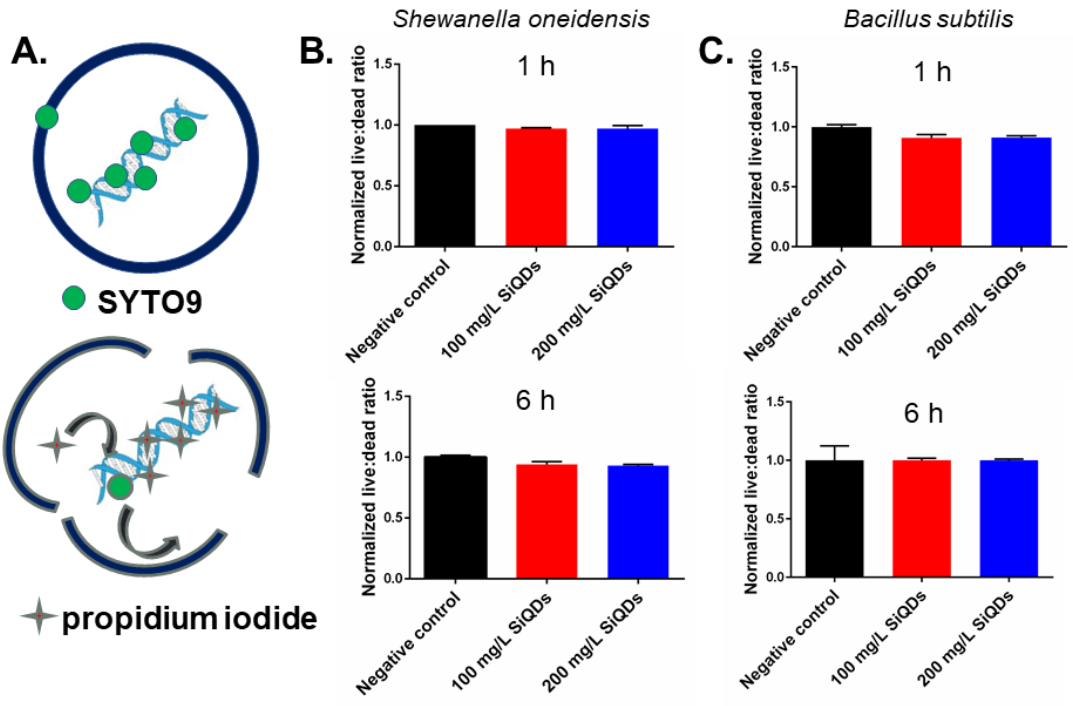

Figure 9: Live-dead membrane integrity assay with bacteria and QDs. A. Schematic showing cell permeable SYTO9 and cell impermeable propidium iodide (PI). B. Data for S. oneidensis after 1 h and 6 h treatment with Si QDs C. Data for B. subtilis after 1 h and 6 h treatment with Si QDs. The error bars denote the standard deviation between two biological replicates.

2.4 Conclusions

SiQDs with good optical properties were synthesized in a low-pressure, non-thermal plasma, and then treated with a microplasma to make them water dispersible. These QDs, made of earth-abundant silicon, have potential as a sustainable alternative to transition metal-based QDs. This work set out to consider potential toxicity of these materials to bacteria, critical components of the food web. The effects of the SiQDs were considered on two different bacteria, one Gram-negative and the other Gram-positive, and compared with the effects of two traditional Cd-based QDs (CdSe and CdSe/ZnS). The SiQDs did not show any effect on the viability of bacteria cells as seen in the colony counting assays, whereas the CdSe QDs exhibited significant dose-dependent toxic effects on the bacteria. The ZnS-coated CdSe QDs showed little to no toxicity to the two bacteria tested. In biological TEM studies the SiQDs showed no association or qualitative impact on bacterial morphology while the CdSe-treated bacteria showed cell membrane damage and filamentation. The ZnS-coated CdSe QDs were seen to exhibit minimal association with the *B. subtilis* cells. Upon exploration of more nuanced bacterial impacts, the SiQDs proved to be benign when considering both respiration and membrane integrity. Overall, based on considerations of bacterial toxicity, this work supports SiQDs as a non-toxic, benign alternative to Cd-based QDs, with the potential to reach comparable luminescent properties. While adding a shell to traditional CdSe QDs appears to be similarly benign, the SiQDs have the additional benefit of being synthesized from an earth-abundant material with more mature recycling infrastructure.[54,55]

2.5 Acknowledgements

This work was supported primarily by the National Science Foundation through the University of Minnesota MRSEC under Award Number DMR-1420013. Part of this work was carried out in the College of Science and Engineering Characterization Facility, University of Minnesota, which has received capital equipment funding from the NSF through the UMN MRSEC program under Award Number DMR-1420013. SKEH acknowledges support through the NSF Graduate Research Fellowship Program under grant NSF GRFP 00039202. NVH acknowledges support through the National Science Foundation Graduate Research Fellowship Program. JNW acknowledges UMN MRSEC REU Site in Nanomaterials supported through the National Science Foundation MRSEC and REU programs under Award Numbers DMR-1263062 & DMR-1420013. EAM acknowledges Lloyd W. Goerke scholarship and the M. Cannon Sneed Memorial award through the UMN Department of Chemistry. The authors would like to thank Fang Zhou for microtoming the biological TEM samples.

Supporting Information

S1. Growth Curve Assay: Bacterial growth rate and replication in presence of SiQDs was assessed through the bacterial growth curve assay. Bacteria were grown in minimal media to an optical density of 0.2 (cell density equivalent to approximately 2 x 10^8 colony forming units/mL) and was diluted in minimal media to achieve half the original cell concentration. The bacterial suspensions were treated with QDs at 50 mg/L, 100 mg/L, or 200 mg/L concentrations. 200 µL of treatment solutions was placed in a 96-well plate, and growth rates and bacterial concentrations were determined by measuring optical density (OD) at 600 nm using a Synergy 2 Multi-Mode Microplate Reader (BioTek, VT). No statistical significance was observed between the growth curves at different SiQD concentration when compared to the negative control.

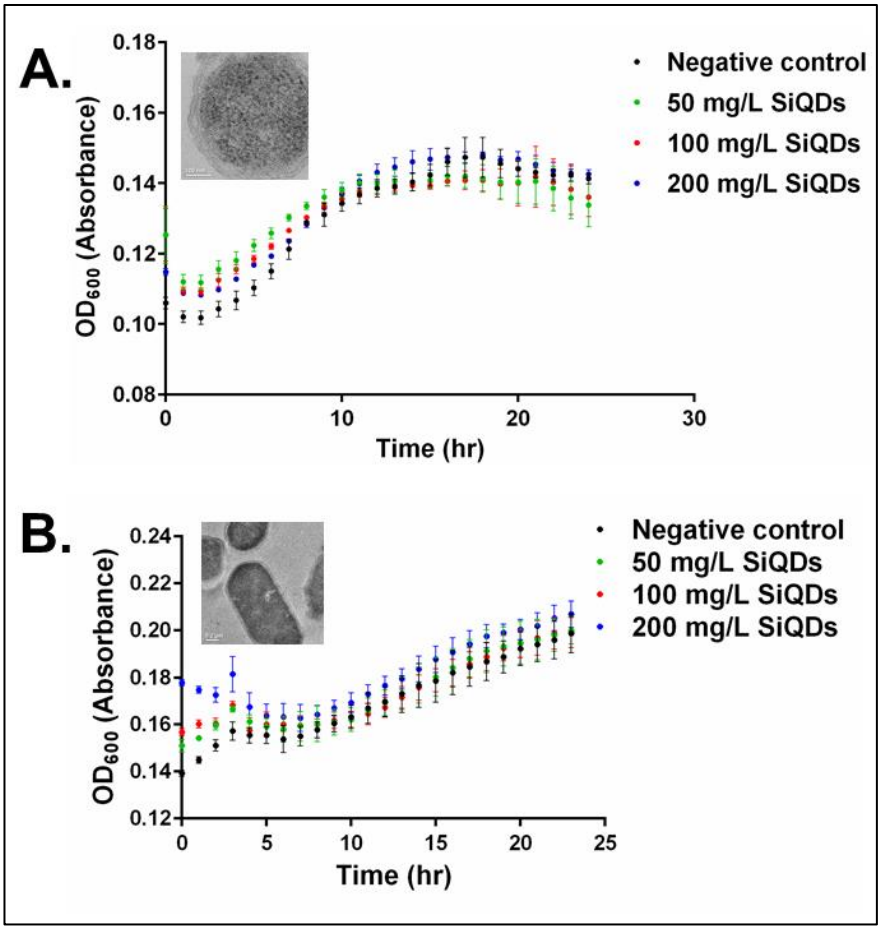

Figure S1: Growth curves of (A) S. oneidensis and (B) B. subtilis in minimal media in the presence of SiQDs.

S2. Physical characterization of Cd-based QDs: Similar to the SiQDs, DLS experiments were performed on both CdSe and CdSe/ZnS QDs to evaluate their hydrodynamic diameters both in water and HEPES buffer (the media used for biological exposures). The measurements were done at QD concentrations of 50 mg/L, 100 mg/L and 200 mg/L to monitor not only the effect of the incubating media, but also QD concentration on aggregate size. Consistent size data was obtained for CdSe QDs, as shown in Figure S2. There was no significant change in aggregate sizes in the two media, at varying QD concentrations.

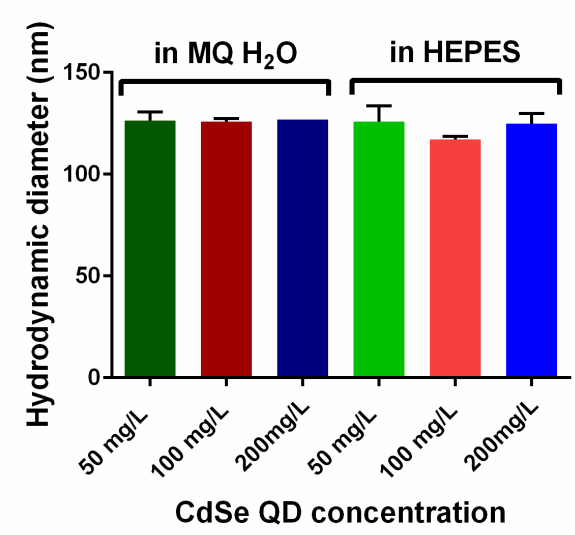

Figure S2: Dynamic light scattering data for CdSe QDs in MQ H_2O and HEPES buffer. No significant difference in hydrodynamic diameter is observed for the two media or among different nanoparticle concentrations.

The DLS data for the CdSe/ZnS QDs fluctuated between replicates, possibly due to interference posed by the fluorescence of the QDs and is not reported here. The zeta potential of the CdSe QDs were measured to be - 66.37 ± 9.2 mV, and that of CdSe/ZnS was measured to be - 90.6 ± 0.5 mV.

S3. Cryogenic TEM of SiQDs on Hydrophilic and Hydrophobic Grids: SiQDs were suspended in ultrapure water at concentration of 3 mg mL^{-1}. The SiQDs were plunge frozen on hydrophobic lacey carbon grids for cryogenic TEM. Images reveal that larger aggregates were present and the ice poorly spread on the grids (Figure S3 A-C). The lacey carbon grids were made hydrophilic through plasma glow discharge. Imaging of samples on these grids revealed more uniform thin vitrified ice, monodispersed particles, and formations of aggregation (Figure S3 D-F). Of note there was also presence of larger, dark contrast, objects on the grids, likely due to ethane contamination or ice crystals (Figure S3 F, yellow box). All images were analyzed with the free NIH ImageJ software. Measurements were made by drawing a line segment across the scale bar and setting the pixel/nm scale. The diameter of the particles was measured by using the oval draw tool to fit an ellipse diameter.

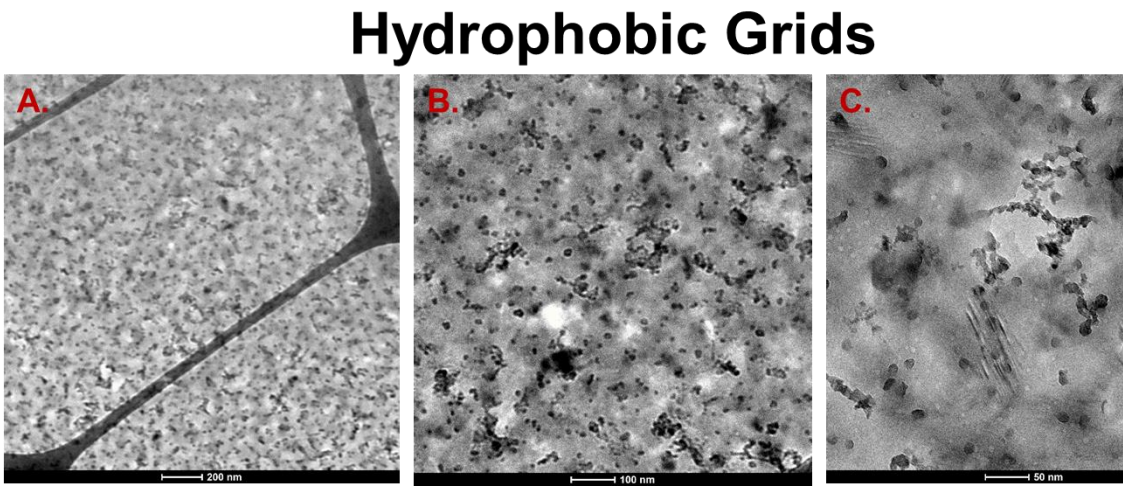

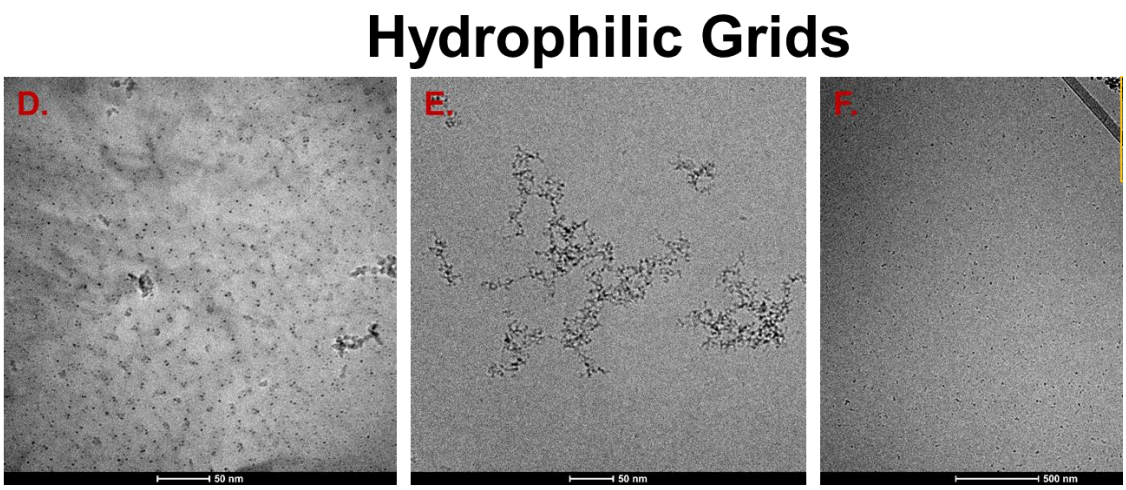

Figure S3: Cryogenic transmission electron micrographs of SiQDs on hydrophobic (top) and hydrophilic grids (bottom). Samples were prepared with a concentration of 3 mg mL^{-1}. A. Dispersion of large particles on the hydrophobic grid. B. Poor ice spreading and possible contamination surrounding particles. C. Representative Thick ice and Crystalline ice. D. Monodispersed SiQDs with average diameter of 3.8 ± 0.04 nm (n=400, mean ± std. error). E. Formation of aggregate particles in vitrified ice. F. Dispersion of larger particles or aggregates with average diameter of 19.2 ± 0.2 nm (n=300, mean ± std. error). Probable ice or ethane contamination indicated by yellow box.

Chapter 3

Adverse Interactions of Luminescent Semiconductor Quantum Dots with Liposomes and a Panel of Bacteria

This work was completed with the assistance of Denise N. Williams, Richard P. Brown, Bo Zhi, Eileen A. McIntire, Natalie V. Hudson-Smith, Prof. Zeev Rosenzweig and Prof. Christy L. Haynes

*co-written with Denise N. Williams

Adapted with permission from Williams et al. *ACS Appl. Nano Mater.* 2018, **1** (9), 4788–4800.

Overview

This paper describes the interactions between luminescent CdSe and ZnSe quantum dots (QD) with phospholipid vesicles (liposomes), which model bacterial membranes, and with *Shewanella oneidensis* MR-1, a Gram-negative bacteria which was previously used to assess the impact of synthetic nanomaterials on the environment. Cadmium-containing luminescent QDs are increasingly used in display, bio-imaging, and energy technologies; however, significant concerns have been raised about their potentially adverse impact on human health and the environment. This study makes use of a broad toolkit of analytical methods to investigate and increase our understanding of the interactions of cadmium-containing and cadmium-free luminescent QDs, with and without a passivating higher bandgap energy ZnS shell, with liposomes and bacterial cells. A unique feature of this study is that all QDs types have the same surface chemistry, being capped with uncharged polyethylene glycol (PEG) ligands. This enables focusing the study on the impact of the QDs core on liposomes and bacterial cells. The study reveals that QDs association with liposome and bacterial cell membranes is imperative, but not sufficient for their adverse impact on liposomes and bacterial cells. The study also shows that cadmium-containing QDs exhibit a higher level of membrane disruption in bacterial cells than cadmium-free QDs. ZnSe QD have low membranal impact, and coating them with a ZnS shell decreases their membrane disruption activity. In contrast, CdSe QDs exhibit a high level of membranal impact, and coating them with a ZnS shell does not decrease, but in fact further increases their membrane disruption activity. This behavior might be attributed to structural irregularities of CdSe/ZnS QDs, which accelerate CdSe/ZnS QDs ion dissolution, and pore formation, and lead to membrane disruption.

3.1 Introduction

In the last two decades luminescent semiconductor quantum dots (QDs) have been incorporated into a broad range of applications including bio-imaging, solar cells, and display technologies.[1-7] Luminescent QDs provide an attractive alternative to organic fluorophores in these applications because of their unique optical properties, including broad absorption peaks with high molar extinction coefficients, size-dependent narrow emission peaks, high emission quantum yield, and high chemical stability and photostability.[8] Historically, cadmium and lead-containing QDs have been widely used because of their excellent photo-physical properties and relatively simple syntheses.[1, 9, 10] However, concerns about the broad use of toxic metal-containing nanomaterials have limited large-scale development and use of QDs technologies, and led to efforts to replace cadmium and lead-containing QDs with alternative non-toxic QDs.[10-12] For example, ZnSe QDs have been explored as a non-toxic alternative to CdS and CdSe QDs.[7, 13, 14] This substitution comes with ease since ZnSe QDs are structurally similar and prepared using the same synthetic methodology as CdSe QDs. This enables replacement of cadmium with zinc in the QD cores while maintaining the same surface chemistry for all four QD types used in our study. It should be noted that other optical nanomaterials, for example InP,[15] graphene,[16] and silicon[17] QDs have been explored as nontoxic alternatives to cadmium-containing QDs in QD-based technologies, as explored in chapters 1 and 2 of this thesis, but variations in their surface chemistry make it difficult to compare their impact on liposomes and cells.[18]

To date, a number of toxicity studies have demonstrated that ZnSe QDs are less toxic than their cadmium-containing counterparts.[12, 19] The adverse effects of cadmium-containing QDs on cells and organisms were attributed to a combination of factors including the association of the QDs with cell membranes, QD ion dissolution, and reactive oxygen species (ROS) generation (particularly when the QDs are irradiated with a UV light); all factors with the capability to negatively impact model membranes and bacterial cells.[12,19] Several studies have found that coating luminescent semiconductor QDs with a higher energy bandgap shell decreases the toxicity of cadmium-containing QDs towards cells and living organisms by inhibiting ROS generation and ion dissolution.[15, 20-22] Other studies revealed that coating cadmium-containing QDs with a passivating shell only delays adverse interactions of luminescent QDs with cells and living organisms.[21, 23-28] Cadmium dissolution is often described as a main contributor to QDs toxicity.[21, 28-30] In contrast, the role of zinc dissolution from commonly used CdSe/ZnS QDs has not been considered as a main contributor to the toxicity of cadmium-containing QDs since the ZnS shell is often assumed to be inert.[25]

Our study describes the interactions between luminescent CdSe and ZnSe QDs with phospholipid vesicles (liposomes), which model the membrane of Gram-negative bacteria, and with *Shewanella oneidensis* MR-1, an environmentally relevant Gram-negative bacterium which is often used as a model organism for bioremediation research due to its metal-reducing capabilities.[31, 32] ZnSe, ZnSe/ZnS, CdSe and CdSe/ZnS QDs were synthesized using nearly identical synthesis methods to insure that the QDs have the same surface chemistry and only differ in their cores. The synthesis, characterization, and

careful control of surface chemistry of luminescent QDs, rather than relying on commercially available QDs with unknown surface content, is imperative to understand their interactions with model membranes and bacterial cells. Our study reveals that cadmium-containing QDs have greater membrane disruption activity than cadmium-free QDs, most likely due to increased membrane association and a higher rate of ion dissolution which destabilizes the liposome and bacterial cell membranes. Surprisingly, coating QDs with a ZnS shell does not always decrease their membrane disruption activity. In CdSe/ZnS QDs, structural irregularities, particularly when the QDs are coated with a thick shell, lead to an increased dissolution rate of the ZnS shell. While zinc ion control measurements reveal that the liposomes are stable in the presence of zinc ions in the sample solutions, it is still possible that the increased rate of zinc ion dissolution adversely impacts the membrane of liposomes and bacterial cells when the CdSe/ZnS QDs dissolve after they associated with the liposome or cell membranes.

3.2 Materials and Methods

3.2.1 Reagents. Zinc stearate (ZnSt), 1-dodecylphosphonic acid (DPA, 95%), zinc formate (98%), and zinc acetate were purchased from Alfa Aesar. 1-Octadecene (ODE), diphenyl phosphine (DPP), sulfur powder, trioctylphosphine (TOP, 97%), tetramethylammonium hydroxide solution (TMAH, 25 wt.% in methanol), tetradecylphosphonic acid (97%), cadmium acetylacetonoate (CdAcAc, 99.9%), sodium chloride, LUDOX TMA colloidal silica (34 wt. % suspension in H_2O), and hexamethyldisilathiane ($(TMS)_2S$, synthesis grade) were purchased from Sigma Aldrich.

Selenium powder (Se, 99.5%), 1-hexadecylamine (HDA, 90%), oleylamine (C_{18} content 80-90%), and sodium hydroxide were purchased from Acros Organic. BD Difco™ Dehydrated Culture Media: LB Broth, Dulbecco's Phosphate-Buffered Saline (without calcium and magnesium), BD Difco™ Dehydrated Culture Media: Granulated Agar, Corning Cellgro DPBS (1X), chloroform, toluene, methanol, HEPES Buffer (1M), and nitric acid (Trace Metal Grade) were purchased from Fisher Scientific. Instrument Calibration Standard 2 (5% HNO_3/ Tr. Tart. Acid/ Tr. HF) for inductively coupled plasma mass spectrometry (ICP-MS) was purchased from Claritas PPT SPEX CertiPrep. DHLA-PEG750-OCH_3 was prepared and purified with slight modifications to a previously reported protocol.[33,34] 1-palmitoyl-2-oleoyl-sn-glycero-3-phosphocholine (POPC), 1-palmitoyl-2-oleoyl-sn-glycero-3-phospho-(1'-rac-glycerol) (sodium salt) (POPG), and 1,2-dioleoyl-sn-glycero-3-phosphoethanolamine-N-(7-nitro-2-1,3-benzoxadiazol-4-yl) (ammonium salt) (NBD-POPE) were purchased from Avanti Polar Lipids, Inc. Calcein disodium salt (calcein) was purchased from Fluka. *Shewanella oneidensis* MR-1 BAA-1096 was purchased from American Type Culture Collection.

3.2.2 ZnSe and ZnSe/ZnS QD Synthesis. ZnSe and ZnSe/ZnS QDs were synthesized according to a previously reported procedure.[14] The reaction was carried out in a 25 ml three-neck round bottom flask under stirring. The zinc precursor solution was prepared in the round bottom flask by dissolving 632 mg (1 mmol) ZnSt powder in 5.0 mL of ODE at 120°C under inert nitrogen gas. The three-neck flask was evacuated out for 30 minutes and then backfilled with nitrogen gas while heating the solution to 280°C. A selenium precursor solution was prepared by dissolving 7.9 mg selenium powder in a solution

containing 17 µl DPP and 670 µL toluene (selenium concentration of 0.15 M). This selenium solution was injected rapidly into the reaction mixture and allowed to react for 5 minutes at 280°C before cooling the flask to room temperature. A second selenium precursor solution was prepared by dissolving 78.9 mg selenium powder in 800 µl TOP (selenium concentration of 1.0 M). This selenium precursor solution was injected into the reaction mixture at room temperature. The reaction mixture was heated and kept at 280°C for 20 minutes, then cooled down to room temperature. The formed ZnSe QDs were immediately coated with a ZnS shell or stored in their reaction mixture at room temperature and away from light. Two precursor solutions were prepared for the ZnS shelling: 1) 32.1 mg sulfur powder in 1 ml TOP (sulfur concentration of 1.0 M), and 2) 632 mg (1.0 mmol) of zinc stearate dissolved in 8 ml ODE. The ZnS shell precursor solutions were injected into the reaction mixture at room temperature. The reaction mixture was then heated, kept at 280 °C for 20 minutes, and finally cooled to room temperature. The resulting ZnSe/ZnS QDs were stored in the reaction mixture at room temperature and away from light. Prior to their immediate future use, QDs were washed multiple times to remove excess reactants.

3.2.3 CdSe and CdSe/ZnS QD Synthesis. CdSe QDs were synthesized according to a previously reported procedure.[35] The reaction was carried out in a 50 ml three-neck round bottom flask under stirring. A cadmium precursor solution was prepared by dissolving 5.0 grams hexadecylamine in a 10 ml TOP solution that also contained 2.1 mmol tetradecylphosphonic acid, and 1.0 mmol of CdAcAc. The solution was heated to 100°C under inert nitrogen gas for the reactants to fully dissolve. The flask was evacuated out

for 30 minutes then backfilled with nitrogen gas. The solution was heated to 250°C, cooled back down to 100°C and vacuumed again for 30 minutes. After backfilling with nitrogen, the vessel was heated to 300°C. A 5 ml selenium precursor solution, which contained 0.84 M selenium powder in TOP, was injected rapidly into the reaction mixture. The CdSe QDs formed instantly and the reaction mixture was cooled to 80°C for overnight annealing. The resulting CdSe QDs were stored in the reaction mixture at room temperature and away from light. CdSe/ZnS QDs were synthesized using successive ionic layer adsorption and reaction (SILAR). SILAR calculation and shelling was carried out following a previously described protocol where 0.3 nm radius monolayers of a ZnS shell are added one at a time.[36] 0.15 μmoles of washed CdSe QDs were added to a solution that contained 6 ml ODE, 4 ml TOP, 6 ml oleylamine, and 10 mg of dodecylphosphonic acid in a 50 ml round bottom flask under nitrogen gas. The solution was heated and kept at 100°C under high vacuum. The flask was backfilled with nitrogen gas. Then, the first aliquot of zinc precursor (0.05 M zinc formate in oleylamine), which was calculated from the core size to add a 0.3 nm radius monolayer of a ZnS shell, was injected over 15 minutes. The reaction mixture was heated and kept at 160°C, and an aliquot of sulfur precursor (0.25 M $(TMS)_2S$ in TOP) was injected over 15 minutes to form the first monolayer of ZnS shell. The QD were then annealed at 160°C for 20 minutes. The reaction mixture was heated and kept at 170°C while the process of adding zinc and sulfur precursors over 15 minutes and annealing over 20 minutes was repeated. The shelling process was repeated, each time at 10°C higher temperature until the desired ZnS shell thickness was realized. Finally, the reaction mixture was heated and kept at 200°C, and

0.5 ml oleic acid was added dropwise over one hour. The reaction mixture was then allowed to slowly cool to room temperature.

3.2.4 Capping Luminescent QD with DHLA-PEG750-OCH_3 Ligands. Luminescent QDs were capped with DHLA-PEG750-OCH_3 ligands (MW= 927 g/mol) to enable their aqueous solution miscibility. The ligand exchange process used to prepare the DHLA-PEG750-OCH_3-coated QDs removed some TOPO ligands from the QD surface and shield the remaining ones from interacting with liposome membranes and bacterial cells.[37] This is an imperative step to minimize the ligand contribution to QD toxicity since TOPO ligands have been shown to be highly toxic.[38] The ligand exchange was carried out by following a previously reported procedure.[39] The DHLA ligand (0.25 mmol), 0.5 mmol sodium hydroxide, 0.13 mmol zinc acetate, and 1 mL of methanol were sonicated together in a septum-closed vial filled under nitrogen gas. 10 nmol of purified QDs were dissolved with a minimal amount of chloroform, dried under vacuum, and put under a flow of nitrogen. The DHLA ligand solution was added to the QD solution, and then left overnight at 50 °C under nitrogen gas. The next day 1 mL of ethyl acetate and enough hexane to separate solvents into two distinct layers were added to the QDs, stirred, and allowed to separate. The hexane layer was removed to waste. The QDs in the ethyl acetate layer were dried under vacuum, and then dispersed in Millipore water. The QD solution was passed through a 0.45 SFCA syringe filter into a 30,000 MWCO spin filtration device for washing using three centrifugation cycles at 2000xg for 5 minutes at room temperature.

3.2.5 Absorbance and Fluorescence Instrumentation. UV-Vis extinction spectra were obtained using a Thermo Scientific Evolution 201 UV-Vis spectrophotometer. Fluorescence spectroscopy measurements were carried out using a PTI-Horiba QuantaMaster 400 fluorimeter, equipped with an integration sphere for emission quantum yield measurements, and with a PicoMaster TCSPC detector for fluorescence lifetime measurements. A Molecular Devices SpectraMax M5 Microplate reader was used to observe of changes in fluorescence emission over time.

3.2.6 Preparation of Calcein-Containing Liposomes. 10:1 molar POPC: POPG liposomes filled with calcein dye were prepared via a dehydration/rehydration method.[40] In a 500 mL round bottom flask, 2 mL of 25 mg/mL POPC and 0.50 mL of 10 mg/mL POPG in chloroform were stirred together under nitrogen gas to create a dry phospholipid film. The flask was further evacuated overnight to remove all organic solvent. A 5 mL stock solution containing 5 mM calcein disodium salt in 2 mM HEPES and 25 mM sodium chloride at pH 7.4 was prepared. 3 mL of the calcein solution was added to the dried lipids. The flask was immersed in dry ice-acetone bath until the solid film began to dissociate from the bottom of the flask. The flask was then placed in a water bath at room temperature to form the liposomes. This process was repeated ten times to ensure dye encapsulation in the liposomes. 1 mL of the liposome solution was extruded 15 times through an Avanti Polar Lipids 50 nm pore mini extruder with a polycarbonate membrane. The liposome sample was then run through a Sepharose CL-4B silica column (10 mm x 100 mm) with free HEPES buffer to remove free fluorophore molecules from the dye-containing liposomes.

3.2.7 Calcein-Containing Liposomes Lysis Assays. Liposome lysis analysis used the time-based function of the PTI-Horiba QuantaMaster 400 fluorimeter. The excitation wavelength was set to 480 nm, the absorbance maximum of the dye. The emission of calcein was observed at 515 nm, until the fluorescence intensity stabilized typically after 15 minutes. The emission of leaked calcein after interactions with each test sample was observed for 20 minutes total, with stirring, at these parameters: 1-2 minutes to determine background fluorescence of liposomes, 15 minutes for substrate to interact with liposomes, 2-3 minutes for maximum liposome lysis to be determined after a 40 µL injection of 1% Triton X-100 in Millipore water.

3.2.8 Preparation of Dye-Free Liposomes. 10:1 molar POPC: POPG dye-free liposomes were prepared via the same methods, with the exception that lipids dried overnight were hydrated with 3mL of 2 mM HEPES and 25 mM sodium chloride solution, followed by dehydration/rehydration and extrusion.

3.2.9 Preparation of NBD-labeled Liposomes. 10:1:0.1 molar POPC: POPG:NBD-POPE liposomes were prepared for a ~1% mol ratio of labeled to unlabeled lipids.[41] In a 250 ml round bottom flask, 400 µL of 25 mg/mL POPC, 100 µL of 10 mg/mL POPG, and 100 µL of 10 mg/mL NBD-POPE in chloroform were stirred together under nitrogen gas to create a dry phospholipid film. The flask was further evacuated overnight to remove all organic solvent. The next day, 7.5mL of 2 mM HEPES and 25 mM sodium chloride at pH 7.4 was used to hydrate the lipids to a 2mM lipid concentration. The flask was taken

through ten freeze/thaw cycles. Finally, 1 mL at a time, the liposome solution was extruded 15 times through an Avanti Polar Lipids 50 nm pore mini extruder with a polycarbonate membrane.

3.2.10 NBD-labeled Liposomes Fluorescence Lifetime Assays. NBD-labeled liposome steady state fluorescence was observed from 495-650nm, with the excitation wavelength set to 470 nm. The fluorescence lifetime of the dye was observed at 515 nm.[42] Steady state and emission readings were conducted of the NBD-labeled liposomes alone, immediately after the addition of 0.5nM QDs, 4 hours after the addition, and 8 hours after the addition. Only data for 4 hours after the addition of QDs is shown.

3.2.11 Bacterial Culture and Colony Counting when Exposed to QD. *Shewanella oneidensis* MR-1 bacteria were cultured by streaking an LB-agar plate with bacteria and then incubating the plate in a 30 °C incubator overnight. Liquid cultures were grown by transferring colony inoculants from the plate to 10 mL of LB broth and incubating for 4 hours at 30 °C in an orbital shaker, to their mid-log phase. Cells were then harvested by centrifugation for 10 minutes at 2000xg, washed in Dulbecco's phosphate-buffered saline (D-PBS) buffer, and suspended in a HEPES buffer (2 mM HEPES and 25 mM NaCl, at pH 7.4). The cultures were then diluted to 0.2 OD at 600 nm (OD600) to achieve a cell density of approximately 2 x 10^8 colony-forming units (CFUs) /mL. Serial 10-fold dilutions of this bacterial suspension were performed to achieve a cell concentration of 10^4 CFUs/mL in HEPES buffer. The resultant diluted bacteria suspension was treated with QDs, in a total volume of 150 µL, at varying concentrations. The QD-exposed cells were

incubated on rotary shaker for 15 minutes, and then the viability of *Shewanella oneidensis* MR-1 bacteria was determined using a drop-plate colony-counting protocol.[43] Six 10 µL droplets of the exposed bacterial suspensions and untreated negative controls were dropped on an LB-agar plate, which were pre-sterilized under UV-illumination for 20 minutes. The droplets were dried under air flow in a biological cabinet, and then incubated at 30°C for 20 hours before colonies were counted using a Bantex Colony Counter 920A.

3.2.12 Inductive Couple Plasma Mass Spectrometry (ICP-MS) of QD, QD Ion Dissolution, and QD Association with Bacteria. Inductive coupled plasma mass spectrometry (ICP-MS) measurements of QDs, bacterial, and QD-bacterial samples were carried out using a PerkinElmer NexION 300D single quad mass spectrometer. The Instrument Calibration Standard 2 was used daily to prepare calibration curves from 0.1 ppb to 1 ppm for the different ion analytes (cadmium, selenium, zinc) possibly generated from the QDs.

Sample preparation for ICP-MS analysis was as follows. For QDs in organic samples, QD sample at predetermined concentration in chloroform was put into a scintillation vial and centrifuged with acetone to precipitate out the QDs. The QDs were allowed to dry, nitric acid was added to dissolve the sample, then Millipore water was added to QD-nitric mixture to dilute nitric acid concentration to 2% by volume. For QDs in aqueous solution, QD samples of predetermined concentrations were dissolved by adding nitric acid to the solution. The solution was kept at room temperature overnight. Millipore water was added to the QD-nitric acid mixtures to dilute the nitric acid concentration to 2% by volume and

a total sample volume of at least 5 mL. For investigation of QD dissolution, known concentrations of QD solution were centrifuged through 30,000 MWCO spin filtration devices at 2000xg and the supernatant analyzed for ion content. The level of association of QDs with *Shewanella oneidensis* determined using ICP-MS measurements was prepped as follows: *Shewanella oneidensis* bacterial cells were cultured in Luria-Bertani (LB) broth overnight. The resulting bacterial suspension was centrifuged for 10 min at 2000xg, washed in Dulbecco's phosphate-buffered saline (D-PBS) buffer, suspended in a HEPES buffer (2 mM HEPES and 25 mM NaCl, at pH 7.4) and the OD was adjusted to 0.8 at 600 nm (OD600). The diluted bacterial suspension was treated with CdSe and CdSe/ZnS QDs at concentrations equivalent to Cd core concentrations of 0.5 mg/L, 1 mg/L and 2mg/L. Similarly, the treatment concentrations used for the ZnSe and ZnSe/ZnS QDs were equivalent to Zn core concentrations of 1mg/L, 2mg/L and 5 mg/L. After an exposure time of 15 mins for the bacteria and QDs, the cells were harvested as pellets by centrifugation at 2000xg for 10 min. At this low speed of centrifugation only bacterial cells are expected to settle down along with any associated QDs, and any free QDs in the supernatant was discarded. These QD-treated bacterial cell pellets were used to perform ICP-MS experiments to assess the presence of Cd or Zn, to confirm any QD association with bacterial cells.

3.2.13 Hyperspectral Imaging of CdSe and CdSe/ZnS QD and Bacteria. Images of *Shewanella oneidensis* MR-1 bacteria following incubation with CdSe or CdSe/ZnS QDs were acquired using high S/N ratio, dark-field Cytoviva® hyperspectral imaging (HSI) (Cytoviva®, Auburn, AL). In these experiments, sample solutions were drop-cast (~3-4

μL) onto a glass slide, which was then sealed with a cover slip and clear nail polish. Slides were examined at 100X magnification with an oil immersion lens under an Olympus BX-41 microscope. Spectral data were acquired with a Cytoviva® spectrophotometer and integrated CCD camera in both the visible and near-infrared range (400-1000 nm). Analysis of the HSI spectra was performed by the Environment for Visualization software (ENVI 4.4 version). Spectral libraries of CdSe and CdSe/ZnS QDs and *Shewanella oneidensis* MR-1 bacteria were used to help analyze HSI spectral angle mapper (SAM) spectral patterns and characterize association of the QDs with the bacterial cells.

3.2.14 High Resolution Transmission Electron Microscopy of QD. High resolution transmission electron microscopy (HR-TEM) images of QDs were obtained using a Titan 80-300 S/TEM, operating at 300 kV with a Gatan OneView imaging camera. QD samples were drop coated onto mesh copper grids with ultrathin carbon film on holey carbon support film (Ted Pella, Inc.) Grids were then placed in vacuum oven overnight before analysis.

3.2.15 Biological Transmission Electron Microscopy of Bacteria Incubated with QD. Biological transmission electron microscopy (BioTEM) images of bacteria exposed to QDs were obtained using a FEI Tecnai T12 TEM after the following preparation. *Shewanella oneidensis* bacteria were cultured in LB broth overnight. The next day, bacteria were washed with DPBS buffer, diluted to an OD of 0.8 (OD600) in HEPES, then exposed to 1 mg/L of CdSe/ZnS QDs for 15 minutes. This bacterial suspension was centrifuged down to a pellet, washed thrice with 0.1 M cacodylate buffer solution, then

resuspended in a fixation buffer of 2.5% glutaraldehyde in 0.1 M sodium cacodylate buffer and fixed for 50 minutes. The fixed bacterial cells were then centrifuged, washed with sodium cacodylate buffer, and dehydrated stepwise with increasing concentration of ethanol (30, 50, 70, 80, 90, 95, and 100% ethanol in water). After the ethanol rinsing steps, the pellet was washed with propylene oxide three times. The resin infiltration steps were performed in the following manner. The pellet was soaked first in a 2:1 propylene oxide: epoxy resin mixture for 2 h, and then in a 1:1 propylene oxide: epoxy resin mixture overnight. Next day, the 1:1 propylene oxide: epoxy resin mixture was removed and replaced with a fresh batch of 1:1 propylene oxide: epoxy resin mixture for 5 h, and finally incubated in a pure resin mixture and infiltrated overnight. The resin sample was then cured in a 40 °C oven for one day and then 60 °C oven for two days. A Leica UC6 microtome and Diatome diamond knife was used to make ultrathin sections (65 nm) of this resin-embedded bacterial sample, and uranyl acetate and lead citrate was used to stain them. These sections were placed on copper TEM grids (Ted Pella Inc.), and imaging was done.

3.3 Results and Discussion

3.3.1 Characterization of Cadmium-Containing and Cadmium-Free QDs. Cadmium-containing CdSe and cadmium-free ZnSe QD were synthesized by the commonly used "hot injection" method.[14, 35] The CdSe and ZnSe QD were coated with a ZnS shell following previously reported procedures.[14, 36] UV-Vis extinction and emission spectra of

CdSe and CdSe/ZnS QD are shown in Figure 1A. The UV-Vis extinction spectra show excitation peaks at 505 nm for CdSe QD, and a red-shifted excitation peak at 552 nm for CdSe/ZnS QD. The emission spectra show corresponding emission peaks at 522 nm for CdSe QD and 580 nm for CdSe/ZnS QD. The emission quantum yields of CdSe and CdSe/ZnS QD were measured to be 13% and 43%, respectively. The full peak width at half maximum (FWHM) of CdSe and CdSe/ZnS QD were 27 and 34 nm, respectively. The UV-Vis extinction and emission spectra for ZnSe and ZnSe/ZnS QD are shown in Figure 1B. The UV-Vis extinction spectra show excitation peaks at 410 and 418 nm for ZnSe and ZnSe/ZnS QD, respectively. The emission spectra show corresponding emission peaks at 418 for ZnSe QD and 423 nm for ZnSe/ZnS QD. The emission quantum yields of the ZnSe QD and ZnSe/ZnS QD were 5% and 10%, respectively. The FWHM of the ZnSe QD and ZnSe/ZnS QD were 17 and 15 nm, respectively. Time-resolved photoluminescence measurements were also carried out to determine the impact of the ZnS shell on the cadmium-containing and cadmium-free QD (see supporting information for details). The fluorescence lifetime of CdSe QD was 29.6 ± 0.4 nsec. It decreased to 16.9 ± 1.0 nsec when the CdSe QD were coated with a ZnS shell to form CdSe/ZnS QD. The fluorescence lifetime of ZnSe QD was 7.4 ± 0.3 nsec. It decreased to 6.4 ± 0.1 nsec when the ZnSe QD were coated with a ZnS shell to form ZnSe/ZnS QD. This decrease in fluorescence lifetime when core QD are passivated with a higher energy bandgap ZnS shell is attributed to increased confinement of the excited electrons in the core QD and is consistent with previous studies.[44] The distinct excitonic peaks in the UV-Vis spectra, the narrow and symmetric emission peaks, and the increase in emission quantum yield with a corresponding decrease in fluorescence lifetime when the QD are passivated with a higher

energy bandgap shell suggest that both the cadmium-containing CdSe and CdSe/ZnS QD, and the cadmium-free ZnSe and ZnSe/ZnS QD are of high quality, and display the photo-physical properties required in luminescent QD-based applications.

A ligand exchange reaction was carried out to replace the organic capping ligands of the QD with uncharged DHLA-PEG750-OCH_3 ligands (Scheme 1). This allowed the QD to be dispersed in aqueous media and made them suitable for the liposome lysis and bacterial viability assays. More importantly, the use of the same capping ligand in all four QD types enabled direct comparison between the membrane disruption activity of cadmium-containing and cadmium-free QD.

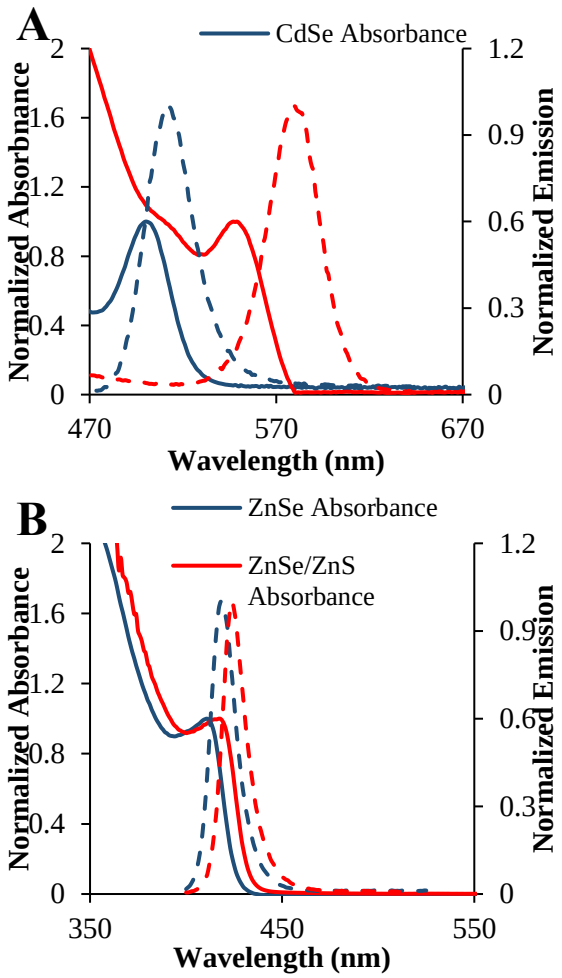

Figure 1. Normalized absorbance and emission spectra of CdSe and CdSe/ZnS QD (λ_{ex} = 375 nm) (A), and ZnSe and ZnSe/ZnS QD (λ_{ex} = 350 nm) (B).

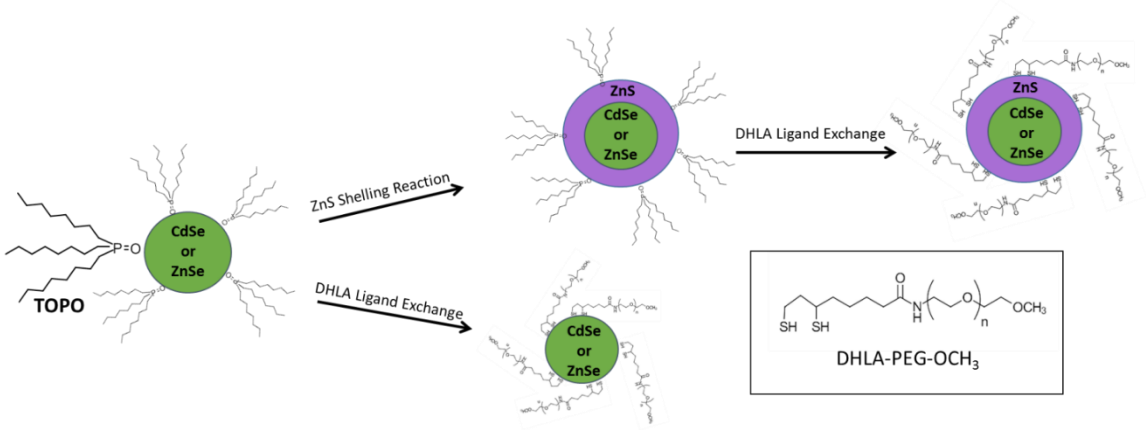

Scheme 1. Schematic of ZnSe and CdSe QD shelling to form ZnSe/ZnS and CdSe/ZnS QD, and their ligand exchange to enable QD dispersity in aqueous solution by replacing hydrophobic TOPO with DHLA-PEG amphiphilic ligands

3.3.2 Interactions of CdSe and ZnSe QD with Liposomes - Liposome lysis assays were carried out to determine the membrane disruption activity of cadmium-containing CdSe and CdSe/ZnS QD, and cadmium-free ZnSe and ZnSe/ZnS QD. Unlike bacteria or other living organisms, liposomes do not possess active mechanisms to degrade QD. Therefore, differences in the interactions between QD and liposomes membranes could only be attributed to differences in association of the QD with the liposome membrane due to differences in QD size, shape, and surface chemistry, and to differences in ion dissolution and reactive oxygen species (ROS) generation that could affect ion interactions with the liposome membrane. It should be noted that the rates of ROS generation are negligible in our experiments, which are conducted under room light conditions in the absence of

intentional QD excitation. Liposomes, with a phospholipid composition that models cell membranes of Gram-negative bacteria, were loaded with 10 mM calcein. Calcein was chosen as the fluorophore for the liposome lysis assays primarily because of its high encapsulation efficiency, and the high anti-leaking stability of calcein-containing liposomes in aqueous solutions.[45] Loading the liposomes with 10 mM calcein resulted in self quenching of the fluorescent calcein molecules. The calcein-containing liposomes were exposed to increasing concentrations of cadmium-containing and cadmium-free QD up to 0.5 mg/mL selenium ion equivalents. The fluorescence of the calcein-containing liposomes was continuously measured at 515 nm (λ_{ex} = 480 nm) during the liposome lysis assays. Membrane disruption of the liposomes led to the release and dilution of calcein in the sample solutions, which in turn led to an increase in calcein fluorescence. The QD were selected to have minimal excitation at 470 nm and minimal fluorescence at 515 nm to minimize spectral overlap with calcein absorption and fluorescence.

Figure 2 describes the liposome lysis efficiency of the cadmium-containing and cadmium-free QD. Figure 2A and shows the temporal dependence of calcein fluorescence (normalized) of the calcein-containing liposomes prior to QD exposure (background fluorescence), following the exposure of the liposomes to CdSe QD (black) and CdSe/ZnS QD (red) which contain 0.5 mg/L selenium ion equivalents in their core, and following the addition of 1% Triton solution to disrupt and release all the calcein molecules from the liposomes. The blue curve follows the fluorescence of calcein-free liposomes when CdSe/ZnS QD with 0.5 mg/L selenium ion equivalents in their core were added to the solution. The slight increase in fluorescence due to direct excitation of the CdSe/ZnS QD

at 470 nm (an unfavorable excitation wavelength) represents the highest level of optical interference in our QD exposure experiments. The level of optical interference is significantly lower when CdSe QD within the same concentration range are added to the calcein-free liposome solutions. The contribution of QD emission due to direct excitation was therefore neglected based on these control measurements. Figure 2A and 2B show that all QD types have membrane disruption activity. Figure 2A shows that CdSe/ZnS QD cause higher liposome lysis compared to non- shelled CdSe QD, which might be attributed to shell instability. In contrast, Figure 2B shows that ZnSe/ZnS QD cause less liposome lysis than non-shelled ZnSe QD, indicating a significantly higher ZnS shell stability on ZnSe QD relative to CdSe QD.

The percent liposome lysis efficiency of CdSe and CdSe/ZnS QD (Figure 2C) and ZnSe and ZnSe/ZnS QD (Figure 2D) was calculated based on the following expression:

$$\% \text{ Lysis} = [(I_{eq} - I_b) / (I_{tri} - I_b)] \times 100 \qquad [1]$$

where I_{eq} is the fluorescence intensity of the liposomes when reaching equilibrium following the exposure of the calcein-containing liposomes to QD; I_b is the background fluorescence of the calcein-containing liposomes prior to QD exposure; and I_{tri} is the fluorescence intensity of the liposome sample following complete disruption and release of calcein molecules due to the exposure of the calcein-containing liposomes to the 1% Triton solution. Figure 2C and 2D show the concentration dependence of the liposome lysis efficiency when the calcein-containing liposomes were exposed to increasing

concentrations of CdSe QD and CdSe/ZnS QD (Figure 2C), and ZnSe and ZnSe/ZnS QD (Figure 2D). The membrane disruption activity is concentration-dependent for all QD types. Cadmium-containing CdSe and CdSe/ZnS QD exhibit higher levels of membrane disruption activity than cadmium-free ZnSe and ZnSe/ZnS QD. For example, exposure of the calcein-containing liposomes to CdSe and CdSe/ZnS QD with 0.5 mg/L selenium ion equivalents in their core resulted in 38 ± 1% and 42 ± 1% liposome lysis efficiency. In contrast, exposure of the calcein-containing liposomes to ZnSe and ZnSe/ZnS QD at 10-fold higher selenium ion equivalents in their cores resulted in 15 ± 4%, and 10 ± 1% liposome lysis efficiency, respectively. Coating ZnSe QD with a ZnS shell decreased their membrane disruption activity almost to the level of liposome lysis observed when the calcein-containing liposomes were exposed to the DHLA-PEG ligands at ppb levels (the levels anticipated if all ligand molecules would be desorbed from the QD surface). In contrast, coating CdSe QD with a ZnS shell slightly increased, rather than decreased, their membrane disruption activity. The differences in lysis efficiency between CdSe and ZnSe QD, and the opposite effect of coating them with a ZnS shell on their membrane disruption activity was unexpected since the synthesis methods used to prepare the CdSe and ZnSe QD and their surface chemistry were nearly identical. The source of this unexpected result is explored in the following paragraphs.

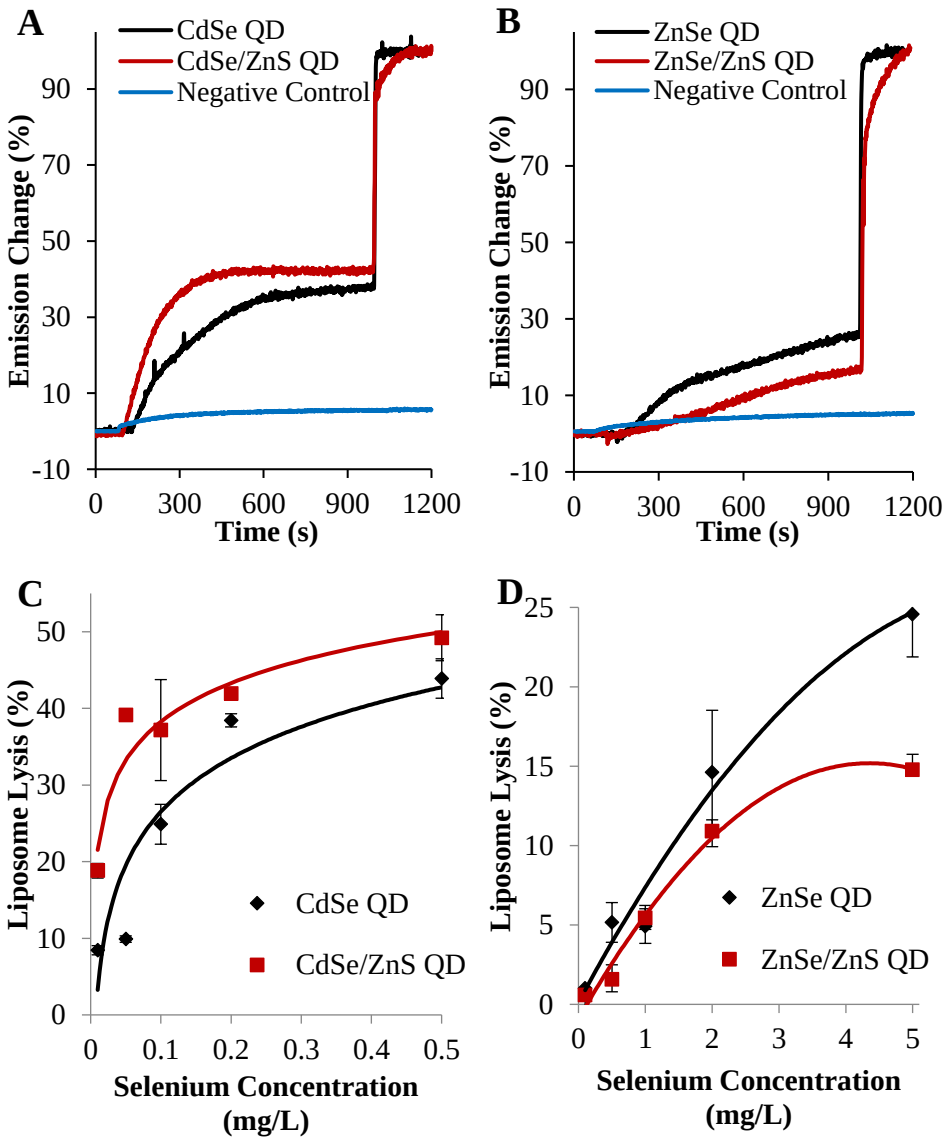

Figure 2. Normalized emission traces comparing the membrane disruption activity of CdSe and CdSe/ZnS QD (A), and ZnSe and ZnSe/ZnS QD (B). The negative control (blue) curves follow the exposure of calcein-free liposomes to CdSe/ZnS QD (A) and ZnSe/ZnS QD (B). The concentration dependence of the liposome lysis efficiency is shown in Figure 2C for CdSe (black) and CdSe/ZnS (red) QD, and in Figure 2D for ZnSe (black) and ZnSe/ZnS (red) QD. Each liposome lysis value is the average of three

replicate measurements (N=3). The error bars are ± standard deviation from the mean value.

3.3.3 Liposomes Lysis Assays of CdSe/ZnS QD with Varying Shell Thickness - Having observed an increase in membrane disruption activity when CdSe QD are coated with a ZnS shell, we investigated how the shell thickness affects the liposome lysis efficiency of CdSe/ZnS QD. Transmission electron microscopy (TEM) measurements were used to confirm an increase in QD size when CdSe QD were coated with a ZnS shell of increasing thickness (see supportive information for details). Figure 3A shows the temporal dependence of the fluorescence of calcein-containing liposomes prior to QD exposure (background fluorescence), following the exposure to CdSe QD (black), and CdSe/ZnS QD with a shell thickness of one monolayer (green), three monolayers (red), and six monolayers (blue). All experiments were conducted with CdSe and CdSe/ZnS QD that contained 0.5 mg/L in their core as was determined by ICP-MS. Control experiments involving the addition of CdSe and CdSe/ZnS QD of the same concentration to liposome-free and calcein-free liposome solutions showed an instant but negligible increase in QD fluorescence under our illumination conditions (λ_{ex} = 480 nm, λ_{em} = 515 nm). The negligible contribution of QD fluorescence is expected since QD concentrations in our liposome lysis experiments are three orders of magnitude lower than the concentration of calcein in the liposome solution following liposome lysis. The liposome lysis efficiencies were calculated from the curves in Figure 3A using equation 1 (see above) as 44 ± 3% for CdSe QD (no shell), 42 ± 1% for CdSe/ZnS QD with one monolayer, 49 ± 3% for CdSe/ZnS QD with three monolayers, and 70 ± 1% CdSe/ZnS QD with six monolayers

ZnS shell thickness. A slower membrane disruption efficiency is observed when the liposomes are exposed to CdSe/ZnS QD with one monolayer shell, a shell thickness that seems to delay but not to prevent the liposome lysis. Further increase in shell thickness results in increasing liposome lysis efficiency, most significantly when the CdSe QD are coated with a thick six-monolayer ZnS shell.

ICP-MS measurements of cadmium, zinc, and selenium ions were used to determine the chemical stability of ZnSe QD, ZnSe/ZnS QD, CdSe QD, and CdSe/ZnS QD with varying shell thickness and concentration. Figure 3B describes the results of ICP-MS measurements used to determine the level of ion dissolution from CdSe and CdSe/ZnS QD with varying ZnS shell thickness between one and six monolayers at increasing concentrations from 0 to 0.5 mg/L selenium ion equivalents in QD which were added to a HEPES buffer at pH 7.4. The QD were incubated in HEPES buffer at room temperature for various time intervals ranging from 15 minutes to 24 hours. The QD were then filtered out by passing the QD solution through a 30K MWCO filter under slow speed centrifugation of 2000xg at room temperature. The levels of cadmium and selenium in the supernatant for all QD were negligible. In contrast, CdSe/ZnS QD exhibited significant zinc ion dissolution over 24 hours, which increased with CdSe/ZnS QD concentration and ZnS shell thickness. It should be noted that it is difficult to quantify the amount of released zinc ions from the QD due to high native levels of zinc in aqueous samples and glassware.[46] Nevertheless, the QD concentration dependence and ZnS shell thickness dependence of zinc ions levels in the samples strongly suggest a significant level of zinc ion dissolution, in the mg/L range, from the CdSe/ZnS QD within the time scale of our

liposome lysis assays. It is therefore fair to conclude that zinc ion dissolution increases the adverse impact of CdSe/ZnS QD on the liposome membranes beyond their impact due membrane association and disruption. It is important to note that the luminescence properties of the CdSe/ZnS QD, including emission quantum yield and peak width, do not change during the 15-minute long incubation and liposome lysis assays, which were conducted in HEPES buffer at pH 7.4 and room temperature as well. This is consistent with previous studies in our laboratory, which showed that a single monolayer of ZnS shell is sufficient to realize ~90% enhancement in luminescence properties of CdSe/ZnS QD, and the value of additional ZnS shell layers is more in delaying the degradation of the core CdSe QD.[44] It is interesting to note that ZnSe/ZnS QD exhibited significantly higher shell stability, and the levels of zinc ions in the supernatants of incubated ZnSe/ZnS QD were negligible (not shown). This was observed even though CdSe and ZnSe QD were coated with the same ZnS shell using nearly identical shelling conditions. The increased ZnS shell stability on ZnSe QD is attributed to a greater crystal plane matching in ZnSe/ZnS than in CdSe/ZnS QD.

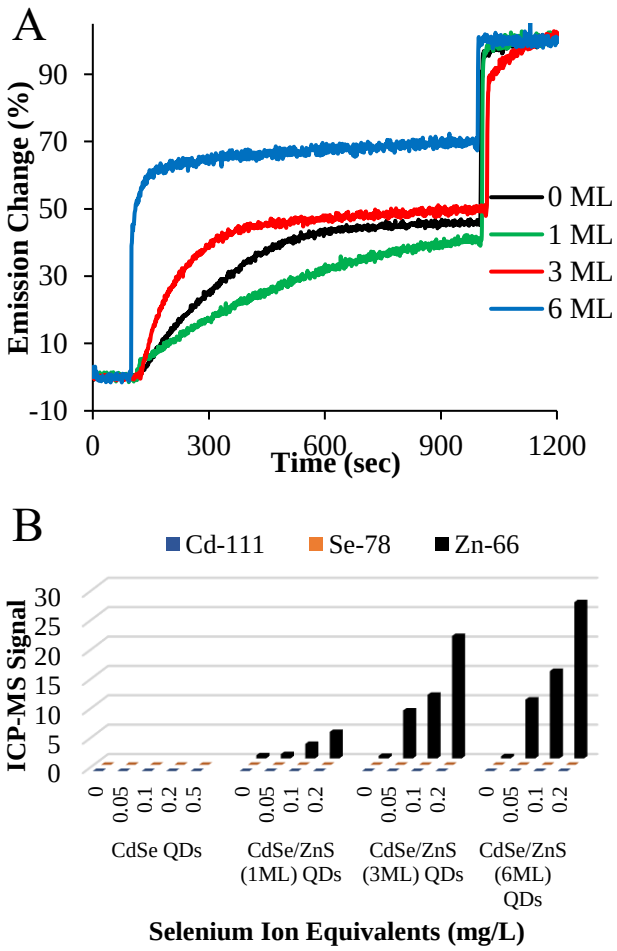

Figure 3. Normalized emission traces from calcein-filled liposomes when exposed to CdSe QD with 0 to 6 monolayers (ML) (A). ICP-MS signal intensities of zinc, cadmium, and selenium ions resulting from the dissolution of CdSe QD and CdSe/ZnS QD with one, three and six monolayers shell in HEPES buffer at pH 7.4 (2B). Only zinc ion dissolution is observed indicating degradation of the ZnS shell. N=3 for each condition, and error bars are omitted for clarity.

3.3.4 Association of QD with Liposomes as a Key Contributor to Liposome Membrane Disruption - The ICP-MS results described above showed negligible cadmium and selenium ion dissolution from CdSe QD during 15-minute long incubation in liposome-free and liposome- containing HEPES buffer solutions at pH 7.4. In addition, ion control experiments revealed a lack of lysis activity when liposomes were incubated for 15 minutes with QD supernatants (no QD in the incubation mixture), and in cadmium and selenium ion solutions at concentrations resulting from total dissolution of CdSe with 0.5 mg/L in their cores. And yet, a measurable difference between the membrane disruption activity of CdSe and ZnSe QD was observed. Based on these results, we hypothesized that QD association with the liposome membranes play a major role in the membrane disruption activity of QD. Association between the QD and the liposome membrane exposes the liposome membranes to residual surfactant molecules, in our system TOPO molecules, and significantly increases the local concentration of dissolved ions when the QD degrade. To validate this hypothesis, we prepared NBD-labeled liposomes and investigated their interactions with CdSe and ZnSe QD. NBD is an environmentally sensitive dye. In the literature, a fluorescence increase and a fluorescence lifetime decrease were reported with decreasing polarity of the NBD environment.[42] In contrast, a fluorescence decrease was reported when NBD molecules react with ROS .[41] Fluorescence spectra of NBD prior to and following exposure of NBD liposomes to CdSe and ZnSe QD are shown in Figures 4A and 4B. The fluorescence spectra of NBD liposomes (λ_{ex} = 470nm and $\lambda_{em\ max}$ = 515nm) prior to and following QD exposure are shown in black and red, respectively. The residual fluorescence spectra of CdSe and ZnSe QD at this unfavorable excitation wavelength are shown in blue. A 6-fold increase in the

fluorescence intensity of the NBD liposomes is observed following their exposure to CdSe (Figure 4A) and ZnSe (Figure 4B) QD. This is attributed to decreased polarity of the NBD environment due to the associating of the PEG-coated QD with the liposome membranes, which effectively shield the NBD headgroup from water molecules and ions in the buffer solution. The lack of fluorescence decrease following the incubation of QD with the liposomes strongly suggests that ROS are not formed and therefore not a significant contributor to membrane disruption under our experimental conditions (short exposure, no UV irradiation). Fluorescence lifetime measurements shown in Figure 4C for CdSe and 4D for ZnSe QD provide additional indication that the QD associate with the liposome membranes. Table 1 summarizes the fluorescence lifetime and the exponential terms used to fit the fluorescence lifetime decay curves of NBD liposomes prior and following a 4-hour long exposure to CdSe and ZnSe QD. A decrease in the fluorescence lifetime from 5.87 ± 0.23 nsec to 5.17 ± 0.03 nsec and to 5.23 ± 0.03 nsec when the NBD liposomes are incubated for 4 hours with CdSe and ZnSe QD, respectively, is observed. Additionally, the fluorescence lifetime decay curve of NBD liposomes prior to QD exposure, is described by two exponential terms with $\tau_1 = 2.81$ nsec and $\tau_2 = 9.58$ nsec with almost equal weights of ~55 and 45%. These two terms are attributed to the NBD heterogeneous environment, which is equally affected by the hydrophobic backbone of the liposome membrane and the outer aqueous environment of the liposomes. A significantly increased mono-exponential character is observed when the PEG-coated QD interact with the liposome membrane. The fluorescence lifetime decay curves (red) are still described by two exponential terms, for CdSe QD $\tau_1 = 3.78$ nsec and $\tau_2 = 9.24$ nsec and for ZnSe QD $\tau_1 = 3.84$ nsec and $\tau_2 = 9.43$ nsec, but their weights change to ~72 and 28% in both QD

types. The decrease in fluorescence lifetime and the increase in mono-exponential character of the fluorescence lifetime decay curves are consistent with a decrease in the polarity of the NBD environment, which is attributed to association of the PEG-coated QD to the NBD liposomes. As expected, the change in NBD fluorescence and fluorescence lifetime does not depend on the QD core composition. It only depends on the surface chemistry of the QD, which is nearly identical for CdSe and ZnSe QD as both QD types undergo a ligand exchange process to replace TOPO with DHLA-PEG molecules to enable aqueous miscibility of the QD. Association of the QD with the liposome membranes is critical to their membrane disruption activity, which depends on their dissolution rate following their association with the liposome membranes.

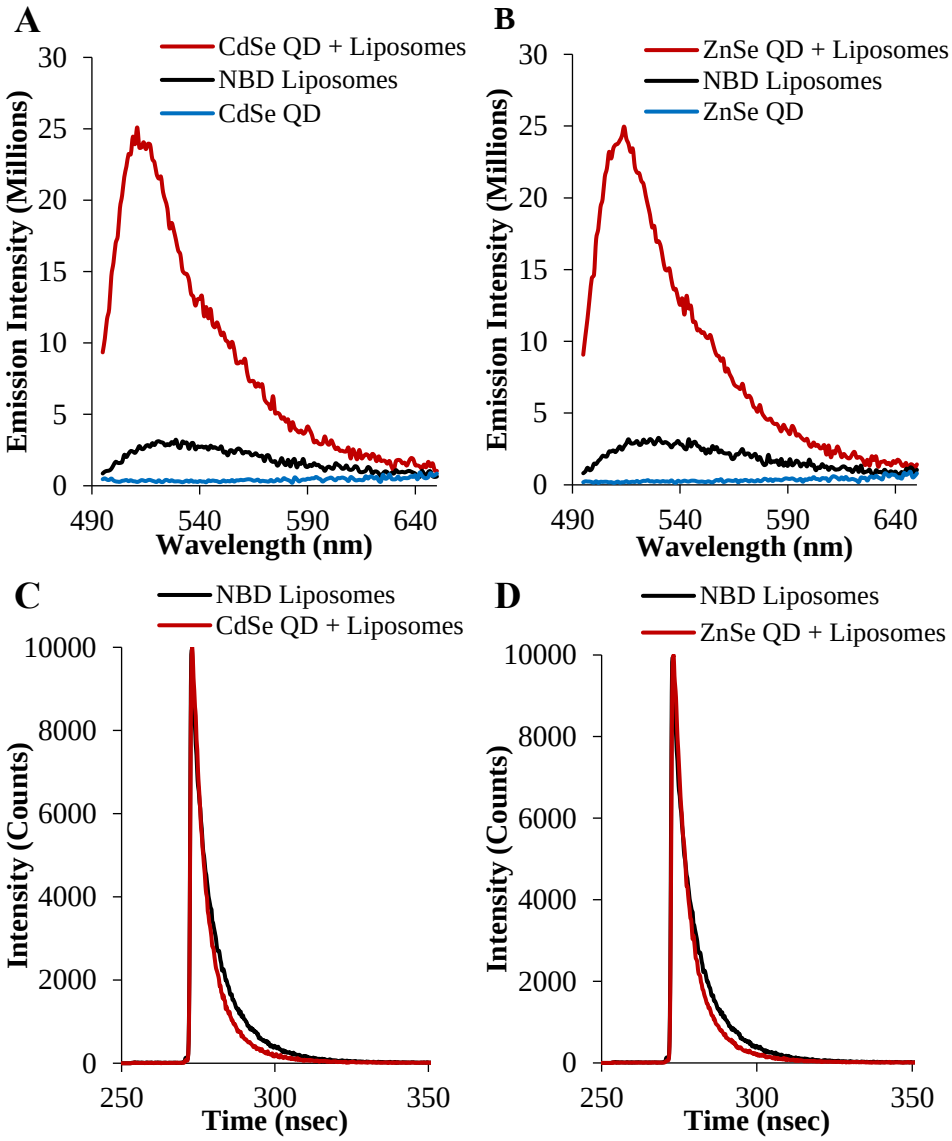

Figure 4. The fluorescence intensity of NBD-labeled liposomes (black), QD (blue), and following a 4-hourlong incubation of NBD liposomes with QD (red) show significant NBD fluorescence increase for both CdSe (A) and ZnSe (B) QD (λ_{ex} = 470nm). Time resolved photoluminescence decay curves of NBD-liposomes (black) and following a 4-hour long incubation with QD (red) for CdSe QD (C) and ZnSe QD (D) show a decrease in fluorescence lifetime (λ_{ex} = 470nm, λ_{em} = 515nm).

	weighted fluorescence lifetime τ (nsec)	τ_1 (nsec)	A_1 (%)	τ_2 (nsec)	A_2 (%)
NBD-Liposomes	5.87 ± 0.23	2.81	54.81	9.58	45.17
CdSe QD and Liposomes	5.23 ± 0.02	3.78	72.51	9.24	27.49
ZnSe QD and Liposomes	5.17 ± 0.03	3.84	72.48	9.43	27.52

Table 1. A summary of the fluorescence lifetime and exponential terms used to fit the fluorescence lifetime decay curves for NBD liposomes prior to and following exposure to CdSe and ZnSe QD. The observed fluorescence lifetime decrease and the change from a bi-exponential to a mono-exponential character of the fluorescence lifetime decay curves are consistent with QD association with the liposome membranes.

3.3.5 The Impact of Cadmium-Free and Cadmium-Containing QD on *Shewanella oneidensis* MR-1 Bacteria. The liposome lysis assays showed membrane disruption activity of all QD types, which is attributed to QD-membrane association that leads to membrane disruption. In our liposome experiments, CdSe and CdSe/ZnS QD showed higher membrane disruption activity than ZnSe and ZnSe/ZnS QD. We hypothesized that the interactions between the QD and negatively charged bacterial membranes would be similar to the interactions of QD with negatively charged liposomes. To test this hypothesis, we investigated the interactions between cadmium-free, ZnSe and ZnSe/ZnS QD, and cadmium-containing CdSe and CdSe/ZnS QD, and *Shewanella oneidensis* MR-1 bacteria. *Shewanella oneidensis* was chosen for the study because it is an environmentally relevant bacteria, which was previously used in similar nanoparticle exposure studies.[31, 32] We utilized TEM, ICP-MS, and hyperspectral imaging measurements to investigate the interactions between QD and bacterial cells, and then measured the impact of QD exposure on bacterial cell viability.

TEM measurements provide qualitative assessment of the interactions between QD and bacteria. Representative TEM images of bacterial cells which were exposed to 1 mg/L CdSe/ZnS QD (the most disruptive QD to liposomes and bacterial cells) are shown in Figure 5. The low magnification required to view the bacteria (scale bars of 0.2 to 1 μm) enables the observation of dark spots, possibly of QD aggregates associated with the cells but not individual QD which are only ~5 nm in diameter. Images A and B show distorted cells with the release of cell organelles as well as disintegrated cell membranes. Dark spots, possibly of QD aggregates, are seen on or near cells in the TEM images. The images

reveal significant damage to the cells due to the interaction with the QD, which is consistent with our QD-liposome lysis assays.

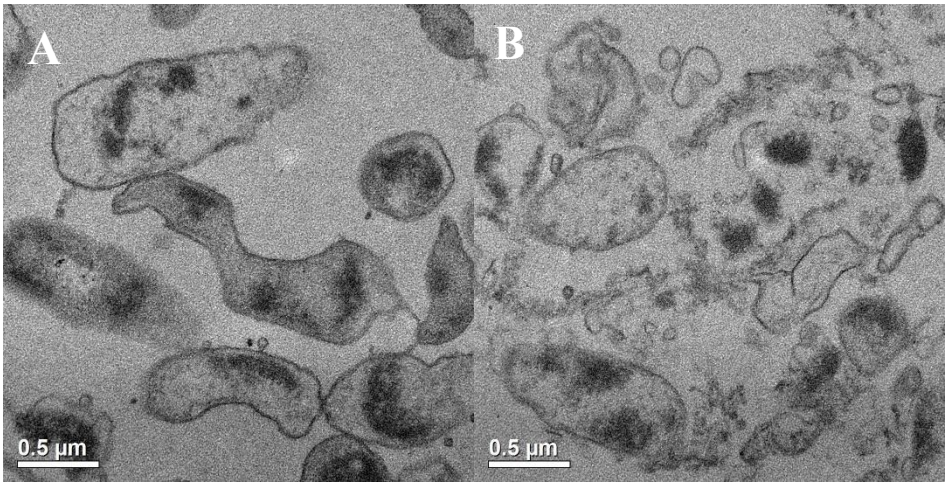

Figure 5. A. and B. Representative biological TEM images of Shewanella oneidensis MR-1 bacteria samples treated with CdSe/ZnS QD at Cd core concentration of 1 mg/L at 15 min.

ICP-MS experiments of washed bacterial samples digested following their incubation with ZnSe, ZnSe/ZnS, CdSe, and CdSe/ZnS QD were used to determine whether all QD associate with *Shewanella oneidensis* MR-1 cells. Control measurements of digested pellets of *Shewanella oneidensis* in the absence of QD show no detectable zinc or cadmium ions. Digested pellets of bacteria that were incubated with 0.5 to 5 mg/L QD in HEPES buffer solutions at pH 7.4 show levels of cadmium (cadmium-containing QD) and zinc (cadmium-free QD) that were significantly higher than the levels of these ions in control QD samples in the absence of bacteria. For example, the washing of 2 mg/L CdSe/ZnS QD control (no bacteria) had a measured cadmium level of 27 µg/L. In contrast, when bacterial cells were exposed to 2 mg/L CdSe/ZnS QD, the level of cadmium pelleted

with the bacteria was about 10-fold higher at 200 µg/L. Interestingly, the level of cadmium and zinc in QD-bacterial samples, which were exposed to CdSe/ZnS and ZnSe/ZnS QD was 3-fold higher than the level of cadmium and zinc in QD-bacterial samples which were exposed to CdSe and ZnSe core QD. The higher affinity of core-shell QD to bacterial cells could be attributed to higher ligand density on core-shell QD due to higher binding affinity of thiolated ligands to the ZnS shell of CdSe/ZnS and ZnSe/ZnS QD than to CdSe or ZnSe QD. The higher levels of cadmium and zinc in QD-incubated bacteria provide additional evidence for QD-bacteria association.

Hyperspectral dark field microscopy was also used to study the interactions between QD and bacterial cells. This technique provides the capability to identify and locate objects, for example nanoparticles and cells, as long as they show unique optical reflectance signature.[47] The hyperspectral data cube acquisition, namely hyperspectral "pushbroom" scanning, generates 3D data consisting of two spatial (x,y) and one spectral (z) dimensions.[48] Hence, a hyperspectral image can be treated as a dark field image with the spectral information associated with each pixel of the image.[49] The work flow includes dark field imaging, hyperspectral data acquisition, spectral library construction, spectral library filtering, and finally, QD and bacterial cell mapping. Figure 6 exhibits the hyperspectral images (left column) of *S. oneidensis*, CdSe QD, and CdSe/ZnS QD, and corresponding spectral libraries (right column) obtained by the region-of-interest (ROI) tool that converts selected pixels into spectral libraries for subsequent QD and bacterial cell mapping in QD-incubated bacterial samples. Specifically, 499 pixels were collected to build *Shewanella oneidensis* library, 438 pixels for CdSe QD, and 403 pixels for

CdSe/ZnS QD. Maximum (max), minimum (min), and mean reflectance intensity are described in the spectral library files, along with standard deviation (±Stdev), from which it can be qualitatively determined that the average reflectance intensity of bacteria is much lower than those of QD. In addition, spectral library function anchored with CytoViva software was performed to cross-compare the libraries of bacteria and QD. Moreover, QD libraries were loaded into the spectral angle mapper (SAM) function to map the location of QD in the hyperspectral images of CdSe and CdSe/ZnS QD. The SAM function provides a convenient and automated mapping method, where the algorithm differentiates the spectral libraries and provides information about the location and analogy of endmember pixels in an input image.[49, 50] This information allows us to map precise QD location and false-color them red. For the next step, the presence of QD co-localized with *Shewanella oneidensis* cells after exposure was investigated using hyperspectral microscopy, as displayed by Figure 7. The pixels representing QD are pseudo-colored with red. In both exposure samples, it is observable that there is proximity between QD and bacteria cells. The proximity, and in many cases overlap, between the spectral signatures for bacterial cells and QD support our conclusion from the liposome assays that the QD associate with the negatively charged membranes. This in turn leads to a high local ion concentration as the QD dissolve. The increase in local ion concentration leads to membrane disruption. As a caveat, the diffraction limit binds this imaging technique, so even overlap of spectral signatures does not guarantee direct physical contact between the micron-scale bacteria (which can be resolved) and the nanoscale QD (which cannot be resolved).

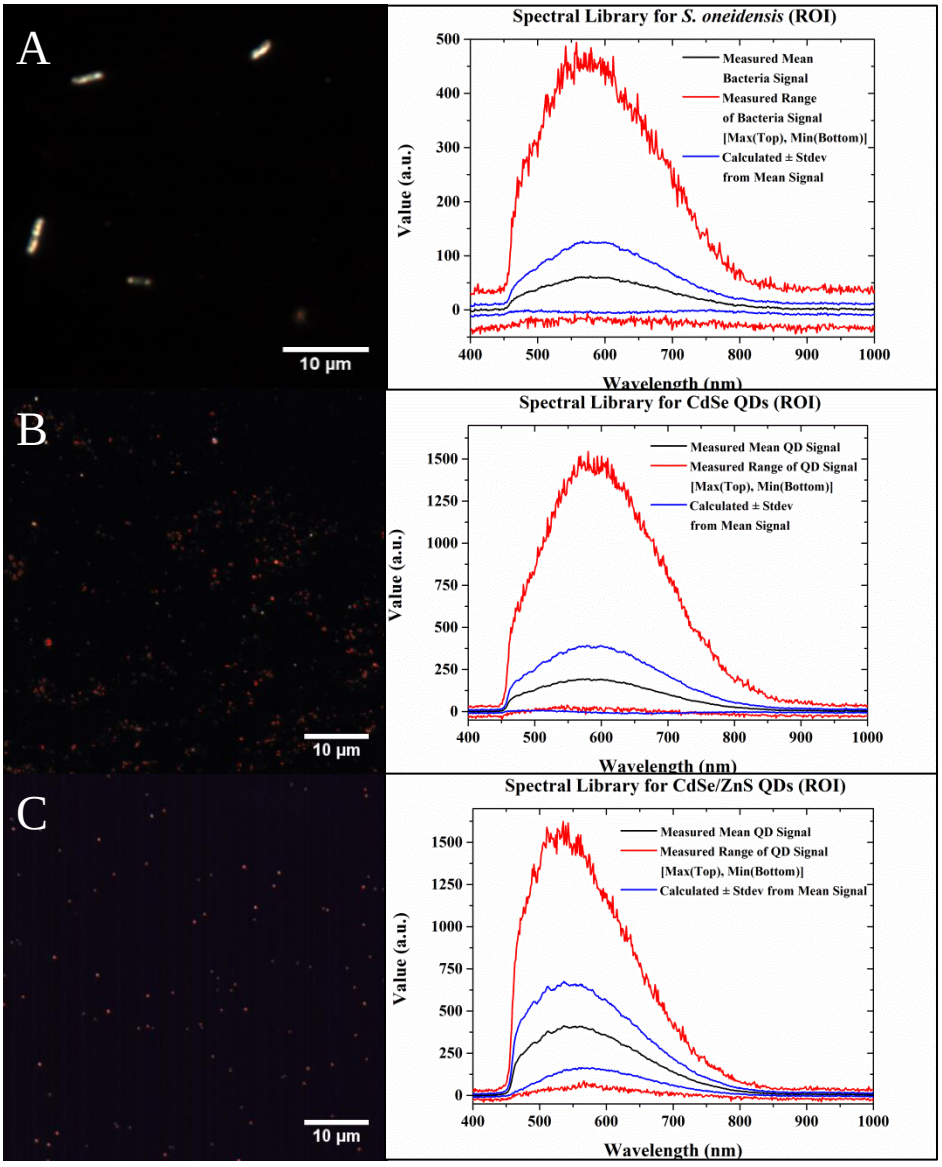

Figure 6. Hyperspectral reflectance microscopy images of Shewanella oneidensis MR-1 (A), CdSe QD (B), and CdSe/ZnS (3ML) QD (C), with the QD false-colored red. The minimum, maximum, and median reflectance spectra for each sample are captured to build a spectral reference library which is shown to the right of each image. The libraries enable identification of bacterial cells and QD in mixed samples.

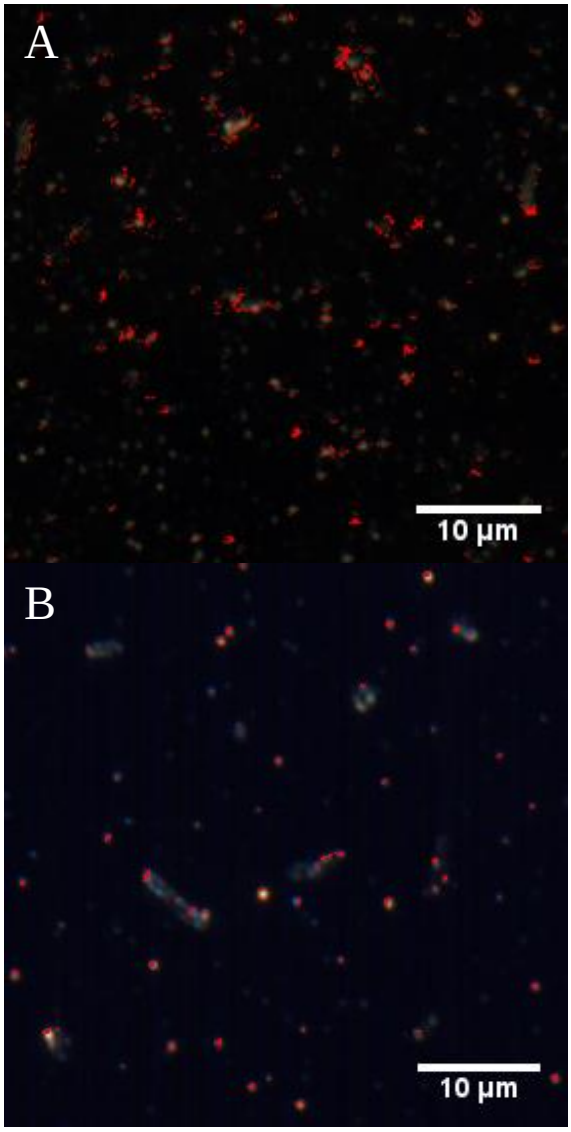

Figure 7. Images of QD-incubated bacteria samples analyzed using the reference spectral libraries of Shewanella oneidensis (gray) exposed to CdSe QD (A) or CdSe/ZnS (3 ML) (B). In both images, pixels displaying the QD spectral signatures are colored red. In many cases, QD are at the vicinity or overlap with bacterial cells, which is indicative of QD membrane association.

Realizing the important role of membrane association on the interactions between QD and liposome, we conducted bacterial viability assays to see if the apparent liposome-QD association and the likely association between bacteria-QD indicated by TEM, ICP-MS, and hyperspectral imaging would lead to dose-dependent impact of QD on *Shewanella oneidensis* MR-1.

Bacterial cell cultures were exposed to ZnSe, ZnSe/ZnS, CdSe, or CdSe/ZnS QD at concentrations ranging from 0.01 to 0.5 mg/L selenium equivalents in the QD cores. Figure 8A shows bacterial cell cultures following exposure to increasing concentrations ranging from 0 to 0.5 mg/L of ZnSe (left) and CdSe (right) QD. Exposure of *Shewanella oneidensis* MR-1 to ZnSe QD had negligible impact on their viability even at the highest concentration of 0.5 mg/L selenium equivalents. Similarly, ZnSe/ZnS QD exposure did not impact bacterial cell viability (Figure SI-5). In contrast, exposure of *Shewanella oneidensis* MR-1 cells to CdSe QD at 0.01 mg/L selenium equivalents led to almost total reduction in *Shewanella oneidensis* viability. In agreement with the liposome assays, an even greater effect was observed when the bacterial cells were exposed to similar levels of CdSe/ZnS QD. To evaluate the relevance of the liposome assays as a model for the bacterial response to QD exposure, we also investigated the impact of CdSe/ZnS QD with varying shell thickness on the viability of *Shewanella oneidensis* MR-1. Figure 8B describes the bacterial cell viability (%) as a function of CdSe/ZnS QD concentration (selenium equivalents) for CdSe QD (black) and CdSe/ZnS QD with shell thickness of one monolayer (green), three monolayers (red), and six monolayers (red). A

concentration-dependent decrease in bacterial viability is shown for all cadmium-based QD, and a greater decrease in bacterial viability is observed for CdSe/ZnS QD with increasing ZnS shell thickness. These results are indicative of the complex nature of the interactions between luminescent QD and bacteria. On one hand, passivating CdSe QD with a higher energy bandgap shell of ZnS is known to decrease the rate of ROS generation when irradiated and lower their toxicity.[15, 20-22] On the other hand, the chemical instability of the shell due to crystal plane mismatches along the core/shell interface[51, 52], particularly in complex aqueous solutions, increases their rate of zinc ion dissolution, and increases QD toxicity against the *Shewanella oneidensis* MR-1 bacteria.

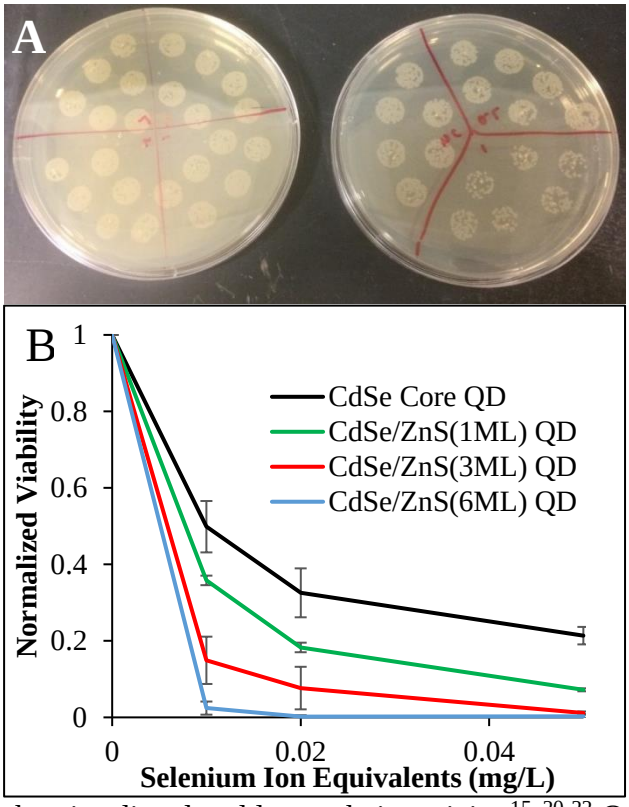

Figure 8. Shewanella oneidensis MR-1 colony growth after exposure to increasing concentrations of ZnSe QD (left) and CdSe QD (right) compared to negative controls (NC) on each plate (A). Exposing the cells to ZnSe/ZnS QD does not impact cell viability (Figure SI-5). In contrast, a significant reduction in viability is seen in Shewanella oneidensis after exposure to CdSe/ZnS QD. Normalized bacterial cell viability as a function of ZnS shell thickness in CdSe/ZnS QD (B). Increasing the QD shell thickness decreases cell viability in a concentration dependent-manner. N=4 biological replicates for each condition, and the error bars represent standard deviation among those replicates.

3.4 Conclusions

This study shows that liposomes with negatively-charged membranes could be used to model the initial interactions between cadmium-free and cadmium-containing QD and *Shewanella oneidensis* MR-1, an environmentally relevant bacteria. Fluorescence assays suggest that ZnSe, ZnSe/ZnS, CdSe, and CdSe/ZnS QD associate with liposome membranes. Association of the QD with liposome membranes leads to membrane destabilization due to a change in the local chemical environment of the phospholipid head groups and a significant increase in local ion concentration when the QD dissolve over time, and finally to membrane disruption. BioTEM, ICP-MS and hyperspectral imaging measurements suggest that the QD also associate with the negatively-charged membranes of *Shewanella oneidensis* MR-1 bacterial cells. Cadmium-free ZnSe and ZnSe/ZnS QD have minimal impact on the viability of *Shewanella oneidensis* MR-1. In contrast, a short exposure time, as short as only 15 minutes, of CdSe or CdSe/ZnS QD to bacterial cells results in a significant reduction in bacterial cell viability. The low level of CdSe and CdSe/ZnS QD of < 0.5 mg/L of selenium in their cores, should not lead to such reduction in bacterial cell viability. Ion control experiments show that even if the CdSe or CdSe/ZnS QD completely dissolve in solution, the resulting ion levels are not sufficient to induce a devastating impact on the cells, and yet exposure of the cells to QD does. The QD impact on liposomes and bacterial cells in this study is attributed to strong association between the QD and liposomes or bacterial cells, which does not cease after the cells are separated from unbound QD to end the exposure.

Surprisingly, the impact of adding a ZnS shell to minimize ROS generation and direct contact between the cadmium-containing cores and the liposomes or bacterial membrane, increases rather than decreases, membrane disruption in both the liposomes and bacterial cultures. These are unwelcome findings since it is generally accepted that shelling cadmium core QD with a ZnS shell would lower QD toxicity due to a reduced rate of ROS generation. However, under our experimental conditions and most likely in even more complex biological/natural solutions, crystal plane mismatches between the core CdSe QD and the ZnS shell leads to inherent chemical instability of CdSe/ZnS QD,[51, 52] and in turn to a high rate of zinc ion dissolution from the QD. The high local concentration of zinc ions results in membrane disruption of the liposomes and adverse impacts on bacterial cell viability. One possible solution is to add an intermediate semiconductor layer of CdS between the CdSe core and ZnS shell (CdSe/CdS/ZnS QD) in an attempt to minimize membrane disruption activity and the impact of cadmium-containing QD on bacterial cell viability. Due to association of the QD with the liposome or cell membranes, the acute QD exposure is turning into a chronic indefinite exposure of the bound QD to the bacterial cells, Furthermore, QD dissolution results in high local ion concentration near the liposome or bacterial cell membrane, which leads to a high level of membrane disruption activity. From the ion-dissolution studies, increased Zn ion dissolution was also observed with increasing shell thickness and concentration, which is another potential cause for toxicity.

3.5 Acknowledgements

Work investigating liposome and bacterial response to quantum dots was supported by the National Science Foundation Center for Chemical Innovation (CCI) program Award CHE-1503408 for the Center for Sustainable Nanotechnology. Work involving bacterial TEM characterization was carried out in the Characterization Facility at the University of Minnesota, which receives partial support from the MRSEC program (DMR-1420013). Denise N. Williams' quantum dot syntheses were supported by the National Science Foundation Award CHE-1506995, including an NSF AGEP graduate fellowship award under CHE-1506995. Supplemental fellowship support to Denise N. Williams and Richard M. Brown was provided by the National Institute of Health Training Grant NIH-T32-GM066706. The authors thank Dr. Alline Myers of the National Institute for Standards and Technology (NIST) Center for Nanoscale Science and Technology for assistance with HRTEM imaging and Fang Zhou at the University of Minnesota for microtoming BioTEM samples.

Supporting Information

S1 TEM of ZnSe, and ZnSe/ZnS QD. High Resolution Transmission Electron Microscopy (HR-TEM) images were obtained to determine the size of core and core/shell QD used in the study. The TEM images revealed the luminescent QD were round and highly crystalline with increasing shape irregularities with increasing shell thickness for CdSe/ZnS QD. The TEM measurements were carried out using a Titan 80-300 S/TEM, operating at 300 kV with a Gatan OneView imaging camera. Samples were prepared by drop coating the QD onto mesh copper grids with ultrathin carbon film on holey carbon support film (Ted Pella, Inc.) Grids were then placed in vacuum oven overnight before analysis.

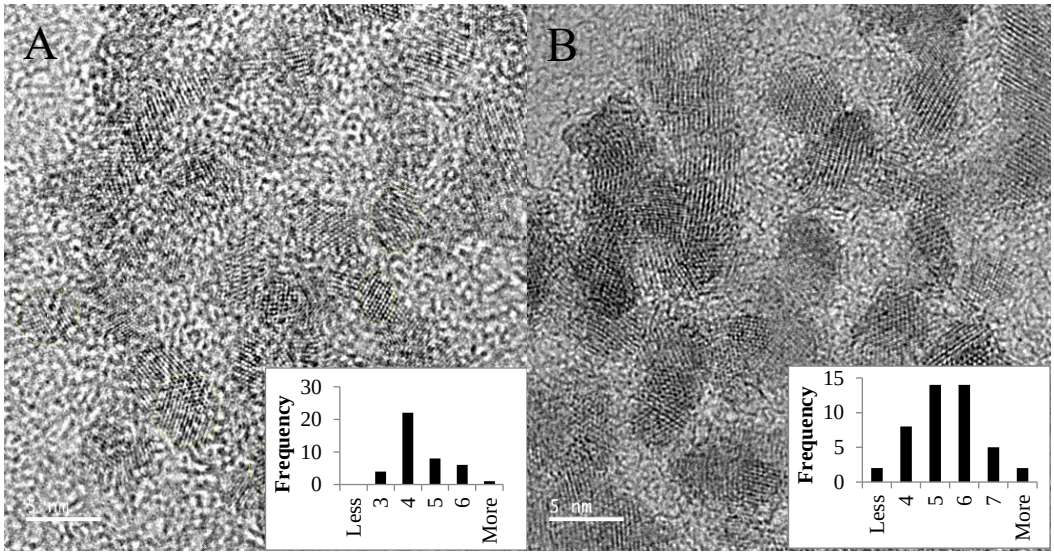

Figure S1 *- TEM images of 3.5 ± 0.4 nm ZnSe core QD (A) and 5.0 ± 1.2 nm ZnSe/ZnS QD (B). These and similar images were used to obtain the QD size distribution. The QD size distribution for each image (N > 50) is shown in the insert.*

TEM of CdSe, CdSe/ZnS (1ML), CdSe/ZnS (3ML), and CdSe/ZnS (6ML) QD.

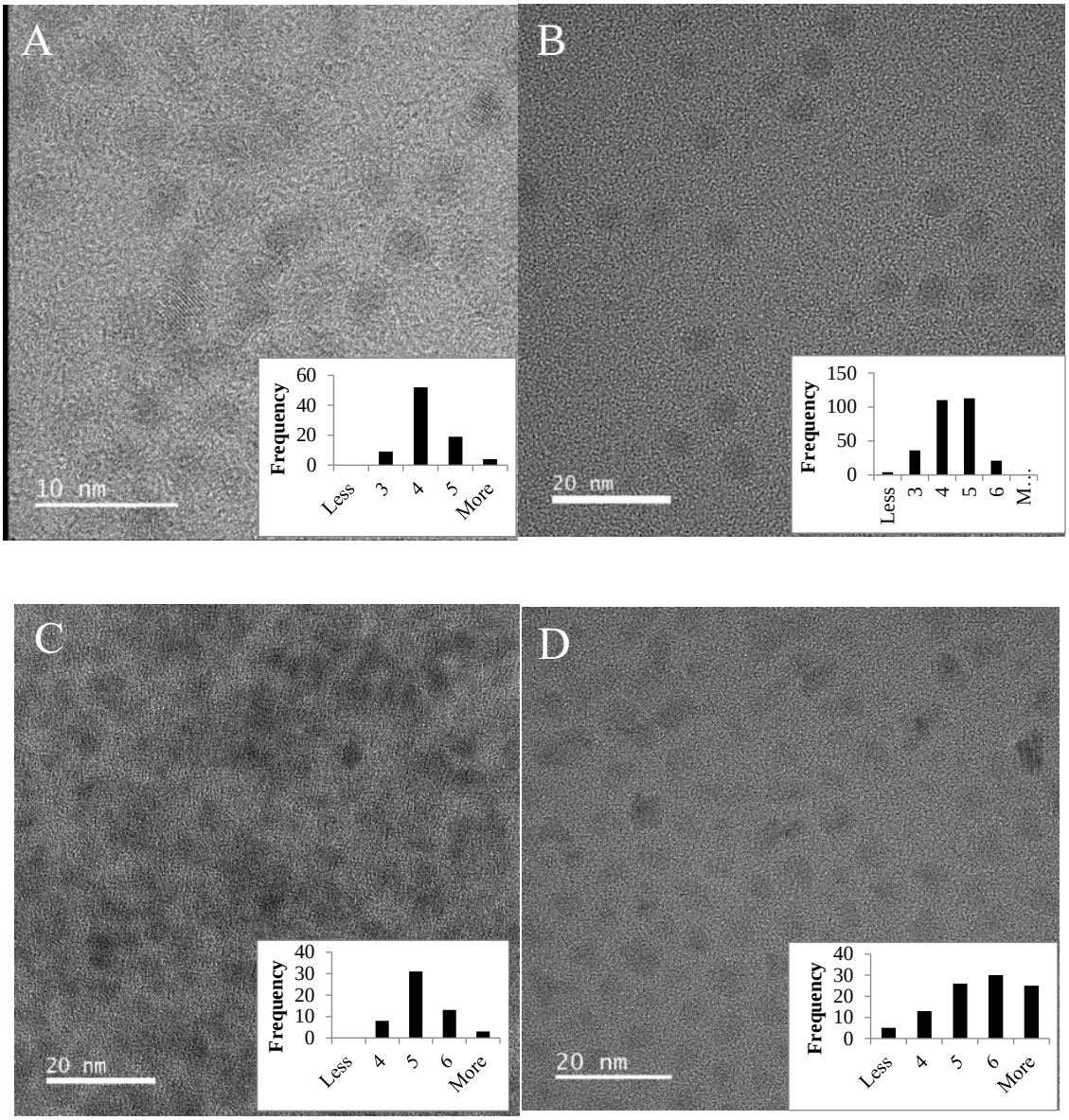

Figure S2. *TEM images of 3.9 ± 0.5 nm CdSe core QD (A), 4.2 ± 0.8 nm CdSe/ZnS (1ML) QD (B), 5.0 ± 0.9nm CdSe/ZnS (3ML) QD (C), and 5.9 ± 0.8 nm CdSe/ZnS (6ML) QD (D). These and similar images were used to obtain the QD size distribution. The QD size distribution for each image (N > 50) is shown in the insert.*

S2 Time resolved photoluminescence measurements of ZnSe and ZnSe/ZnS QD. Time resolved photoluminescence measurements were carried out to determine the impact of the ZnS shell on the QD optical performance and to assess the quality of the luminescent QD. The LUDOX TMA colloidal silica standard in water, λ_{em} = 372 nm, was used as the standard. The decrease in fluorescence lifetime of core QD when passivated with a higher energy bandgap shell is attributed to increased confinement of the excited electrons in the core QD, and is consistent with previous studies.[1]

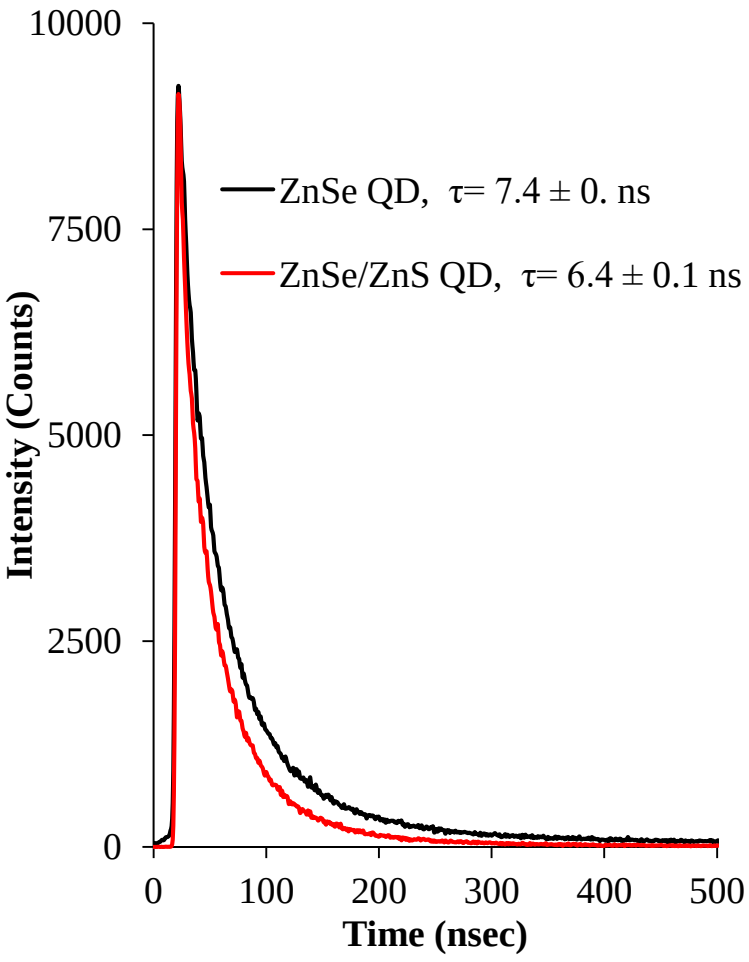

Figure S3. *Time resolved photoluminescence decay curves of ZnSe and ZnSe/ZnS QD in hexane. A decrease in the fluorescence lifetime of the ZnSe QD is observed when they are coated with a higher energy bandgap shell.*

S3 Time resolved photoluminescence measurements of CdSe, CdSe/ZnS (1ML), CdSe/ZnS (3ML), and CdSe/ZnS (6ML) QD.

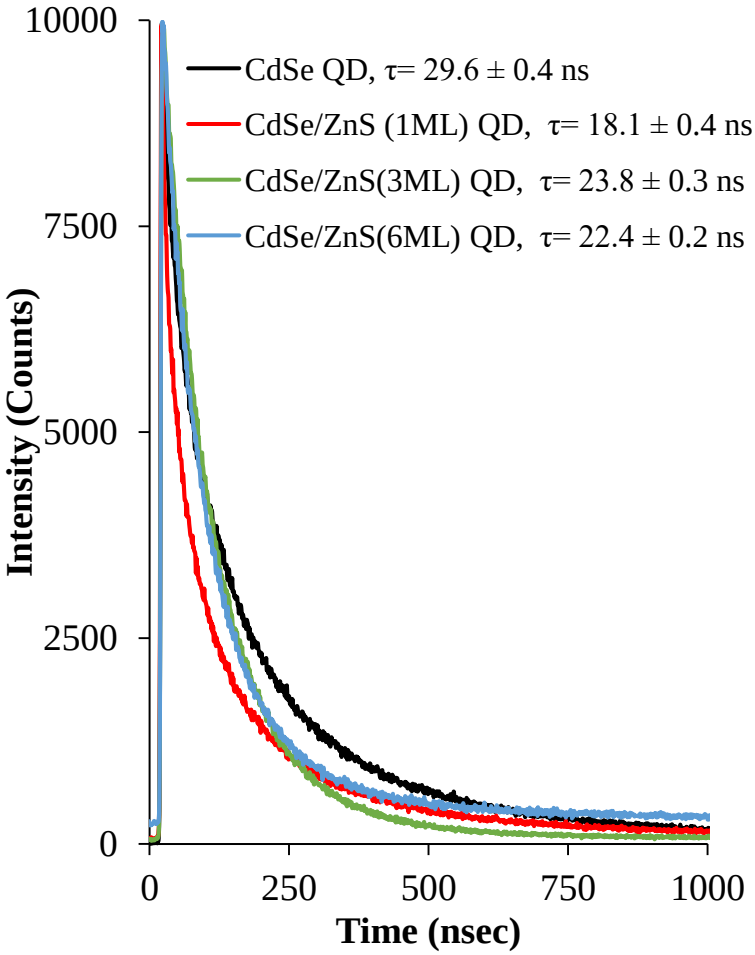

Figure S4. *Time resolved photoluminescence decay curves of CdSe, CdSe/ZnS (1ML), CdSe/ZnS (3ML), and CdSe/ZnS (6ML) QD in chloroform. The fluorescence lifetime of the CdSe QD decreases significantly when they are coated with a higher energy bandgap ZnS shell. The majority of the impact is realized when the CdSe QD are coated with one monolayer ZnS shell.*

S4 Dynamic Light Scattering (DLS) Measurements of Liposomes when Exposed to Zinc and Cadmium Ions. DLS measurements were used to determine the size distributions of liposomes before and after >15minute exposures to 1% Triton X solution, 1-20 ppm cadmium ion, and 1-20 ppm zinc ion control solutions. Measurements were carried out in triplicate to determine the mean liposome size and standard deviation. The DLS measurements were carried out on using a Malvern Zetasizer Nano ZS. Figure S5 shows the impact of liposome exposure to 1% Triton X solution (curve color), 20 ppm zinc ions, and 20 ppm cadmium ions on their structural integrity. The concentration of zinc and cadmium ion was chosen as 20 ppm since this is the upper limit of ion concentration in our QD experiments if they completely dissolve. Significant changes to the liposome size distribution were detected only following the exposure of the liposomes to Triton X. The lack of changes in the liposome size distributions following the addition of ions indicates that the dissolution of free QD that are not associated with the liposome membrane is not a major contributor of QD-induced membrane disruption.

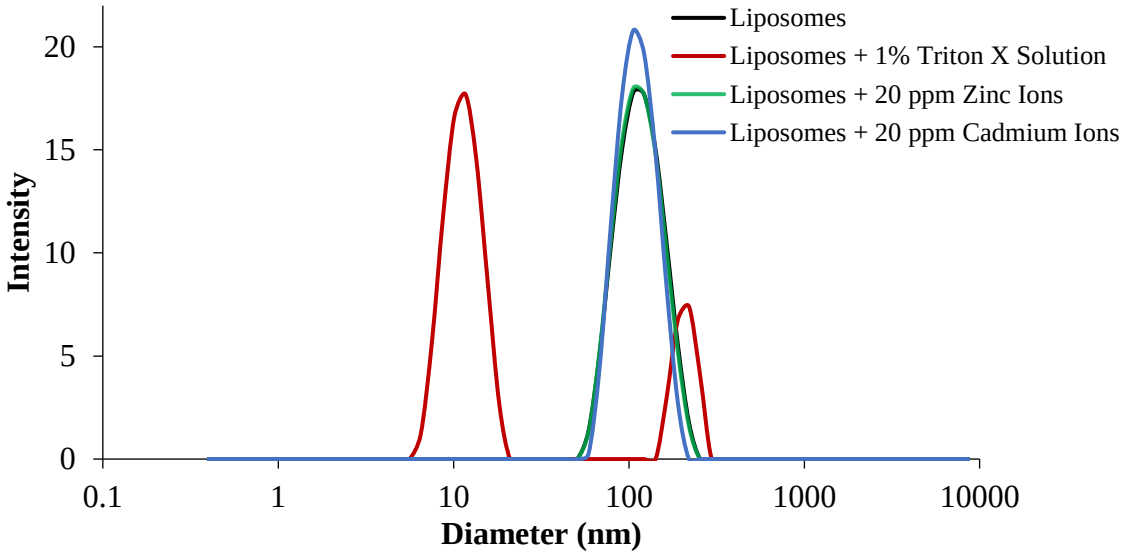

Figure S5. *DLS size distribution of POPC:POPG liposomes in HEPES solution at pH 7.2 (curve color), and the same liposomes following 15 minute-long exposure to 1% Triton X solution (curve color), 20 ppm zinc ions (curve color), and 20 ppm cadmium ions (curve color). The DLS data show that the impact of zinc and cadmium ions under our exposure conditions (20 ppm for 15 minutes) is negligible.(Note: 'Liposomes' and 'Liposomes + 20 ppm Zinc Ions' data overlay each other.)*

S5 Bacterial viability studies of *Shewanella oneidensis* MR-1 cells exposed to ZnSe and ZnSe/ZnS QD. *Shewanella oneidensis* MR-1 bacteria were treated with QD for 15 minutes at varying concentrations, and their viability was determined using a drop-plate colony-counting protocol on the next day.[2] Bacterial cell cultures of *Shewanella oneidensis* MR-1 exposed to ZnSe and ZnSe/ZnS QD indicated QD had negligible impact on cell viability even at the highest concentration of 5mg/L zinc ion equivalents in the core (0.5 mg/L selenium equivalents). This is contrary to the results of bacterial exposures to CdSe and CdSe/ZnS QD (Figure 7 in the main paper), which demonstrated that exposing the bacterial cells to cadmium-containing QD induces a concentration-dependent decrease in bacterial cell viability at similar selenium ion concentration equivalents.

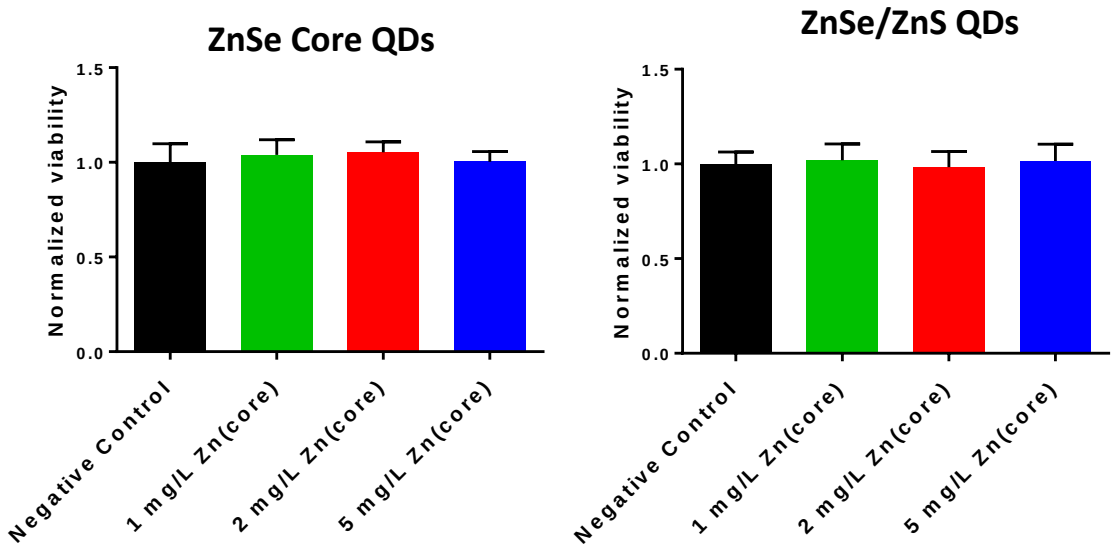

Figure S6*. Viability of Shewanella oneidensis MR-1 following their exposure to increasing concentrations of ZnSe (A) and ZnSe/ZnS (B) QD. The viability values are normalized to negative controls of unexposed bacteria cells. N=4 biological replicates for each condition, and the error bars represent standard deviation among those replicat*es.

References

1. Lyons, T.; Williams, D.; Rosenzweig, Z., Addition of Fluorescence Lifetime Spectroscopy to the Tool Kit Used to Study the Formation and Degradation of Luminescent Quantum Dots in Solution. Langmuir 2017, *33*, 3018-3027.
2. Feng, Z.; Gunsolus, I.; Qiu, T.; Hurley, K.; Nyberg, L.; Frew, H.; Johnson, K.; Vartanian, A.; Jacob, L.; Lohse, S.; Torelli, M.; Hamers, R.; Murphy, C.; Haynes, C., Impacts of Gold Nanoparticle Charge and Ligand Type on Surface Binding and Toxicity to Gram-negative and Gram-positive Bacteria. *Chem. Sci.* **2015,** *6*, 5186-5196.

Chapter 4

Transformations and Environmental Impacts of Copper Zinc Tin Sulfide Nanoparticles & Thin Films

This work was completed with assistance from Nancy Trejo, Eileen A. McIntire, Natalie V. Hudson-Smith, Prof. Eray Aydil, and Prof. Christy L. Haynes

Overview

Quarternary chalcogenide copper zinc tin sulfide (CZTS) nanoparticles have applications as p-type absorber materials in solar cells, and can be used as a more benign alternative to copper indium gallium selenide (CIGS) materials. CZTS materials are known for their optical properties, such as an ideal band gap and high absorption coefficient for solar radiation, that make them attractive options for use in photovoltaic cells. In this work, we explore the toxicity of CZTS nanoparticles using an environmentally relevant bacteria model *Shewanella oneidensis* MR-1. This study also focuses on understanding the stability of CZTS-based thin films and their direct interaction with bacterial cells. Bacterial cell viability is assessed by colony-counting methods, and the stability of the nanoparticles and thin films, along with the mechanisms of toxicity, are investigated using tools such as biological transmission electron microscopy (TEM), inductively coupled plasma mass spectrometry (ICPMS), and assays to monitor reactive oxygen species (ROS) generation. The CZTS nanoparticle suspensions show significant acute toxic effects to bacterial cells, but longer term (72 h) exposure of bacterial cells to CZTS-based thin films do not exhibit similar detrimental effects to bacterial viability.

4.1 Introduction

Harnessing solar energy and utilizing it to meet global energy demands has become an extremely important field of research, since solar energy is a vast resource of energy that can help produce clean, renewable electricity.[1- 2] The photovoltaic effect, which is the conversion of light energy to electricity, was first discovered by Alexander Edmond Becquerel in 1839,[3] and the application of semiconductor materials for this purpose was established with the discovery of photosensitivity and photoconductivity in selenium.[4] In the last 50 years, due to the depletion of fossil fuel reserves, as well as general environmental concerns, solar photovoltaic cells have become one of the leading contenders in the renewable energy resource field.[5-6] For solar cells to be truly effective and sustainable, the technologies need to have high energy conversion efficiencies and be fabricated from cheap, environment-friendly, and earth-abundant materials.[7] Currently, silicon-based solar cells dominate the photovoltaic market due to being inexpensive and the raw material silicon being largely available in the earth's crust.[8,9] But silicon-based technologies have some drawbacks such as high manufacturing costs and low light harvesting and conversion efficiencies.[10,11] Research is ongoing to improve the photoconversion efficiency of solar cells by synthesizing materials with higher absorption coefficients and direct bandgaps,[12] as opposed to silicon which is an indirect band-gap material. Chalcogenide semiconducting materials such as GaAs, CdTe, and $CuIn_xGa_{1-x}Se_2$ (CIGS) have garnered interest in the last decade due to their direct bandgaps and ability to be utilized in thin-film technologies, thus lowering manufacturing costs compared to silicon-based photovoltaics.[7,13,14,15,16] CIGS-based solar cells have been reported to show a

record efficiency of 21.7% at the laboratory scale.[17] However, the toxicity of Cd-based absorber materials, and the scarcity of Te, Ga, and In are major limitations to the widespread use of these absorber materials, including CIGS.[7] Recently, CZTS (copper zinc tin sulfide) materials have been introduced as a potentially more benign p-type absorber material for use in solar cells,[18,19,20,21,22] due to the use of less toxic metals Cu and Sn. CZTS materials have a high absorption coefficient of 10^4 cm^{-1} and an ideal optical band gap of 1.5 eV.[23] The efficiency of CZTS solar cells have increased over time with optimization of materials and synthetic routes, and the highest reported efficiency to date is 12.6%.[24] Even though the Shockley-Queisser photon balance calculations show that the theoretical limit for CZTS is 32.2%,[25] there are various factors responsible for the lower efficiency obtained experimentally. One of the major reasons for this is the formation of secondary phases, as well as various defect complexes.[9] Research is ongoing to minimize these effects through the use of different growth techniques as well as various vacuum and non-vacuum thin film deposition processes that can decrease the generation of secondary phases and defects.[26,27,28] Solution-based, inexpensive thin film deposition processes using a hydrazine-based solution of CZTS have also been reported,[29] but the toxic and explosive nature of hydrazine renders this route less desirable. CZTS nanocrystal-based processes offer a safer and more controlled solution-based method for the synthesis of high quality CZTS nanomaterials and production of thin films.[22] Nanocrystal-based thin film coatings can be formed through techniques such as drop-casting, dip-coating, spin-coating, and printing.[21]

Even though CZTS nanomaterials and thin films have received significant attention due to

their optical properties and use of earth-abundant as well as benign metals, studies on the biological and environmental impacts of these potentially important materials are lacking. To the best of our knowledge, one study has been reported investigating the antibacterial properties of CZTS nanoparticles against pathogenic bacteria, to assess the potential application of CZTS nanoparticles in antibiotics.[30] This study infers that CZTS nanoparticles have antibacterial effects on Gram-positive and Gram-negative pathogenic bacteria. In light of the potential applications of the CZTS nanoparticles, especially in the field of photovoltaics, we need to think beyond potential application as antibiotics about the inevitable release of the nanoparticles into the environment in the near future. The CZTS nanoparticles as part of devices can be disposed of in wastewater streams, landfills, or seawater, and it is important to preemptively investigate and unerstand their environmental interactions.

Bacteria are ubiquitous in the ecosystem, form the lowest trophic level in the ecological pyramid, have important roles in decomposition, nutrient cycling, and bioremediation, and thus were chosen as the model organism in this study. *Shewanella oneidensis* MR-1, is a Gram-negative, environmentally-beneficial bacteria species known to be a robust model which has been shown to withstand the effect of a number of engineered nanomaterials.[31,32] In our work, CZTS nanocrystal suspensions are synthesized using a thermal decomposition of metal precursors method, and thin films were prepared by drop-casting the nanocrystal suspensions on soda-lime glass. To introduce CZTS nanocrystals to aqueous bacterial suspensions for toxicity assessment, the non-polar moieties on the surface of initially synthesized nanocrystals were exchanged with polar groups, and the CZTS nanocrystals were dispersed in water.[33]

Higher solar cell efficiencies were observed in CZTS nanocrystal thin films that have been annealed in a sulfur atmosphere at high temperature.[21,34,22] Due to this reason, thin film stability and bacterial viability studies were performed using both the as-deposited unannealed films as well as the annealed thin films. This work investigated the toxic effect of the CZTS nanoparticles and thin films on *Shewanella oneidensis* MR-1 using a drop-plate colony counting assay. Also, mechanisms of nanoparticle toxicity such as metal ion release, damage to the cell membrane through association, and reactive oxygen species (ROS) generation were also explored. Ion dissolution from CZTS nanocrystals and CZTS thin films are probed as well to characterize how the material transforms in aqueous environments, and how that trannsformation impacts bacteria.

4.2 Methods

4.2.1 Materials

Oleic acid (technical grade, 90%), oleylamine (OLA) (technical grade, 70%), toluene (HPLC grade, 99.9%) were purchased from Sigma-Aldrich. Reagent alcohol (histological grade, 90% ethyl alcohol, 5% methyl alcohol, 5% butyl alcohol) was purchased from Fisher Scientific. Copper(II), zinc(II), and tin(IV)-diethyldithiocarbamate complexes were synthesized from sodium diethyldithiocarbamate trihydrate (ACS reagent, Sigma Aldrich), copper(II) chloride dihydrate (ACS grade, 99+%), zinc chloride (reagent grade, 98%), and tin(IV) chloride pentahydrate (98%). Sulfur was purchased from Cerac, Inc. (99.999%), and the soda lime glass (SLG) substrates were purchased from Valley Design Corp.

4.2.2 Characterization

The CZTS nanocrystals were imaged with a JEOL 6500 field-emission scanning electron microscope (SEM). The elemental composition was determined using a Thermo-Noran Vantage energy dispersive X-ray spectrometer (EDS) installed on the SEM. Raman scattering spectra were collected using a backscattering geometry on a WITec alpha300 spectrometer, an Nd:YAG laser (532 nm), and a DV401 CCD detector. X-ray diffraction (XRD) from the nanoparticles was collected using a Bruker D8 Discover Co Kα radiation source and a 0.8 mm beam collimator. XRD patterns were converted to Cu Kα radiation using JADE analysis software from Materials Data Incorporated.

4.2.3 Synthesis of 5 nm CZTS Nanocrystals

CZTS nanocrystals were synthesized by thermal decomposition of copper diethyldithiocarbamate (107.9 mg), zinc diethyldithiocarbamate (54 mg), and tin diethyldithiocarbamate (106.8 mg) precursors. This procedure is described by Khare *et al.*[35] The three precursors were dissolved in oleic acid (OA, 4 mL) and 1-octadecene (ODE, 36 mL) and then heated to 60 °C in a 100 mL three neck flask. The flask was attached to a Schlenk line and degassed and purged with nitrogen three times. After the third nitrogen purge, the flask was heated to 175 °C and oleylamine (0.9 mL) was quickly injected into the flask. The reaction temperature was maintained at 175 °C for 10 minutes, after which the flask cooled naturally to 40 °C. The solution was split equally into two centrifuge tubes. Both centrifuge tubes were centrifuged with reagent-alcohol to remove olelylamine (OLA) and unreacted intermediates. After centrifuging for 10 minutes at 4000 rpm, the supernatant was discarded, and the solid product was dispersed in toluene with 10^{-4} v/v% oleic acid. The dispersions were combined into one vial, and then the solid nanocrystals were

precipitated again with centrifugation in reagent alcohol for 10 minutes. The supernatant was discarded, and the CZTS nanocrystals were dispersed in toluene with 10^{-4} v/v% oleic acid.

4.2.4 Extraction of 5 nm CZTS nanoparticles in water

The CZTS nanocrystals were extracted into water as described by Tosun *et al.*[33] First, the nanocrystals were extracted into formamide by mixing 5 mL formamide, 1 mL 1.28 g/mL K_2S solution in water, and 1 mL CZTS nanocrystals (~30 mg/mL) dispersed in toluene with 10^{-4} v/v% oleic acid. The mixture was stirred for 24 hours to extract the CZTS nanocrystals from toluene/oleic acid into the formamide phase. The vial was removed from the stir plate, 2 mL toluene was added, and the mixture was allowed to settle for 5 minutes. The top, clear toluene layer was carefully removed with a glass pipette, while the bottom, dark formamide layer was transferred into a centrifuge tube with 6 mL acetonitrile. The formamide phase was centrifuged for 10 minutes at 4000 rpm. The supernatant was discarded, and the remaining precipitate was sonicated and dispersed in 4 mL formamide. After the nanocrystals were dispersed, they were precipitated again by centrifuging with 2 mL each of acetone, acetonitrile, and toluene for 10 minutes. Again, the supernatant was discarded, and the precipitate was dissolved in 4 mL formamide. Crashing out and dispersing in formamide was repeated 1-2 times to remove K_2S. After the last precipitation, the CZTS nanocrystals were dispersed in water.

4.2.5 Synthesis of 40 nm CZTS nanoparticles and film fabrication

~40-nm-diameter CZTS nanocrystals were synthesized as described by Chernomordik *et al*[36] and used to prepare CZTS films on soda lime glass substrates. Copper

diethyldithiocarbamate (54 mg), zinc diethyldithiocarbamate (30 mg), and tin diethyldithiocarbamate (53.4 mg) precursors were mixed with OA (5 mL) and heated to 60 °C in a 25 mL three neck flask. In a separate 100 mL three neck flask, OLA was also heated to 60 °C. Both flasks were attached to a Schlenk line and degassed/purged with nitrogen three times. The flask containing the precursors was heated to 140 °C to dissolve the solids, while the flask containing OLA was heated to 340 °C. The precursor flask was cooled to 75 °C and quickly injected with a syringe into the preheated OLA. After injection, the temperature was maintained for 10 minutes. The reaction solution was allowed to naturally cool to 40 °C. OLA and unreacted intermediates were removed by repeated precipitation of the CZTS nanocrystals with reagent-alcohol under centrifugation for 10 minutes at 4000 rpm. The supernatant was discarded and the solid products were dispersed in toluene with 10^{-4} v/v% oleic acid. The nanocrystals were precipitated a second time with reagent alcohol, the supernatant was discarded, and the CZTS nanocrystals were finally dispersed in toluene with 10^{-4}v/v% oleic acid. The CZTS nanocrystal dispersions (~30 mg mL^{-1}) were drop cast onto soda lime glass substrates to form CZTS films (~1 μm thick). The substrates coated with CZTS film were placed in quartz tubes (10 cm long with 1 cm inner diameter) along with 14 mg sulfur and evacuated to 10^{-6} Torr. The tubes were flame sealed and annealed at 600 °C for 1 hour.

4.2.6 Bacterial culture

Shewanella oneidensis MR-1 stock was a gift from the lab of Jeff Gralnick at the University of Minnesota. The bacteria were stored at -80 °C before being inoculated onto LB broth agar plates, which were incubated at 30 °C until use.

4.2.7 Colony-counting viability assays

Colony counting experiments were performed to assess the dose-dependent effect of the CZTS nanoparticles at 50 mg/L, 100 mg/L, and 200 mg/L concentrations.[32] Currently, there are no data regarding the environmentally relevant concentrations of CZTS, so we used a higher end concentration to assess the worst case scenario of accumulation of the particles in the environment as well as bioaccumulation. Bacteria liquid cultures were grown in Luria Broth media (Difco LB Broth, Miller) for 4 h at 30 °C to mid-log phase from colony inoculants on solid agar plates. Bacterial cells were harvested by centrifugation for 10 min at 2000xg, washed in Dulbecco's phosphate-buffered saline (D-PBS) buffer, and suspended in a HEPES buffer (2 mM HEPES and 25 mM NaCl, at pH 7.4). The cultures were then diluted to OD 0.2 at 600 nm (OD600) to achieve a cell density of approximately 2 x 10^8 colony-forming units (CFUs)/mL. Serial 10-fold dilutions of this bacterial suspension were performed at this stage to achieve a cell concentration of 10^4 CFUs/mL in HEPES buffer. The resultant diluted bacteria suspension was then treated with 5 nm CZTS nanoparticles at various concentrations (50 mg/L, 100 mg/L and 200 mg/L) and incubated for 15 min. An adapted drop-plate method was used for the *S. oneidensis* cells, where six 10 µL droplets of the exposed bacterial suspensions as well as untreated negative controls were dropped on an LB-agar plate, which had been pre-sterilized under UV-illumination for 20 min. The droplets were dried under air flow in a biological cabinet and were incubated at 30 °C for 20 hours before colonies were counted using a Bantex Colony Counter 920A. The viability of cells from each treatment was reported as a ratio to the control samples. The experiments were done using three materials replicates of CZTS nanoparticles repeated three times (three biological replicates) for each batch of particles.

4.2.8 Ion dissolution quantification

Ion dissolution from the CZTS nanoparticles over time in suspension was quantified using inductively coupled plasma mass spectrometry (ICPMS). The nanoparticles were incubated in HEPES media for 15 min at the same concentrations (50 mg/L, 100 mg/L, and 200 mg/L) that were used for the bacterial viability studies. After the incubation, each suspension was centrifuged using an ultracentrifuge at 61579xg for 30 min at 4°C. The resultant supernatant was collected and used for ICPMS. The ICPMS analyses were done on a Thermo Scientific XSeries-2 ICP-MS using CCT/KED more (Collision Cell Technology/Kinetic Energy Dispersion). The carrier gas is argon, and the CCT gas was a helium & hydrogen blend.

4.2.9 Ion-control experiments with *S. oneidensis*

The concentration of dissolved metal ions obtained from the ICPMS data was used to perform ion control experiments with bacteria so that nanoparticle-specific effects could be distinguished from soluble ion effects. Bacteria were exposed to equivalent concentrations of metal ions for 15 min, and colony-counting experiments were performed. $CuCl_2$, $ZnCl_2$, $SnCl_2$ and $SnCl_4$ were used as the source of the ions in these experiments.

4.2.10 Biological TEM analysis

Bacteria culture, with an OD of 0.8 at 600 nm in HEPES, was exposed to the nanoparticles at 100 mg/L concentration for 15 min, then pelleted, washed thrice with 0.1 M cacodylate buffer solution, and resuspended in a fixation buffer of 2.5% glutaraldehyde in 0.1 M

sodium cacodylate buffer and fixed for 50 minutes. The pellet was washed with sodium cacodylate buffer and dehydrated stepwise with a series of aqueous ethanol solutions of increasing concentration (30, 50, 70, 80, 90, 95, and 100% ethanol in water). After the washing steps with ethanol, the pellet was washed with propylene oxide three times, and the resin infiltration steps were performed. The pellet was soaked for 2 h in a 2:1 propylene oxide:epoxy resin mixture. This was replaced with a 1:1 propylene oxide: epoxy resin mixture, and the pellet was incubated in this mixture overnight. After this, the pellet was incubated in a fresh batch of 1:1 propylene oxide: epoxy resin mixture for 6 h, and finally placed in a pure resin mixture and infiltrated overnight. The resin sample was then cured in a 40 °C oven for one day and then 60 °C oven for two days. Ultrathin sections (65-nm-thick) were sectioned using a Leica UC6 microtome and Diatome diamond knife, then stained with uranyl acetate and lead citrate. These sections were placed on copper TEM grids (Ted Pella Inc.), and imaging was done using an FEI Tecnai T12 TEM.

4.2.11 Total ROS generation analysis

An abiotic assessment of ROS generation in HEPES buffer media (in absence of bacteria) was performed using the 2′,7′-dichlorofluorescin diacetate (DCFDA, also known as H_2DCFDA) assay.[37,38] DCFDA in DMSO stock solution (20 mM) was diluted 100-fold in HEPES buffer. Then, 50 μL of DCFDA working solution was mixed with 200 μL of CZTS nanoparticle solution of 50 mg/L, 100 mg/L and 200 mg/L. A negative control for the experiment was performed by adding the DCFDA solution to HEPES buffer, while a positive control experiment was done by adding the DCFDA solution to 1 M hydrogen peroxide solution. Each condition in the experiment was performed in triplicate in a 96-

well optical bottom plate (Costa, Corning, NY). The fluorescence counts were recorded by a Synergy 2 Multi-Mode microplate reader (BioTek, Winooski, VT) at Ex/Em: 485/525 nm for 2.5 h.

4.2.12 Short-term (15 min) incubation of thin films with bacteria

Bacteria were grown for 4 h in LB broth and then washed with DPBS and diluted in HEPES buffer to an OD of 0.2 (10^8 CFU/mL). 1 mL of the bacterial solution was dropped on top of the thin film (either annealed or unannealed), left to sit for 15 min, then pipetted out, and diluted to a cell concentration of 10^4 CFU/mL through serial dilution. The exposures were done simultaneously with 3 annealed and 3 unannealed thin films. The controls for the experiment included cells incubating on a soda-lime glass substrate without CZTS, as well as cells not exposed to anything. After the serial dilution, 10 μL aliquots of the bacterial suspensions were dropped on an LB-agar plate, including the negative controls, and the plates were incubated at 30 °C for 20 hours. The number of colonies on the plate corresponding to each exposure conditions were counted on the next day using a Bantex colony counter 920A.

4.2.13 Long-term (72h) incubation of thin films with bacteria

Since the bacterial cells do not remain viable in HEPES buffer for extended time periods, prolonged exposures were done in LB broth media and aqueous minimal media (buffered with 10 mM HEPES and containing 11.6 mM NaCl, 4.0 mM KCl, 1.4 mM $MgCl_2.6H_2O$, 2.8 mM Na_2SO_4, 2.8 mM NH_4Cl, 0.088 mM Na_2HPO_4, 0.051 mM $CaCl_2$, and 100 mM sodium lactate as nutrient source). For the experiments, the bacteria were grown in LB

broth overnight, then washed with DPBS and suspended in either LB broth or minimal media (depending on the final exposure media). The OD was adjusted to 0.2, and 1 mL aliquots of the diluted cell suspensions were pipetted into 9 mL of fresh media. The CZTS thin films were introduced into the culture tubes, and incubated in a rotary shaker at 30 °C for 72 h. The exposures were done simultaneously with 3 annealed and 3 unannealed thin films. The controls for the experiment included cells incubating on a soda-lime glass substrate without added CZTS, as well as cells not exposed to anything. After the 72 h time period, aliquots of the exposed bacterial suspensions were collected, diluted to cell concentrations of 10^4 CFU/mL, and the drop-plate colony counting assay was performed. Additionally, culture tubes with the media (without any bacteria) and the films were incubated simultaneously under the same conditions, and aliquots were collected and ICPMS was performed to assess any dissolution to constituent ions.

4.2.14 Thin film incubation with MQ water, HEPES and artificial seawater

CZTS thin films were incubated in three different media for 72 h; then, aliquots of the exposed media were collected and ICPMS was performed.

4.3 Results and discussion

4.3.1 Synthesis and characterization of CZTS nanoparticles and thin films

The synthesized nanoparticles were imaged with SEM (Figure 1). Figure 1a-d shows the top view and cross sections for CZTS NP films made from ~40-nm-diameter CZTS crystals before annealing and after annealing. The CZTS NP films were ~1-µm-thick before annealing and ~0.6-µm-thick after annealing. After annealing, the film grains grew to 250

± 100 nm. Figure 1e shows the SEM of ~5-nm-diameter CZTS NPs. EDS revealed near stoichiometric ratios of Cu, Zn, Sn, and S. Specifically, from EDS, the 5-nm-diameter CZTS NPs were composed of 26.4% Cu, 12% Zn, 12.5% Sn, and 49% S while the 40-nm-diameter CZTS NPs contained 24.8% Cu, 13% Zn, 13.2% Sn, and 49% S. After annealing, the films composed of 40-nm-diameter CZTS NPs were composed of 21.6% Cu, 11.1% Zn, 11.6% Sn, and 55.7% S.

X-ray diffraction from the NPs revealed the presence of the expected CZTS phase. Fig 2 shows the XRD from the 5-nm-diameter CZTS NPs, 40-nm-diameter CZTS NP films, and 40-nm-diameter CZTS NP films after annealing. All XRD diffraction peaks match with diffraction from the CZTS kesterite phase (ICDD ref 00-026-0575). The diffraction peak widths decrease with increasing NP size and with annealing treatment. Larger NPs and annealed NPs have larger crystals with more planes available to strengthen the diffraction signal. The number of matching diffraction peaks to CZTS increases with NP size and with annealing treatment. Both the 5-nm-diameter NPs and films made from 40-nm-diameter NPs show diffraction from the (112), (220), and (312) planes, but the films with 40-nm-diameter NPs also show diffraction from the (200) and (224) planes. Annealing the films with 40-nm-diameter NPs results in additional diffraction from the (110), (103), (202), (211), (224), and (008) planes. The CZTS diffraction pattern shares similar peaks with ZnS and tetragonal Cu_2SnS_3. However, the diffraction peaks from (202) and (211)were absent in ZnS and were small in tetragonal Cu_2SnS_3.Therefore, the CZTS phase was confirmed in the annealed films with 40-nm-diameter NPs.

To confirm the phase of the 5-nm-diameter NPs and films with 40-nm-diameter NPs, Raman spectroscopy was performed. XRD combined with Raman spectroscopy can unambiguously confirm the CZTS phase. Figure 3 shows the Raman spectra for 5-nm-diameter NPs, films with 40-nm-diameter NPs, and films with 40 nm NPs after annealing. All three spectra reveal the characteristic peak for CZTS at ~336-338 cm^{-1}. This can be assigned to the A mode of kesterite CZTS. The 5-nm-diameter CZTS NPs exhibit a weak, broad peak due to phonon confinement in smaller nanoparticles. Taken together, the CZTS phase was confirmed within the detection limits of EDS, Raman spectroscopy, and XRD.

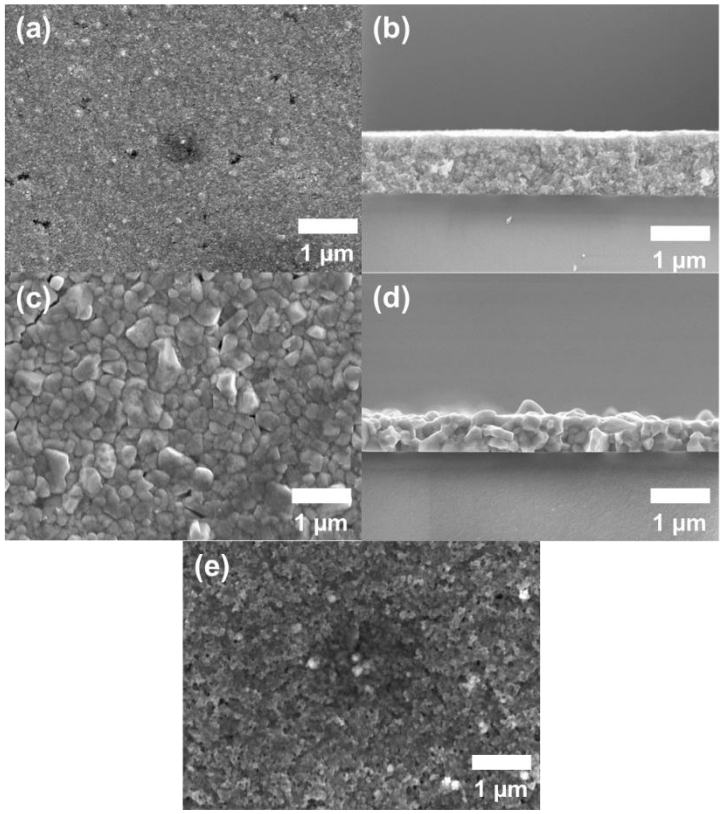

Figure 1: Scanning electron micrograph top view and cross sections for 40-nm-diameter CZTS NP films (a,b) before annealing and (c,d) after annealing 600°C for 1 hour. (e) Scanning electron micrograph for 5-nm-diameter CZTS NPs.

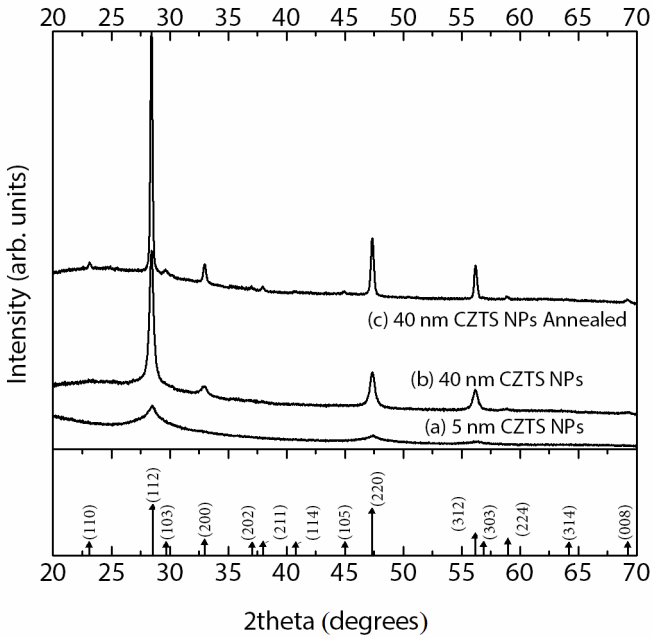

Figure 2: X-ray diffraction spectra of (a) 5-nm-diameter CZTS NPs, (b) film with 40-nm-diameter CZTS NPs, and (c) film with 40-nm-diameter CZTS NPs annealed at 600 °C for 1 hour.

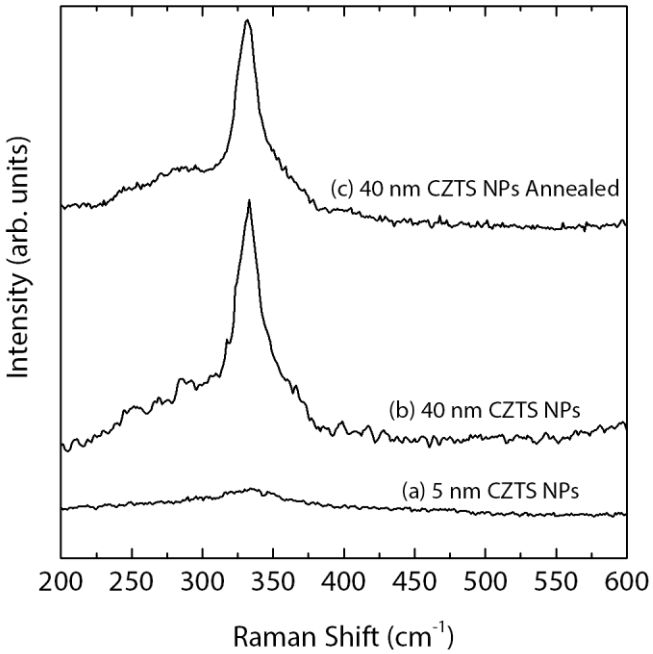

Figure 3: Raman spectra of (a) 5-nm-diameter CZTS NPs, (b) film with 40-nm-diameter CZTS NPs, and (c) film with 40-nm-diameter CZTS NPs annealed at 600 °C for 1 hour.

4.3.2 Bacterial viability assays and investigation of mechanisms of toxicity

4.3.2.1 Colony-counting viability assays

Drop-plate colony counting assays were performed to assess bacterial cell viability after exposure to CZTS nanoparticles. The concentration of bacterial cells at which distinct and non-overlapping colonies can form was first ascertained, and the diluted bacterial suspensions were exposed to CZTS nanoparticle solutions at increasing concentrations of 50 mg/L, 100 mg/L and 200 mg/L. Since the number of colonies that form on the LB-agar plate after 20 h incubation indicate the number of viable cells that were present in the suspension during nanoparticle exposure, any decrease in the number of colonies as compared to the negative controls indicates toxic effects of nanoparticles or nanoparticle transformation products.

In this experiment with aqueous CZTS (5-nm-diameter) nanoparticle suspension, significant toxic effects to the bacterial viability were observed. Also, an increase in the toxic effect was observed over time, depending on how long after the synthesis the nanoparticle suspension was used, indicating that the CZTS nanoparticles transformed as they aged. Bacterial exposure experiments were performed after 2 days, 2 weeks, and 7 weeks after the initial synthesis of the nanoparticles to characterize this effect, and the results are shown in Figure 4. The experiments were repeated with 2 material replicates, twice (2 biological replicate for each material replicate) and 3 analytical replicates for every experiment. Statistical analysis for these experiments was performed using one-way ANOVA, followed by post-hoc Tukey's multiple comparisons tests (GraphPad Prism software, La Jolla, CA). All values plotted are the mean ± standard deviation (SD), and the statistical significance is indicated using asterisks (p values < 0.0001 indicated by ****,

0.0001 to 0.001 indicated by ***, 0.001 to 0.01 indicated by **, and 0.01 to 0.05 indicated by *).

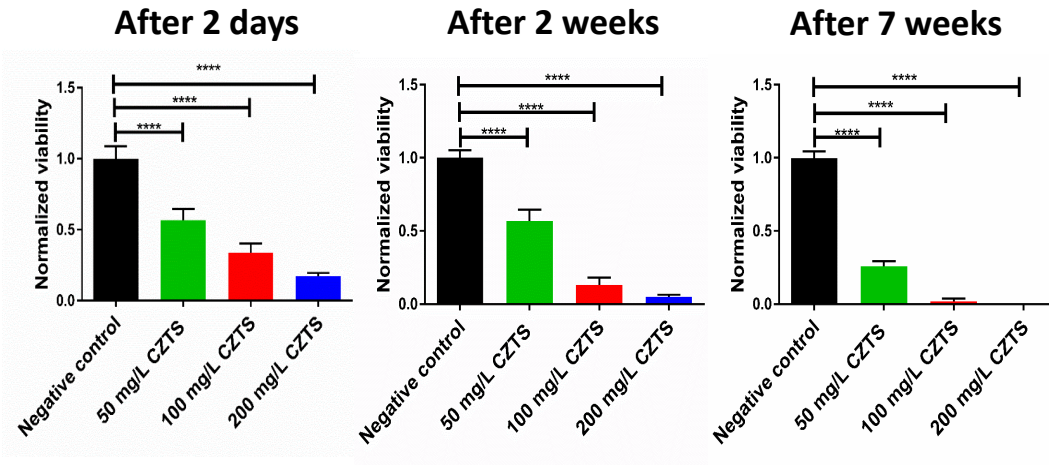

Figure 4: Bacterial viability of S. oneidensis in the presence of CZTS nanoparticles after various post-synthesis ageing times (as noted) assessed using drop plate colony counting.

It is clear from the data in Figure 4 that the CZTS nanoparticles become more toxic to the bacteria as they age following synthesis. The observed toxicity can be due to a number of factors such as the effect of dissolved ions, disruption of cell surface structures, or reactive oxygen species generation. The observation with other nanomaterials of increasing toxicity over time due to gradual ion dissolution has been reported in other studies.[39,40]

4.3.2.2. Ion dissolution quantification

To assess the concentration of dissolved ions in solution, the nanoparticle suspensions were incubated in HEPES buffer, and then ultracentrifuged to separate out the nanoparticles. The supernatants were collected, and the presence of dissolved metal was quantified using

ICPMS. The data are shown in Figure 5.

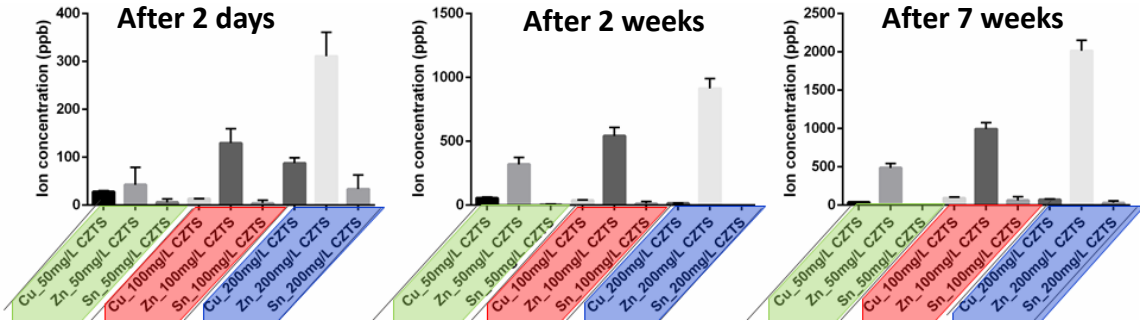

Figure 5: Dissolved metal concentrations as obtained by ICPMS technique in CZTS nanoparticle suspension 2 days, 2 weeks and 7 weeks after initial nanoparticle synthesis. Note the different y-axis scale bars between the 3 different timepoints.

An increasing trend in the dissolution of Zn was observed with increased concentration of CZTS suspension as well as increased time gap after synthesis.

4.3.2.3 Ion-control experiments

Bacteria viability was monitored in the presence of metal ions, using ion concentrations as obtained from ICPMS in the previous section. On exposure to only Zn^{2+} ions, no significant deccrease in bacterial cell viability was observed, except in the case of the highest concentration of Zn^{2+} ions at 2011.7 ppb, where the viability was still at 81% After the addition of Cu^{2+} ions along with the Zn^{2+} ions, drastic decreases in cell viability were observed (Figure 6). Synergistic toxicity of heavy metals such as copper and zinc is a possibility and has been reported previously.[41] The effects of heavy metals such as copper and zinc on microorganism growth are widely studied in literature.[42] Heavy metals can inhibit cellular functions through oxidizing vital enzymes or interacting with DNA. Even

though copper is an essential micronutrient for living organisms, it is also known for its antimicrobial properties. Cu^{2+} ions can bind with the sulfhydryl groups in proteins and enzymes, and thus hinder normal cellular metabolism.[43] Zn^{2+} ions can prohibit the function of the Mg^{2+} transporter MgtA by competing as substrates.[44] These effects can contribute to the toxic effects the CZTS nanoparticle suspension as a result of production of dissolved ions. However, the cell viability decrease measured in the CZTS nanoparticle suspension is still not completely explained by the presence of Cu^{2+} and Zn^{2+} ions. The ion exposure experiments were repeated twice (two biological replicate) with three analytical replicates for each condition both times. Statistical analysis for these experiments was performed using one-way ANOVA, followed by post-hoc Tukey's multiple comparisons tests (GraphPad Prism software, La Jolla, CA). All values plotted are the mean ± standard deviation (SD), and the statistical significance is indicated using asterisks (p values < 0.0001 indicated by ****, 0.0001 to 0.001 indicated by ***, 0.001 to 0.01 indicated by **, and 0.01 to 0.05 indicated by *).

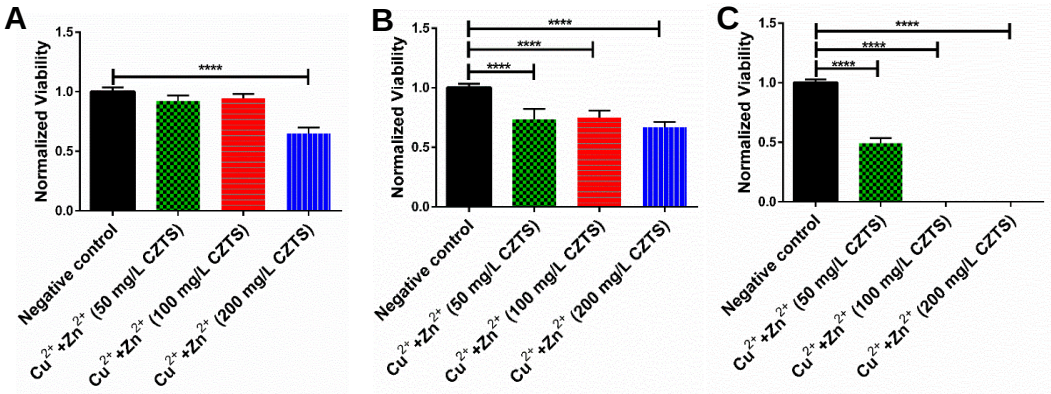

Figure 6: Bacterial viability results after being exposed to Cu^{2+} and Zn^{2+} ion concentrations corresponding to 50 mg/L, 100 mg/L and 200 mg/L CZTS nanoparticle concentration at A. 2 days, B. 2 weeks and C. 7 weeks after nanoparticle synthesis.

One thing to keep in mind is that the slow release of ions from the nanoparticles might have a different impact to the bacterial viability than a single dose of ions as is used in case of the ion control experiments.

Only small amounts of tin were detected in the supernatant, and we were interested in assessing the effect of tin ions on bacteria. However, most tin compounds are reported to be polar covalent, so ion control experiments with tin compounds is difficult. We attempted to use both $SnCl_2$ and $SnCl_4$ as our tin ion controls, but any effects observed could be due to the compound rather than the tin ions. On introduction of these compounds separately to the bacterial suspension, an increase in toxicity was observed compared to the Cu^{2+} + Zn^{2+} controls. The toxic effect of the combined ions after the addition of the tin compounds was even more than what was observed in presence of the nanoparticle suspension. This result further suggests the hypothesis that the toxic effect observed after addition of the tin compounds is caused by the tin compounds as a whole rather than the Sn components of the CZTS.

4.3.2.4 Biological TEM analysis

Biological TEM helps with the qualitative assessment of nanoparticle interaction with bacterial cells and provides an excellent tool to visualize any association of nanoparticles with cells. Figure 7 shows the results obtained after treating the *S. oneindensis* cells with 100 mg/L of CZTS nanoparticle suspensions.

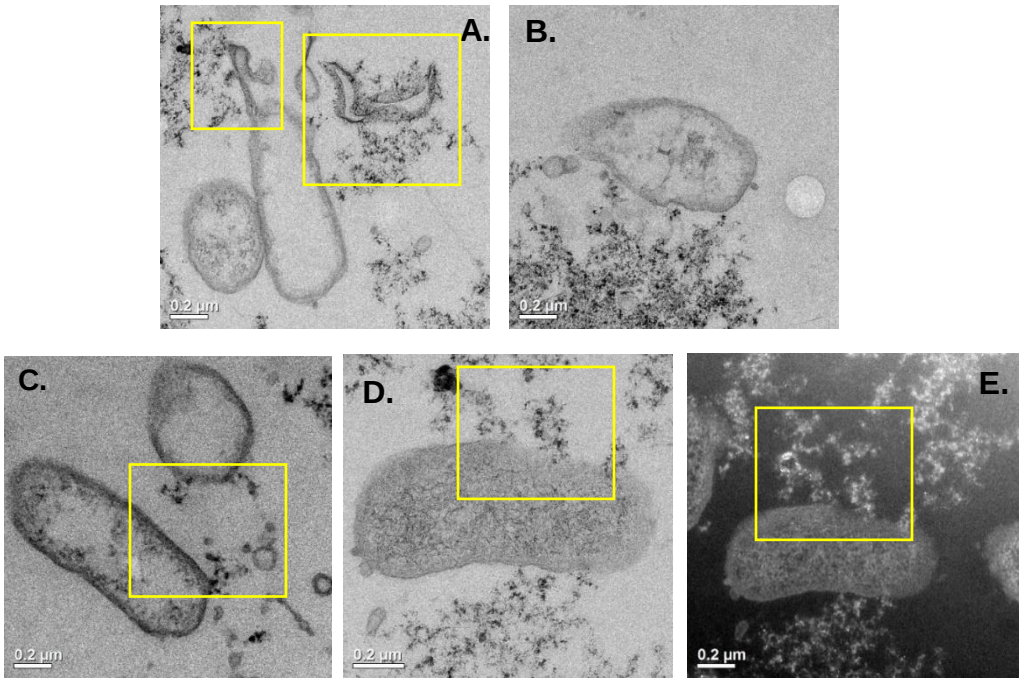

Figure 7: Biological TEM images of S. oneidensis after being exposed to CZTS nanoparticles exhibiting A. severe cellular membrane damage and B. association of nanoparticles with the bacterial cell membrane. C. and D. show more cell membrane association of nanoparticles and E. is the dark-field counterpart of D.

As seen in the images, the CZTS nanoparticles inflict severe damage on the *S. oneidensis* cells. In image A (Figure 7), the nanoparticle clusters are pulling at the cell membrane, and a disintegrated cell membrane structure surrounded by nanoparticles is observed as well. The other images show nanoparticle association with the cell membrane, and as seen in image C, partial disruption of the cell membrane. Image E is a dark field version of the bright field image D. Dark field TEM imaging can be helpful in identifying nanoparticles in a biological matrix, due to the electron scattering from nanoparticles with high mass and crystallinity as opposed to the matric around them, which makes them light up.[45] It is evident from the images that the association of the nanoparticles with the bacterial cells

contributes to severe damage of the cell structures, likely having an effect on cell viability. These are representative images obtained after investigating at least 20 bacterial cells on 2 TEM grids.

4.3.2.5 ROS generation assay

Semiconductor nanoparticles such as CIGS and CdSe have been reported to produce reactive oxygen species through the formation of e^-/h^+ pairs by moving electrons from its valence band to its conduction band.[46,47,48] This is especially likely in CZTS materials with a small band gap of 1.5 eV. While ROS is naturally occurring and managed in biological systems, excess ROS can be extremely harmful as they may induce macromolecule oxidation, changes in gene transcription, as well as damage to cell organelles.[49]

The DCFDA assay was performed to assess the ROS generation from 5-nm-diameter CZTS nanoparticles. As observed from Figure 8A, dose-dependent ROS generation was observed. To obtain a clear view of the CZTS nanoparticle ROS generation plots, the data was plotted without the very large positive control response to 1 M hydrogen peroxide solution (Figure 8B). From this plot, it is evident that there is a progressive increase in the ROS generation over the incubation time. Based on this data, it can be inferred that CZTS nanoparticles produce ROS, and the amount of ROS generated is directly related to the nanoparticle concentrations and incubation times.

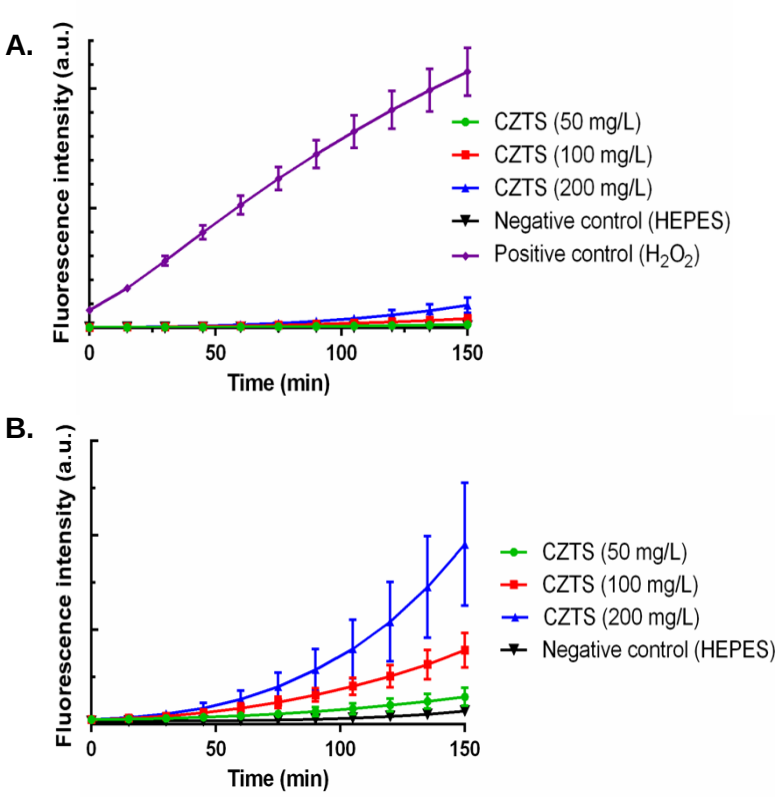

Figure 8: A. Abiotic ROS generation by CZTS nanoparticles assessed using the DCFDA assay. B. Data as shown in 8A, but without the positive control to get a clear look at the CZTS-specific ROS generation. The fluorescence intensity is reported in arbitrary units (a.u.). Each condition was repeated three times in 96-well optical bottom plates (Costa, Corning, NY).

4.4 Bacterial incubation with CZTS thin films

Toxicity studies are generally done using nanoparticle suspensions, and it's not common to assess the toxicity of nanoparticle-based thin films. As p-type absorber material in solar cells, CZTS nanoparticles will be potentially used in commercial products as thin films. Thus, at the end of their life when they were disposed of, they may enter the environment as thin films. It is of interest to assess how these thin films will behave in different media as well how they will affect bacterial viability.

4.4.1 Short-term exposure with 40-nm-diameter CZTS nanoparticle thin films

After short-term exposure of *S. oneidensis* bacterial suspension on CZTS (40-nm-diameter) thin films for 15 min, the bacterial cells were collected, diluted, and 10 µL aliquots dropped

on LB-agar plates. After overnight incubation, no changes in bacterial viability (number of colonies formed) was observed when compared to the negative controls. The experiment was done with three annealed and three unannealed films, along with three glass substrates.

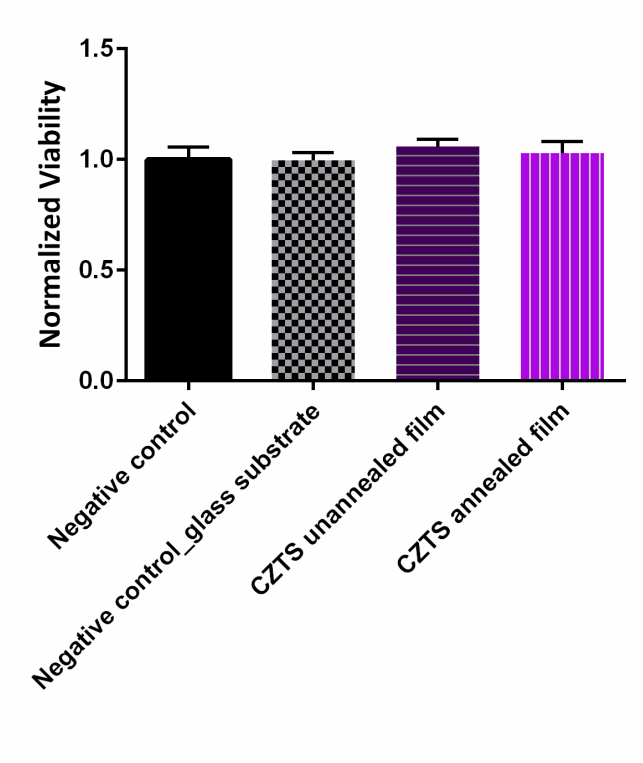

Figure 9: No significant toxic effect was observed upon incubating the bacterial suspension over nanoparticle-assembled CZTS thin films for 15 min.

4.4.2 Long-term exposure with 40-nm-diameter CZTS nanoparticle thin films

For a longer term comparison, the thin films, both annealed and unannealed, were incubated in the presence of bacterial cells in nutrient-rich LB medium as well as relatively nutrient-sparse minimal media with lactate. The exposures were carried out for 72 h, and the 10 μL droplets of the exposed bacterial suspensions were placed on LB-agar plates, and standard colony counting assays were performed. Also, ICPMS was performed on media exposed to the thin films under same conditions without the bacteria to characterize any dissolution from the thin films.

For both the LB-broth media and minimal media, no significant differences in colony counts were observed in comparison to the negative controls even after 72 hours of exposure. In LB-broth, ion dissolution was quantified using ICPMS. The ion dissolution data is shown in Figure 10A. We hypothesize that even if the dissolved ions had a detrimental effect on some portion of the first generation of cells, the surviving bacteria were able to recover in subsequent generations after a long exposure, especially in the presence of nutrient-dense LB broth. Surprisingly, no significant toxic effect was observed in a nutrient sparse minimal media either (Figure 11). Figure 11A shows the ion dissolution data of the thin films in minimal media. From the ion dissolution data, it can be concluded that the unannealed films leach more copper and zinc ions whereas the annealed films leach more tin. Statistical analysis for these experiments was performed using one-way ANOVA, followed by post-hoc Tukey's multiple comparisons tests (GraphPad Prism software, La Jolla, CA). All values plotted are the mean ± standard deviation (SD), and the statistical significance is indicated using asterisks (p values < 0.0001 indicated by ****, 0.0001 to 0.001 indicated by ***, 0.001 to 0.01 indicated by **, and 0.01 to 0.05 indicated by *).

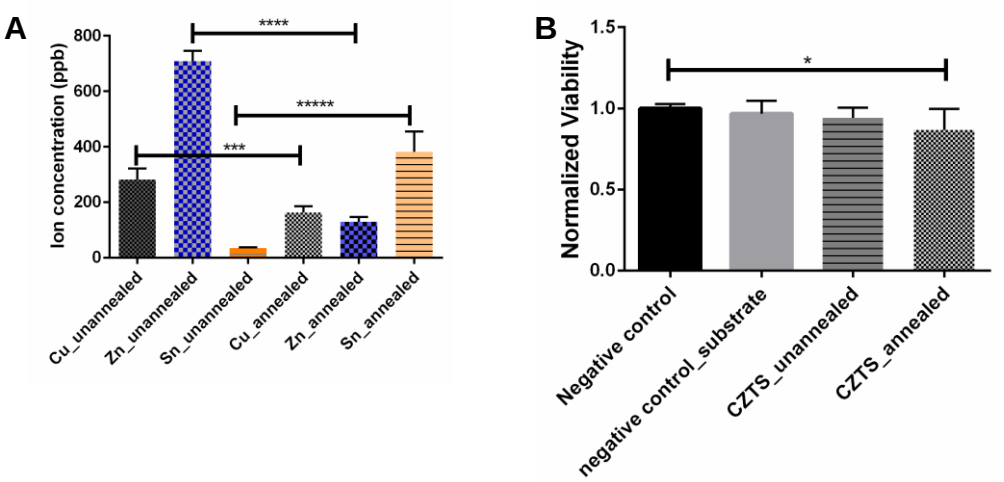

Figure 10: A. Ion dissolution from the unannealed and annealed in LB broth media is shown. B. No significant loss in viability is observed in case of the unannealed films. And only a slight loss in viability is observed in case of the annealed films.

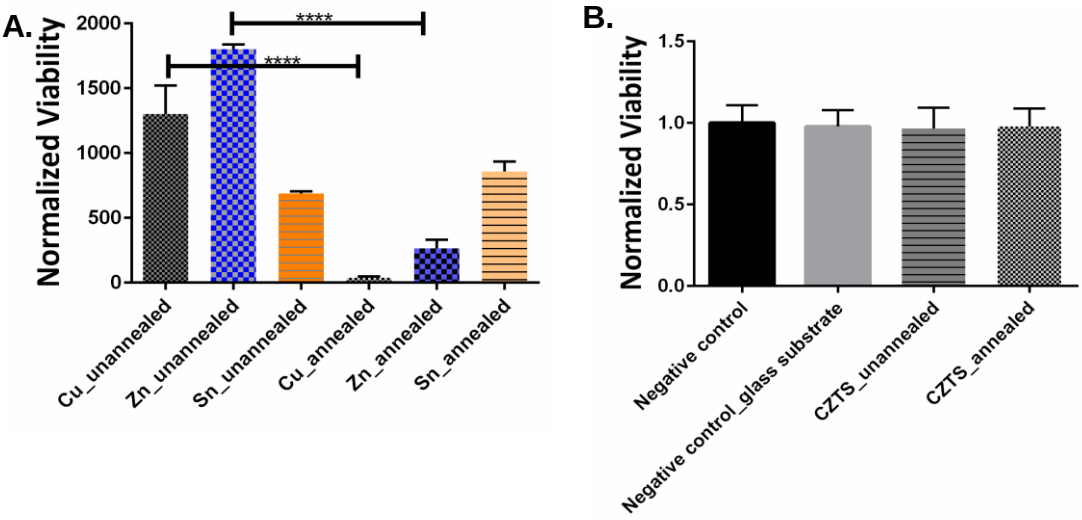

Figure 11: A. Ion dissolution from the unannealed and annealed in minimal media is shown. B. No significant loss in viability is observed in case of the unannealed or annealed films.

Thus, even though serious toxic effects were observed in *S. oneidensis* on exposure to 5-nm-diameter CZTS nanoparticle suspension, in the case of the thin films made with 40-nm-diameter particles, no toxicity was observed in the time frame of our experiments. This is a partially positive development in terms of using CZTS thin films, especially since no toxic effect was observed even in minimal media, which mimics the nutrient-scarce natural environment. It will be interesting to see future work involving other, more complex organisms, as well as gene expression studies.

4.4.3 Long-term exposure with 5-nm-diameter CZTS nanoparticle thin films

5-nm-diameter CZTS particles are generally not considered as good candidates for thin film preparation due to their tendency to produce cracks in the thin films leading to shorts.[36] However, similar experiments were completed with thin films made from 5-nm-diameter CZTS nanoparticles to explore any difference in dissolution and toxicity of these particles in thin films compared to the 40-nm-diameter nanoparticle thin films.

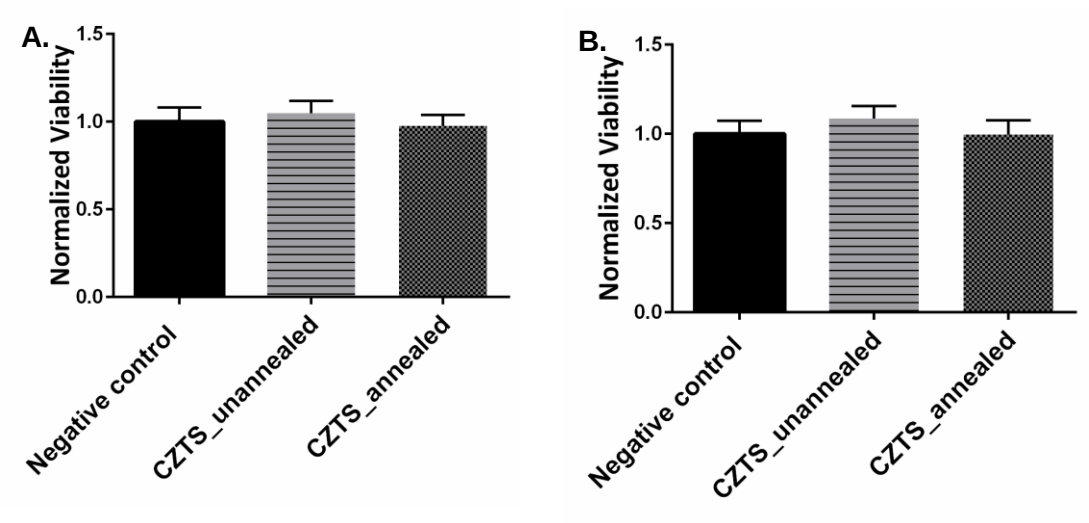

Figure 12: No significant loss in viability is observed in case of the unannealed or annealed films made using 5-nm-diameter CZTS nanoparticles in A. LB media or B. minimal media over a time period of 72h.

As with the 40-nm-diameter CZTS nanoparticle thin films, no significant loss in bacterial viability was observed in either LB or minimal media. Thus, it can be concluded that thin films made out of 5-nm-diameter nanoparticles as well as 40-nm-diameter nanoparticles do not pose any viability threats to *S. oneidensis* bacteria in the 72 h time period. The incubations were performed using three each of annealed and unannealed films in the presence of bacteria in LB media in separate culture tubes, and the resulting bacteria from each tube were washed and dropped on three LB-agar plates to assess their viability. All values plotted are the mean ± standard deviation (SD), and the statistical significance is indicated using asterisks (p values < 0.0001 indicated by ****, 0.0001 to 0.001 indicated by ***, 0.001 to 0.01 indicated by **, and 0.01 to 0.05 indicated by *).

4.4.4 CZTS thin film exposure to different media

CZTS thin films (annealed and unannealed) were incubated in three different media for 72 h to assess their stability and dissolution properties. The media used were MQ water (pH 7.2), HEPES buffer (pH 7.4), and substitute seawater (pH 8.08). The substitute seawater was obtained from Ricca Chemical that's prepared following the ASTM D1141 protocol.

After incubating the films in these media for 72 h, supernatants were collected and ICPMS performed (Figure 13). The results showed that the films showed more dissolution in MQ water than in HEPES or seawater. In MQ water, the unannealed films showed more copper and zinc dissolution, and the annealed films showed more tin dissolution. In both HEPES and seawater the unannealed films showed significant zinc dissolution (though much less than in water). The higher ionic strength in HEPES and seawater, than MQ water, possibly contributes to the decrease in dissolution of the thin films as ions.

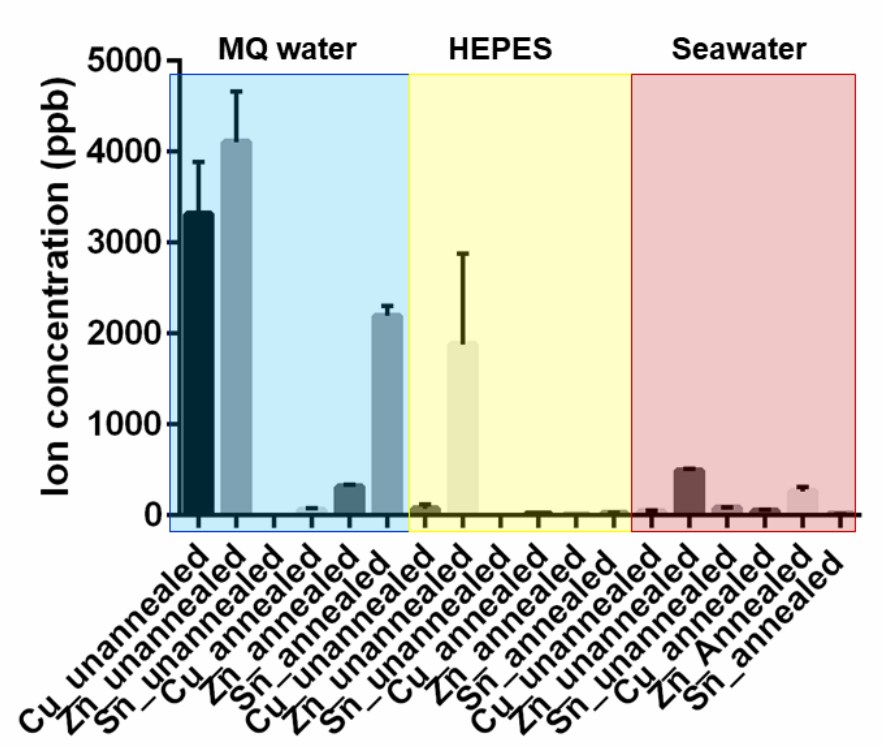

Figure 13: Dissolution data of thin films in MQ water, HEPES media and substitute seawater as obtained from ICPMS.

4.5 Conclusion

The 5-nm-diameter CZTS suspension posed significant toxicity to the bacteria model *S. oneidensis MR-1*. Dissolved ions in the suspension were partially responsible for the toxicity of the nanoparticles. Association of the nanoparticles with bacterial cells were observed using biological TEM, and significant cellular damage was noticed. Dose-dependent generation of ROS was observed under abiotic conditions. Thus the presence of dissolved ions, in conjunction with NP-inflicted damage to cell structures and ROS are responsible for the observed toxicity of CZTS. The 40-nm-diameter thin films, either annealed or unannealed, did not pose significant toxicity to the bacterial cells for a short term (15 min) or long term (72 h) exposure. Even though ion dissolution was observed, they did not pose any toxic effect on the bacterial cells, or at least there was significant recovery in the 72 h time period in the nutrient-rich media. Similar results were obtained from experiments performed with 5-nm-diameter CZTS thin films as well. Thus, it can be concluded that the size of the NPs did not affect their toxicity in the thin film form within the experimental timeframe considered here. Since thin films are more likely to be introduced into the environment than nanoparticle suspensions, this is an optimistic development from an environmental point of view.

Chapter 5

Viability Studies and Mechanistic Assessment of the Toxicity of Cadmium-based and Cadmium-free QDs on a Panel of Bacteria

This work is in collaboration with Denise N. Williams and Prof. Zeev Rosenzweig.

5.1 Introduction

Nanotechnology as a field of research and industry has been growing rapidly in the last 20 years. One of the novel and unique types of nanoparticles are quantum dots (QDs). QDs are nanocrystals made of semiconducting materials that show size-dependent photoluminescence due to quantum confinement effects. Due to their unique properties, there is a lot of research focusing on their applications in areas like optoelectronics and nanodiagnostics.[1] These applications include the use of these QDs in devices such as electronic screens (backlighting of liquid crystal displays), solar cells, light emitting devices (LEDs), and photodiodes. Research is also ongoing to explore their application in biomedical imaging.[2] With this increase in interest and applications, there is a high possibility that these QDs will end up in the environment (through wastewater streams or landfills). As such, it is important to explore and understand how the QDs will behave once they get into the ecosystem.

Cd-based QDs are the most commonly used, but the presence of Cd makes them less ideal than many alternative semiconducting materials due to concerns about their effects on the environment. Cd^{2+} is a known carcinogen to humans, and can also cause DNA damage in cells through oxidative stress while inducing mitochondrial damage and apoptosis.[3]

In chapter 3, we explored the comparative toxicities and associative interactions of 4 different QDs with a bacterial model: CdSe cores, CdSe/ZnS, ZnSe cores and ZnSe/ZnS.[4] The Cd-based QDs proved to be significantly toxic to the model bacteria *Shewanella oneidensis* MR-1, whereas the Zn-based QDs were non-toxic under the conditions

considered. Interestingly, the CdSe/ZnS QDs proved to be more toxic than the bare CdSe cores, even though it has been reported that addition of a shell can mitigate the toxicity.[5] It has also been reported that the main source of toxicity in CdSe/ZnS QDs is due to their association with the cell surface.[6] In chapter 3 we examined both Cd dissolution and QD association with bacterial cells. While no Cd dissolution was observed under the experimental conditions, associative interactions of the QDs with the cell surface and damage to the cells were noted.

In the present study, we focus in on the Cd-based QDs and Cd-free QDs to assess if the results obtained were specific to *S. oneidensis* MR-1 bacterial cells, or if they are generalizable across other bacteria; accordingly, a panel of three Gram-negative, environmentally relevant bacteria was employed.[7] The three bacterial strains are *Acinetobacter baylyi* ADP1, *Shewanella oneidensis* MR-4, and *Pseudomonas aeruginosa* PAO1. *A. baylyi* are aerobic, non-pathogenic, and found in soil and aquatic environments. They are able to metabolize plant degradation products.[8] *S. oneidensis* MR-4 exhibit metal-reducing properties (like *S. oneidensis* MR-1) and can dissimilate and metabolize many different metals.[9] *P. aeruginosa* PAO1 is a ubiquitous bacteria and has great metabolic diversity.[10] It is important to note here, even though all these bacteria metabolize exogenous substances, only *S. oneindensis* MR-4 can respire and metabolize metals. Since, bacterial association is an important pathway for toxicity in this context, it is important to understand the difference in the cell surface of these three bacteria.[11] Gram-negative bacterial surfaces present lipopolysaccharides (LPS), which play an important role in their association with foreign materials such as nanoparticles. Smooth LPS is composed of an O-antigen (O-Ag), complete core oligosaccharides, and the lipid A, while rough LPS lacks

O-Ag but possesses lipid A and progressively shorter core oligosaccharides.[12] Out of the four bacteria, *P. aeruginosa* and *A. baylyi* have smooth LPS, whereas *S. oneidensis* MR-1 and *S. oneindensis* MR-4 have rough LPS.

To assess the toxicity of the four different QDs (CdSe, CdSe/ZnS, ZnSe, and ZnSe/ZnS) on three different bacteria, a drop plate colony counting assay was employed.[13] Any interaction between the bacterial cell surface with the QDs was investigated using biological TEM imaging. It is also of interest to assess the mechanistic pathways of the toxicity utilizing gene expression studies, so gene expression studies employing qPCR techniques will be performed in the future.

5.2 Methods

5.2.1 Synthesis of QDs

5.2.1.1 CdSe and CdSe/ZnS QD synthesis. CdSe QD were synthesized according to a previously reported procedure.[14] The reaction was carried out in a 50 ml three-neck round bottom flask under stirring. A cadmium precursor solution was prepared by dissolving 5.0 grams hexadecylamine in a 10 mL trioctylphosphine (TOP) solution that also contained 2.1 mmol tetradecylphosphonic acid, and 1.0 mmol of CdAcAc (cadmium acetylacetonate). The solution was heated to 100°C under inert nitrogen gas until the reactants to fully dissolve. The flask was under vacuum for 30 min, then backfilled with nitrogen gas. The solution was heated to 250°C, cooled back down to 100°C and vacuumed again for 30 minutes. After backfilling with nitrogen, the vessel was heated to 300°C. A 5 mL selenium precursor solution, which contained 0.84 M selenium powder in TOP, was

injected rapidly into the reaction mixture. The CdSe QD formed instantly and the reaction mixture was cooled to 80°C for overnight annealing. The resulting CdSe QD were stored in the reaction mixture at room temperature and away from light. CdSe/ZnS QD were synthesized using successive ionic layer adsorption and reaction (SILAR). SILAR calculation and shelling was carried out following a previously described protocol where 0.3nm radius monolayers of a ZnS shell are added one at a time.[15] 0.15 μmoles of washed CdSe QD were added to a solution that contained 6 ml ODE, 4 ml TOP, 6 ml oleylamine, and 10 mg of dodecylphosphonic acid in a 50 ml round bottom flask under nitrogen gas. The solution was heated and kept at 100°C under high vacuum. The flask was backfilled with nitrogen gas. Then, the first aliquot of zinc precursor (0.05 M zinc formate in oleylamine), which was calculated from the core size to add a 0.3 nm radius monolayer of a ZnS shell, was injected over 15 minutes. The reaction mixture was heated and kept at 160°C, and an aliquot of sulfur precursor (0.25 M $(TMS)_2S$ in TOP) was injected over 15 minutes to form the first monolayer of ZnS shell. The QD were then annealed at 160°C for 20 minutes. The reaction mixture was heated and kept at 170°C while the process of adding zinc and sulfur precursors over 15 minutes and annealing over 20 minutes was repeated. The shelling process was repeated, each time at 10°C higher temperature until the desired ZnS shell thickness was realized. Finally, the reaction mixture was heated and kept at 200°C and 0.5 ml oleic acid was added dropwise over one hour. The reaction mixture was then allowed to slowly cool to room temperature.

5.2.1.2 ZnSe and ZnSe/ZnS QD synthesis. ZnSe and ZnSe/ZnS QD were synthesized according to a previously reported procedure.[14] The reaction was carried out in a 25 ml

three-neck round bottom flask under stirring. The zinc precursor solution was prepared in the round bottom flask by dissolving 632 mg (1 mmol) ZnSt powder in 5.0 mL of ODE at 120°C under inert nitrogen gas. The three-neck flask was vacuumed out for 30 minutes and then backfilled with nitrogen gas while heating the solution to 280°C. A selenium precursor solution was prepared by dissolving 7.9 mg selenium powder in a solution containing 17 µl DPP and 670 µL toluene (selenium concentration of 0.15 M). This selenium solution was injected rapidly into the reaction mixture and allowed to react for 5 minutes at 280°C before cooling the flask to room temperature. A second selenium precursor solution was prepared by dissolving 78.9 mg selenium powder in 800 µl TOP (selenium concentration of 1.0 M). This selenium precursor solution was injected into the reaction mixture at room temperature. The reaction mixture was heated and kept at 280°C for 20 minutes, then cooled down to room temperature. The formed ZnSe QD were immediately coated with a ZnS shell or stored in their reaction mixture at room temperature and away from light. Two precursor solutions were prepared for the ZnS shelling: 1) 32.1 mg sulfur powder in 1 ml TOP (sulfur concentration of 1.0 M), and 2) 632 mg (1.0 mmol) of zinc stearate dissolved in 8 ml ODE. The ZnS shell precursor solutions were injected into the reaction mixture at room temperature. The reaction mixture was then heated, kept at 280 °C for 20 minutes, and finally cooled to room temperature. The resulting ZnSe/ZnS QD were stored in the reaction mixture at room temperature and away from light. Prior to their immediate future use, QD were washed multiple times to remove excess reactants.

5.2.1.3 Capping luminescent QD with DHLA-PEG750-OCH_3 ligands. Luminescent QDs were capped with DHLA-PEG750-OCH_3 ligands (MW= 927 g/mol) (DHLA is dihydrolipoic acid) to enable their aqueous solution miscibility.[16] These are the same ligands that were used for capping the QDs discussed in Chapter 3. The ligand exchange process used to prepare the DHLA-PEG750-OCH_3-coated QDs removed some TOPO ligands from the QD surface and shielded the remaining ones from interacting with bacterial cells. This is an imperative step to minimize the ligand contribution to QD toxicity since TOPO ligands have been shown to be highly toxic.[17] The ligand exchange was carried out by following a previously reported procedure. The DHLA ligand (0.25 mmol), 0.5 mmol sodium hydroxide, 0.13 mmol zinc acetate, and 1 mL of methanol were sonicated together in a septum-closed vial filled under nitrogen gas. 10 nmol of purified QDs were dissolved with a minimal amount of chloroform, dried under vacuum, and put under a flow of nitrogen. The DHLA ligand solution was added to the QD solution, and then left overnight at 50 °C under nitrogen gas. The next day, 1 mL of ethyl acetate and enough hexane to separate solvents into two distinct layers were added to the QD, stirred, and allowed to separate. The hexane layer was removed to waste. The QDs in the ethyl acetate layer were dried under vacuum, and then dispersed in Millipore water. The QD solution was passed through a 0.45 SFCA syringe filter into a 30,000 MWCO spin filtration device for washing using three centrifugation cycles at 2000xg for 5 minutes at room temperature.

5.2.2 Bacterial Culture and Colony Counting when Exposed to QD

Shewanella oneidensis MR-4 was obtained from Daad Saffarini (Dept of Biological Sciences, University of Wisconsin – Milwaukee). *Acinetobacter baylyi* (ATCC®

33305™), and *Pseudomonas aeruginosa* (ATCC® 47085™) were purchased from the American Type Culture Collection (Manassas, VA). Bacteria were stored in a -80 °C freezer. When needed, bacteria were cultured by streaking an LB-agar plate with bacteria and then incubating the plate in a 30 °C incubator overnight. Liquid cultures were grown by transferring colony inoculants from the plate to 10 mL of LB broth and incubating for 4 hours at 30 °C in an orbital shaker, to their mid-log phase. Cells were then harvested by centrifugation for 10 minutes at 2000xg, washed in Dulbecco's phosphate-buffered saline (D-PBS) buffer, and suspended in a HEPES buffer (2 mM HEPES and 25 mM NaCl, at pH 7.4). The cultures were then diluted to 0.2 OD at 600 nm (OD600) to achieve a cell density of approximately 2 x 10^8 colony-forming units (CFUs) /mL. Serial 10-fold dilutions of this bacterial suspension were performed to achieve a cell concentration of 10^3 CFUs/mL in HEPES buffer. The resultant diluted bacteria suspension was treated with QDs, in a total volume of 150 µL, at varying concentrations of 0.5-5 mg/L of core cadmium or zinc concentration. The QD-exposed cells were incubated on rotary shaker for 15 minutes, and then the viability of *Shewanella oneidensis* MR-1 bacteria was determined using a drop-plate colony-counting protocol.[18] Six 10 µL droplets of the exposed bacterial suspensions and untreated negative controls were dropped on an LB-agar plate, which were pre-sterilized under UV-illumination for 20 minutes. The droplets were dried under air flow in a biological cabinet, and then incubated at 30°C for 20 hours before colonies were counted using a Bantex Colony Counter 920A.

5.2.3 Biological transmission electron microscopy of bacteria incubated with QD. Biological transmission electron microscopy (BioTEM) images of all the bacterial strains

exposed to QDs were obtained using a FEI Tecnai T12 TEM after the following preparation. Bacteria were cultured in LB broth overnight. The next day, bacteria were washed with DPBS buffer, diluted to an OD of 0.8 (OD600) in HEPES, then exposed 1 mg/L of CdSe/ZnS QD for 15 minutes. This bacterial suspension was centrifuged down to a pellet, washed thrice with 0.1 M cacodylate buffer solution, then resuspended in a fixation buffer of 2.5% glutaraldehyde in 0.1 M sodium cacodylate buffer and fixed for 50 minutes. The fixed bacterial cells were then centrifuged, washed with sodium cacodylate buffer, and dehydrated stepwise with increasing concentration of ethanol (30, 50, 70, 80, 90, 95, and 100% ethanol in water). After the ethanol rinsing steps, the pellet was washed with propylene oxide three times. The resin infiltration steps were performed in the following manner. The pellet was soaked first in a 2:1 propylene oxide: epoxy resin mixture for 2 h, and then in a 1:1 propylene oxide: epoxy resin mixture overnight. Next day, the 1:1 propylene oxide: epoxy resin mixture was removed and replaced with a fresh batch of 1:1 propylene oxide: epoxy resin mixture for 5 h, and finally incubated in a pure resin mixture and infiltrated overnight. The resin sample was then cured in a 40 °C oven for one day and then 60 °C oven for two days. Leica UC6 microtome and Diatome diamond knife was used to make ultrathin sections (65 nm) of this resin-embedded bacterial sample, and uranyl acetate and lead citrate was used to stain them. These sections were placed on copper TEM grids (Ted Pella Inc.), and imaging was done.

5.3 Results and discussion

5.3.1 Bacterial viability assay with *A. baylyi*

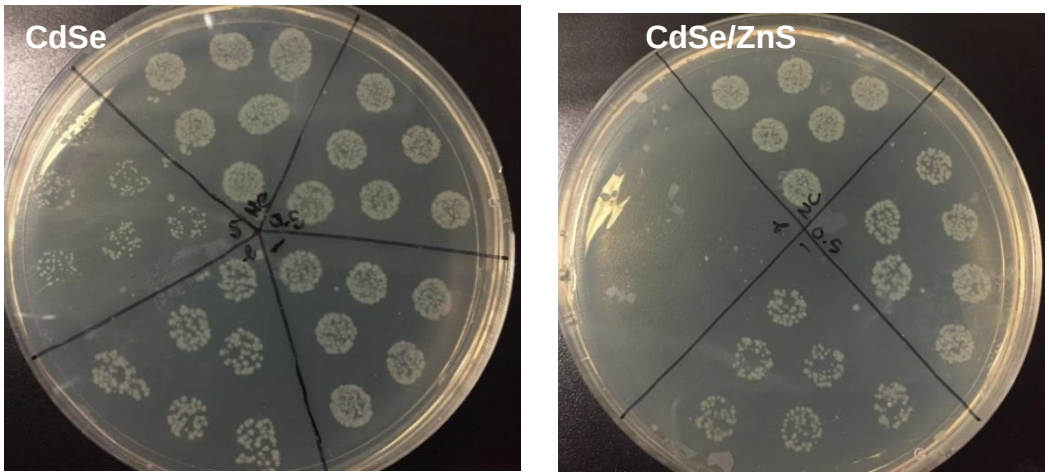

Figure 1: Images of representative LB-agar plates after drop-plate assay with A. baylyi (10^4 CFU/mL) and CdSe (left) and CdSe/ZnS (right) QDs. On the left, the QD concentrations clockwise from the top are: negative control, 0.5, 1, 2, 5 mh/L. One the right, the QD concentrations clockwise from the top are: 2 mg/L, negative control, 0.5, and 1 mg/L.

Drop-plate colony counting assay was performed with *A. baylyi* in the presence of CdSe (0.5-5 mg/L of Cd core concentration) and CdSe/ZnS (0.5-2 mg/L of Cd core concentration). These concentration ranges were chosen based on our previous work (Chapter 3) on *S. oneindensis* MR-1, where toxicity of CdSe and CdSe/ZnS QDs were observed at similar concentrations. We chose not to use higher than 2 mg/L of Cd core concentration in the case of CdSe/ZnS due to 100% loss in viability at that concentration. In initial replicates, a cell concentration of 10^4 CFU/mL was chosen to match the experimental conditions used in Chapter 3 with *S. oneindensis* MR-1.[4] However, at this cell concentration, it was difficult to count the colonies as they are overlapping and not discrete. Even in that circumstance, the dose-dependent toxicity of both the QDs was still visually noticeable, along with the fact that the core/shell QDs appeared more toxic than

the unshelled cores. To do quantitative colony counting experiments, the cell concentration was diluted to 10^3 CFU/mL, and countable colonies were obtained. As seen in Figure 2, the CdSe/ZnS QDs posed the highest toxicity to *A. baylyi* cells. This was similar to the results that were obtained for *S. oneidensis* MR-1 where the CdSe/ZnS posed more toxic effect to the bacteria, though the *A. baylyi* proved more resilient to the Cd-based QD toxicity. In the case of *S. oneidensis* MR-1, at CdSe exposure conditions of 0.5 mg/L core Cd concentration, roughly 10% of the bacteria remained viable. However, in the case of *A. baylyi*, we see no decrease in viability at that concentration. It is worth noting here that all the experimental conditions, including culture media in case of *S. oneidensis* MR-1 and *A. baylyi* were kept constant, thus this difference in viability values is not due solution-based transformation difference that yields the differential toxicity (though it could still be based on bacteria action on the QDs). In the case of the CdSe/ZnS QDs, a concentration of 0.5 mg/L wiped out all viable colonies, which is not something we see in case of *A. baylyi*. In presence of the Zn-based QDs, no significant toxicity was observed (Figure 3). The experiments were done with one batch of QDs (one material replicate) twice (on bacteria cultured on different days), with three analytical replicates each time. Statistical analysis for these experiments was performed using one-way ANOVA, followed by post-hoc Tukey's multiple comparisons tests (GraphPad Prism software, La Jolla, CA).

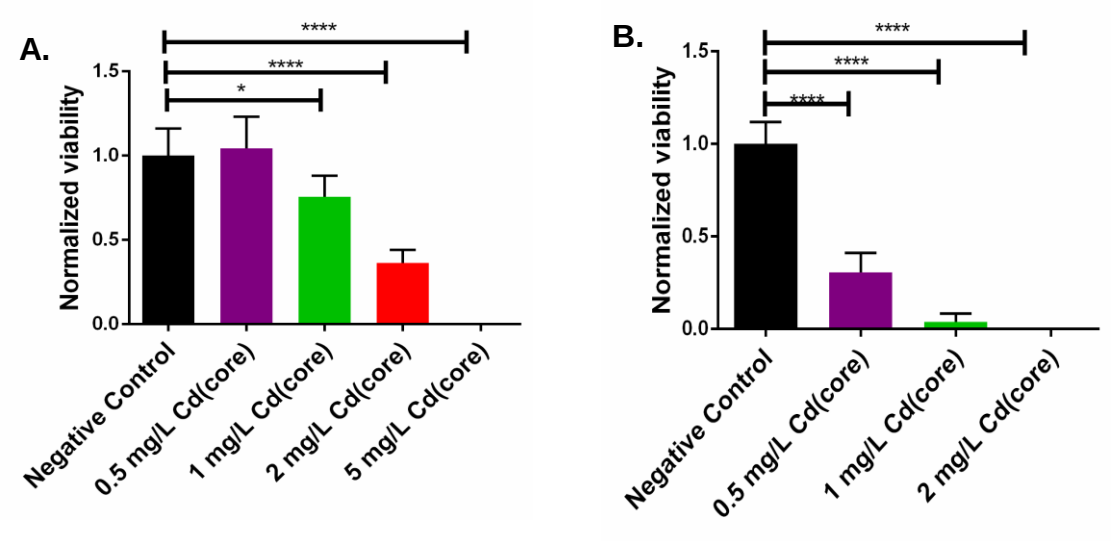

Figure 2: Drop-plate colony counting assay with A. baylyi in presence of A. CdSe QDs and B. CdSe/ZnS QDs. All values plotted are the mean ± standard deviation (SD), and the statistical significance is indicated using asterisks (p values < 0.0001 indicated by ****, 0.0001 to 0.001 indicated by ***, 0.001 to 0.01 indicated by **, and 0.01 to 0.05 indicated by *).

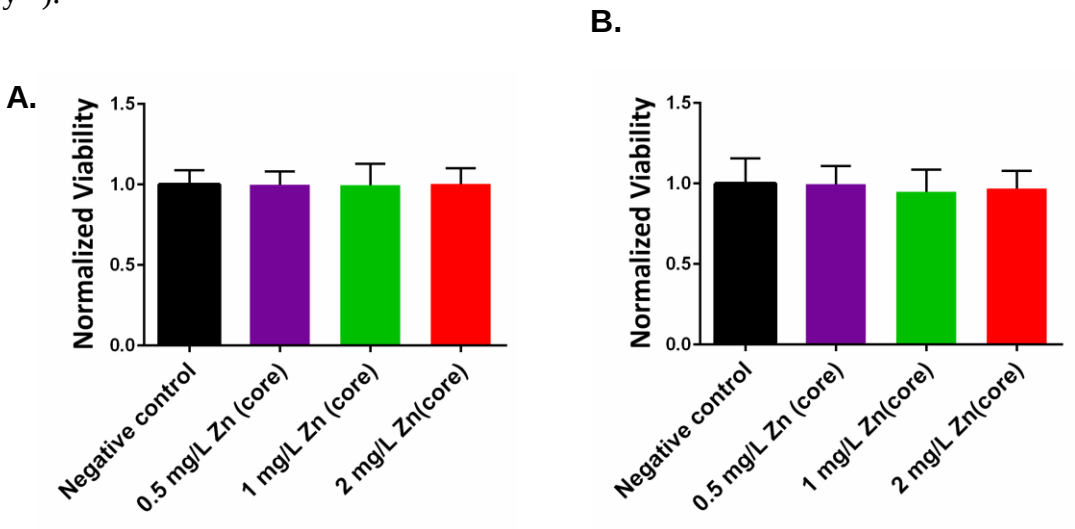

Figure 3: Drop-plate colony counting assay with A. baylyi in presence of A. ZnSe QDs and B. ZnSe/ZnS QDs. All values plotted are the mean ± standard deviation (SD), and the statistical significance is indicated using asterisks (p values < 0.0001 indicated by ****, 0.0001 to 0.001 indicated by ***, 0.001 to 0.01 indicated by **, and 0.01 to 0.05 indicated by *).

5.3.2 Bacterial viability assay with *S. oneidensis* MR-4

For *S. oneidensis* MR-4, similar dose-dependent toxicities were observed for both CdSe and CdSe/ZnS (shown in Figure 4). Experiments were done with one material replicate, one biological replicate, and three analytical replicates for each. Similar to *A. baylyi*, the quantum dots posed significantly less toxicity in case of *S. oneidensis* MR-4. For the CdSe/ZnS QDs at a concentration of 0.5 mg/L of QDs, 17% of viable colonies remained for *S. oneidensis* MR-4, whereas no viable colonies remained in *S. oneindensis* MR-1. In presence of the Zn-based QDs, no significant toxicity was observed (Figure 5). Statistical analysis for these experiments was performed using one-way ANOVA, followed by post-hoc Tukey's multiple comparisons tests (GraphPad Prism software, La Jolla, CA).

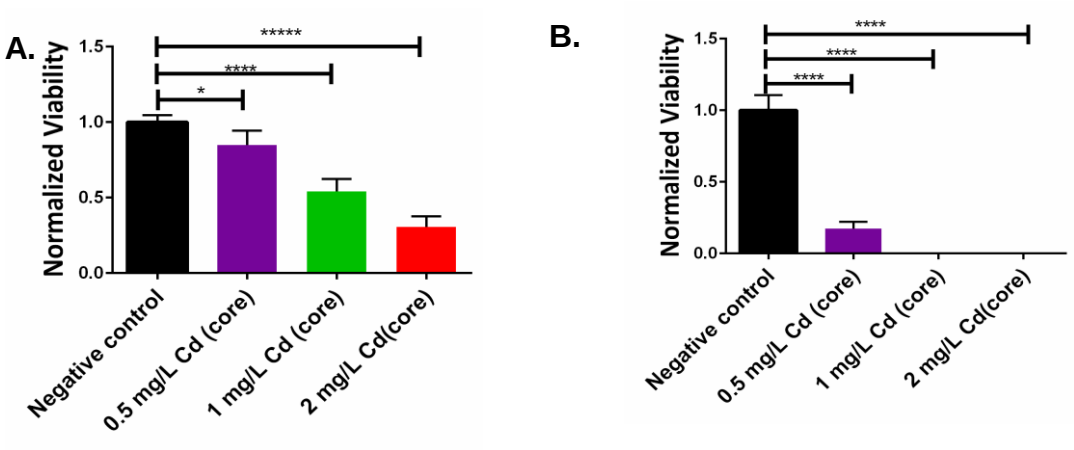

Figure 4: Drop-plate colony counting assay with S. oneindensis MR-4 in presence of A. CdSe QDs and B. CdSe/ZnS QDs. All values plotted are the mean ± standard deviation (SD), and the statistical significance is indicated using asterisks (p values < 0.0001 indicated by ****, 0.0001 to 0.001 indicated by ***, 0.001 to 0.01 indicated by **, and 0.01 to 0.05 indicated by *).

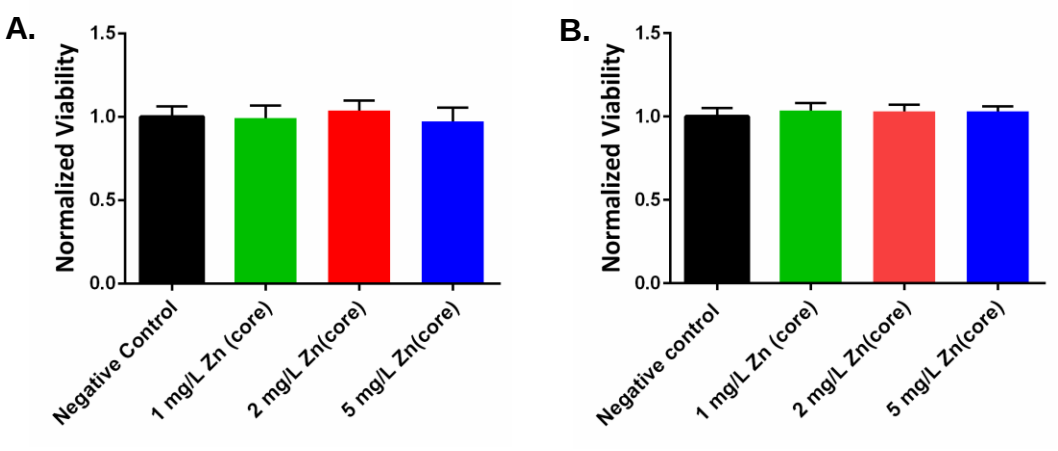

Figure 5: Drop-plate colony counting assay with S. oneidensis MR-4 in presence of A. ZnSe QDs and B. ZnSe/ZnS QDs. All values plotted are the mean ± standard deviation (SD), and the statistical significance is indicated using asterisks (p values < 0.0001 indicated by ****, 0.0001 to 0.001 indicated by ***, 0.001 to 0.01 indicated by **, and 0.01 to 0.05 indicated by *).

5.3.3 Bacterial viability assay with *P. aeruginosa*

Similar toxicity results as before were obtained when *P. aeruginosa* was treated with the CdSe, CdSe/ZnS, ZnSe and ZnSe/ZnS QDs (Figure 6 and 7).

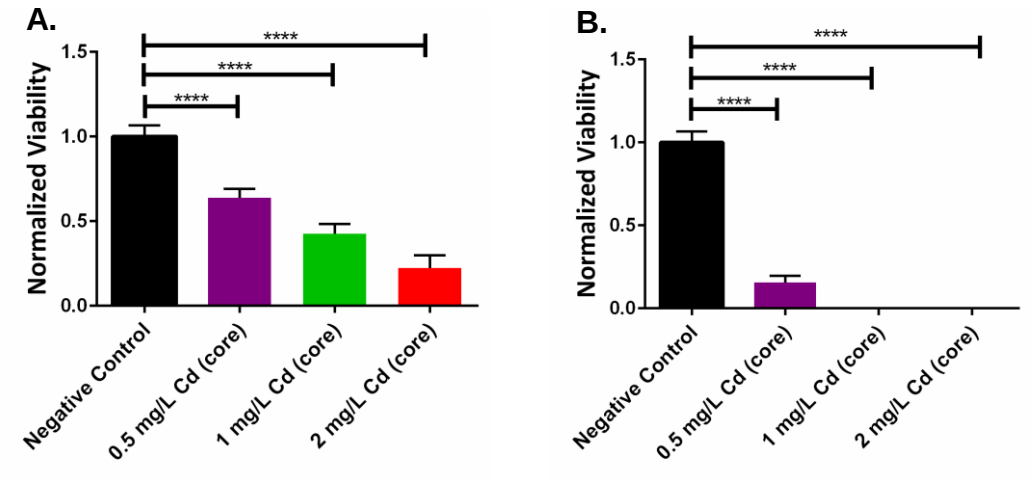

Figure 6: Drop-plate colony counting assay with P. aeruginosa in presence of A. CdSe QDs and B. CdSe/ZnS QDs. All values plotted are the mean ± standard deviation (SD), and the statistical significance is indicated using asterisks (p values < 0.0001 indicated by ****, 0.0001 to 0.001 indicated by ***, 0.001 to 0.01 indicated by **, and 0.01 to 0.05 indicated by *).

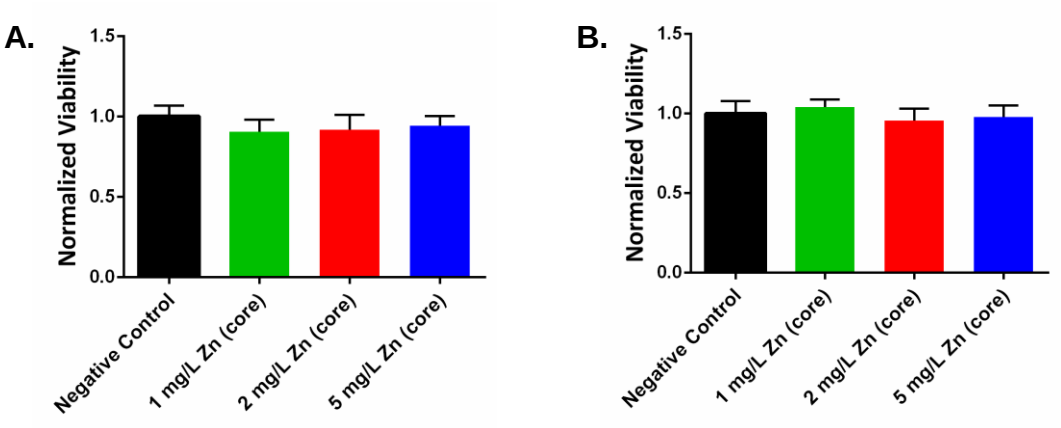

Figure 7: Drop-plate colony counting assay with P. aeruginosa in presence of A. ZnSe QDs and B. ZnSe/ZnS QDs. All values plotted are the mean ± standard deviation (SD), and

the statistical significance is indicated using asterisks (p values < 0.0001 indicated by ****, 0.0001 to 0.001 indicated by ***, 0.001 to 0.01 indicated by **, and 0.01 to 0.05 indicated by *).

From the viability studies reported here, it is obvious that the different Gram-negative bacteria have similar responses to treatment with the QDs. Even though two of the bacteria have rough LPS and two have smooth LPS, that does not seem to play any significant role, as far as cell viability is concerned. Since the different LPS structures might be expected to impact QC association with the bacterial membrane, biological TEM was performed on bacteria treated with QDs.

5.3.4 Biological TEM

Biological TEM is an excellent tool for qualitative visualization of any damage to the bacterial cellular structures, as well as association between the QDs and bacterial cells. As seen in Figure 8, damage to the *A. baylyi* cell membrane and spillage of cytoplasm is observed in the samples treated with unshelled CdSe QDs. Also, abnormal elongation of cells, known as filamentation, is observed (as shown in Figure 8B in the red rectangle). Filamentation occurs when a cell continues to elongate but does not undergo cell division due to inhibition of chromosome replication caused by DNA damage.[19] In the presence of CdSe/ZnS core-shell QDs, damaged bacterial cells, and some polyp like formations (as shown in Figure 8F in the red square, possibly from a disintegrating cell membrane) were observed.

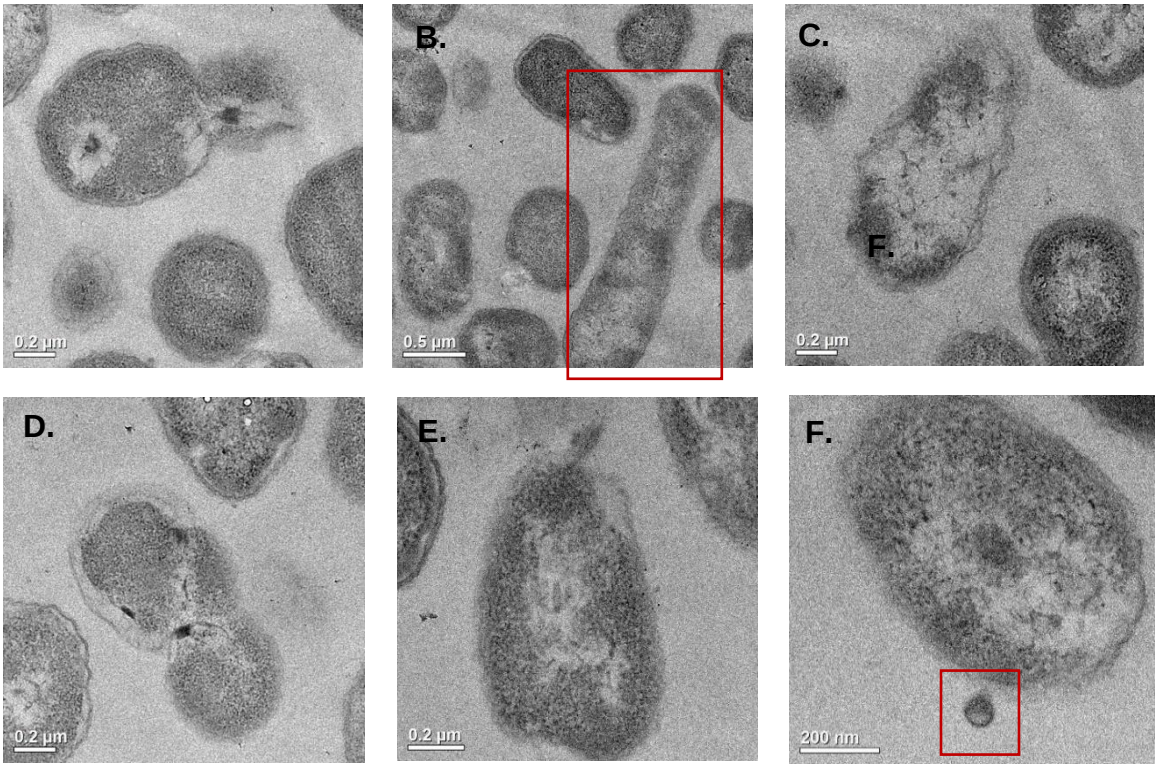

Figure 8: Biological transmission electron micrographs for A. baylyi after treatment with QDs. A., B and C. Micrographs show bacteria treated with unshelled CdSe QDS while D., E., and F. micrographs show bacteria treated with core/shell CdSe/ZnS QDs.

In case of *P. aeruginosa,* significant damage to cell membrane and cellular structures was observed, as shown by the red boxes in Figure 9.

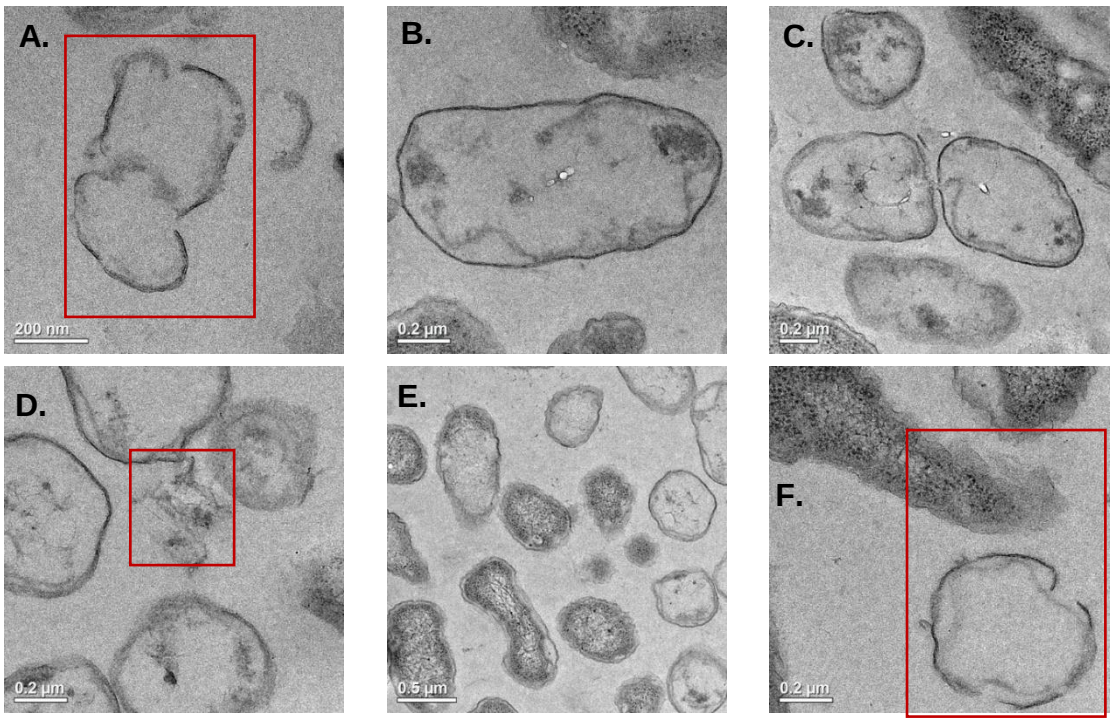

Figure 9: Biological transmission electron micrographs for P. aeruginosa after treatment with QDs. A., B and C. Micrographs show bacteria treated with unshelled CdSe QDS while D., E., and F. micrographs show bacteria treated with core/shell CdSe/ZnS QDs.

In case of *S. oneidensis* MR-4, due to thickness of the TEM sample slices, it was difficult to obtain clear images. I have included some representative images here, that show damage to cells, but it is difficult to confirm these results.

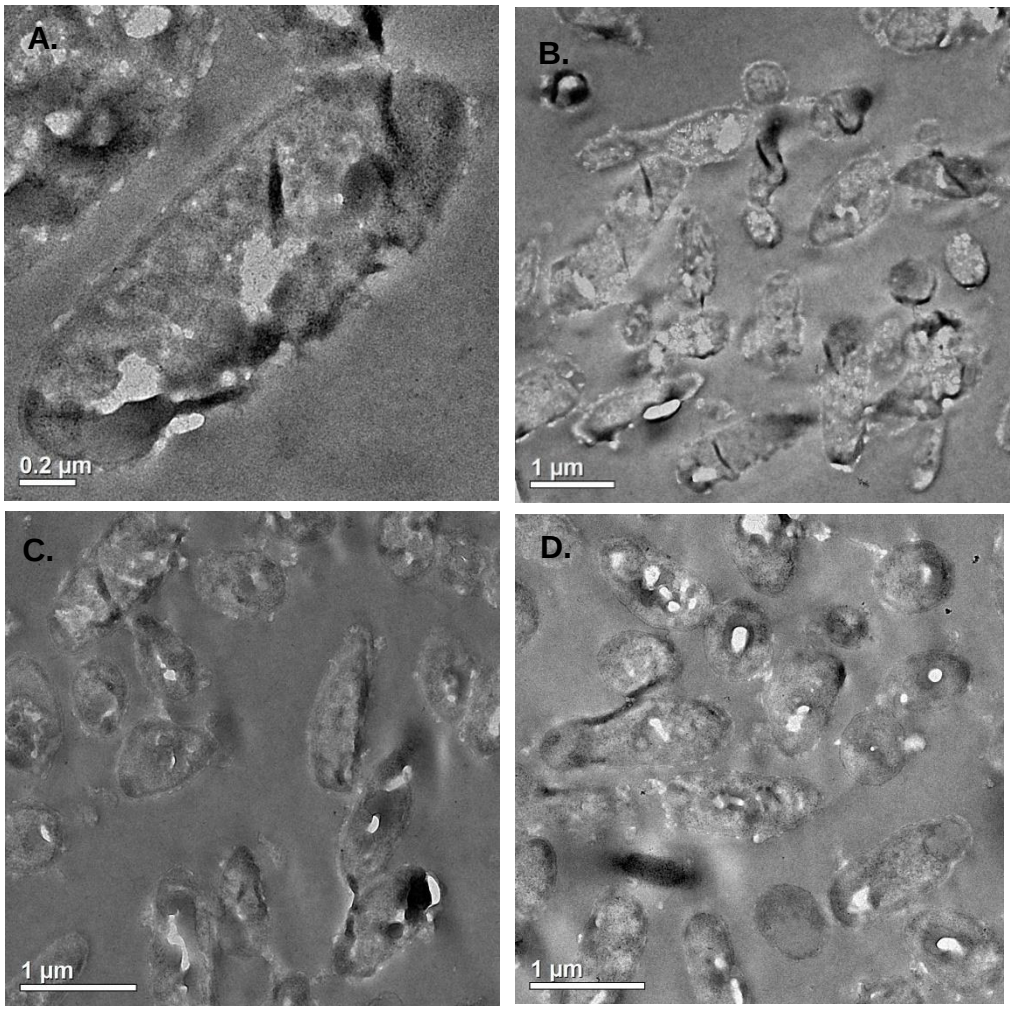

Figure 10: Biological transmission electron micrographs for S. oneindensis MR-4 after treatment with QDs. A.,and B. Micrographs show bacteria treated with unshelled CdSe QDS while C., and D. micrographs show bacteria treated with core/shell CdSe/ZnS QDs.

5.4 Conclusion

From the results of this work, it is obvious that the CdSe and CdSe/ZnS QDs show similar dose-dependent toxicity to *A. baylyi*, *S. oneidensis* MR-4, and *P. aeruginosa*, as was reported previously for *S. oneidensis* MR-1. In case of the Zn-based QDs, no toxicity was observed. For all three bacteria, biological TEM shows damage to cells on treatment with both CdSe and CdSe/ZnS. Because it is clear that there is significant toxicity, in the future qPCR experiments will be done to assess any changes in gene expression to get further mechanistic insights into the toxicity caused by Cd-based QDs.

Bibliography:

Chapter 1

(1) Hardman, R. Review A Toxicologic Review of Quantum Dots : Toxicity Depends on Physicochemical and Environmental Factors. *Environ Health Perspect.* **2012**, *114* (2), 165–172.

(2) Michalet, X.; Pinaud, F. F.; Bentolila, L. a; Tsay, J. M.; Doose, S.; Li, J. J.; Sundaresan, G.; Wu, a M.; Gambhir, S. S.; Weiss, S. Quantum Dots for Live Cells, in Vivo Imaging, and Diagnostics. *Science* **2005**, *307* (5709), 538–544.

(3) Reed, M. A.; Aggarwal, R. J.; Matyi, R. J.; Moore, T. M.; Wetsel, A. E. Observation of Discrete Electronic States in a Zero-Dimensional Semiconductor Nanostructure *Phys. Rev. Lett.* **1988**, *60* (6), 535.

(4) Resch-genger, U.; Grabolle, M.; Cavaliere-jaricot, S.; Nitschke, R.; Nann, T. Quantum Dots versus Organic Dyes as Fluorescent Labels. *Nat. Methods.* **2008**, *5* (9), 763–775.

(5) Piccinno, F.; Gottschalk, F. Industrial Production Quantities and Uses of Ten Engineered Nanomaterials in Europe and the World. *J. Nanopart. Res.* **2012**, *14*, 1109.

(6) Lopes, T.; Mestre, N. C.; Maria, S.; Sabóia-morais, T.; João, M. Environmental Behaviour and Ecotoxicity of Quantum Dots at Various Trophic Levels : A Review. *Environ. Int.* **2017**, *98*, 1–17.

(7) Danek, M.; Jensen, K. F.; Murray, C. B.; Bawendi, M. G. Synthesis of Luminescent Thin-Film CdSe / ZnSe Quantum Dot Composites Using CdSe

Quantum Dots Passivated with an Overlayer of ZnSe. *Chem. Mater.* **1996**, *8* (1), 173–180.

(8) Dabbousi, B. O.; Mikulec, F. V; Heine, J. R.; Mattoussi, H.; Ober, R.; Jensen, K. F.; Bawendi, M. G. (CdSe) ZnS Core - Shell Quantum Dots : Synthesis and Characterization of a Size Series of Highly Luminescent Nanocrystallites. *J. Phys. Chem.* **1997**, *101*, 9463–9475.

(9) Rzigalinski, B. A.; Strobl, J. S. Cadmium-Containing Nanoparticles : Perspectives on Pharmacology and Toxicology of Quantum Dots I. *Toxicol. Appl. Pharmacol.* **2009**, *238* (3), 280–288.

(10) Bimberg, D. Quantum Dots for Lasers , Amplifiers and *Computing. J. Phys. D: Applied Physics* **2005**, *38*(13), 2.

(11) Derfus, A. M.; Chan, W. C. W.; Bhatia, S. N. Probing the Cytotoxicity of Semiconductor Quantum Dots. *Nano Lett.* **2004**, *4*(1), 11-18.

(12) Kairdolf, B. A.; Smith, A. M.; Stokes, T. H.; Wang, M. D.; Young, A. N.; Nie, S. Semiconductor Quantum Dots for Bioimaging and Biodiagnostic Applications. *Annual Rev. Anal. Chem.* **2013**, *6,* 143-162

(13) Riley, E. A.; Hess, C. M.; Reid, P. J. Photoluminescence Intermittency from Single Quantum Dots to Organic Molecules: Emerging Themes. *Int. J. Mol. Sci.* **2012**, *13* (10), 12487–12518.

(14) Alivisatos, A. P.; Gu, W.; Larabell, C.Quantum Dots as Cellular Probes. *Annu. Rev. Biomed. Eng.* **2005**, *7*, 55–76.

(15) Winnik, F. M.; Maysinger, D.*Acc. Chem. Res.* **2013**, *46* (3), 672-680.

(16) Fu, P. P.; Xia, Q.; Hwang, H.; Ray, P. C. ScienceDirect Mechanisms of

Nanotoxicity : Generation of Reactive Oxygen Species 5. *J. Food Drug Anal.* **2014**, *22* (1), 64–75.

(17) Tian, P.; Tang, L.; Teng, K. S.; Lau, S. P. Graphene Quantum Dots from Chemistry to Applications. *Mater. Today Chem.* **2018**, *10*, 221–258.

(18) Bacon, M.; Bradley, S. J.; Nann, T. Graphene Quantum Dots. *Part. Part. Syst. Charact.* **2014**, *31*, 415–428.

(19) Ponomarenko, L. A. Chaotic Dirac Billiard in Graphene Quantum Dots. **2008**, *320*, 356-358.

(20) Barreiro, A.; Zant, H. S. J. Van Der; Vandersypen, L. M. K. Quantum Dots at Room Temperature Carved out from Few-Layer Graphene.*Nano Lett.* **2012,** *12*, 6096-6100.

(21) Nakada, K.; Fujita, M.; Dresselhaus, G.; Dresselhaus, M. S. Edge State in Graphene Ribbons : Nanometer Size Effect and Edge Shape Dependence. *Phys. Rev. B* **1996**, *54* (24), 954–961.

(22) Chen, W.; Li, F.; Wu, C.; Guo, T. Optical Properties of Fluorescent Zigzag Graphene Quantum Dots Derived from Multi-Walled Carbon Nanotubes. *Appl. Phys. Lett.* **2014**, 104, 063109.

(23) Zhang, Z. Z.; Chang, K. Tuning of Energy Levels and Optical Properties of Graphene Quantum Dots. *Phys. Rev. B* **2008**, *77*, 235411.

(24) Mueller, M. L.; Yan, X.; Mcguire, J. A.; Li, L. Triplet States and Electronic Relaxation in Photoexcited Graphene Quantum Dots. *Nano Lett.* **2010**, *10*, 2679–2682.

(25) Isley, S. L.; Penn, R. L. Titanium Dioxide Nanoparticles : Effect of Sol - Gel pH

on Phase Composition , Particle Size , and Particle Growth Mechanism. *J. Phys. Chem. C* **2008**, *112*, 4469–4474.

(26) Pan, D.; Guo, L.; Zhang, J.; Xi, C.; Xue, Q.; Huang, H.; Li, J.; Zhang, Z. Cutting Sp 2 Clusters in Graphene Sheets into Colloidal Graphene Quantum Dots with Strong Green Fluorescence. *J. Mater. Chem.* **2012**, *22*, 3314–3318.

(27) Raeyani, D.; Shojaei, S.; Kandjani, S. A.; Wlodarski, W. Synthesizing Graphene Quantum Dots for Gas Sensing Applications. *Procedia Eng.* **2016**, *168*, 1312–1316.

(28) Liu, F.; Jang, M.; Ha, H. D.; Kim, J.; Cho, Y. Facile Synthetic Method for Pristine Graphene Quantum Dots and Graphene Oxide Quantum Dots : Origin of Blue and Green Luminescence. *Adv. Mater.* **2013**, *25*, 3657–3662.

(29) Zhou, L.; Geng, J.; Liu, B. Graphene Quantum Dots from Polycyclic Aromatic Hydrocarbon for Bioimaging and Sensing of Fe 3 + and Hydrogen Peroxide. *Part. Part. Syst. Charac.* **2013**, *30* 1086–1092.

(30) Kharangarh, P. R.; Umapathy, S.; Singh, G. Effect of Defects on Quantum Yield in Blue Emitting Photoluminescent Nitrogen Doped Graphene Quantum Dots. J. Appl. Phys. **2017**, *122*, 145107.

(31) Luo, Y.; Xu, Y.; Li, M.; Sun, L.; Hu, G.; Tang, T.; Wen, J.; Li, X. Tuning the Photoluminescence of Graphene Quantum Dots by Fluorination. J. Nanomater. **2017**,Article ID 9682846.

(32) Sun, J.; Yang, S.; Wang, Z.; Shen, H.; Xu, T.; Sun, L.; Li, H. Ultra-High Quantum Yield of Graphene Quantum Dots : Aromatic-Nitrogen Doping and Photoluminescence Mechanism. *Part. Part. Syst. Charac.* **2015**, *32*, 434–440.

(33) Abbas, A.; Tuti, L.; Phan, A. N. Biomass-Waste Derived Graphene Quantum Dots and Their Applications. *Carbon N. Y.* **2018**, *140*, 77–99.

(34) Kumawat, M. K.; Thakur, M.; Gurung, R. B.; Srivastava, R. Graphene Quantum Dots for Cell Proliferation , Nucleus Imaging , and Photoluminescent Sensing Applications. *Sci. Rep.* **2017**, *7*, 15858..

(35) Wang, Z. G.; Zhou, R.; Jiang, D.; Song, J. E.; Xu, Q.; Si, J.; Chen, Y. P.; Zhou, X.; Gan, L.; Li, J. Z.; Zhang, H.; Liu, B. Toxicity of Graphene Quantum Dots in Zebrafish Embryo. *Biomed. Environ. Sci.*, **2015**, *28* (5), 341–351.

(36) Dooley, K.; Zon, L. I. Zebrafish : A Model System for the Study of Human Disease. *Curr. Opin. Genet. Div.* **2000**, *10*, 252–256.

(37) Roy, P.; Periasamy, A. P.; Lin, C.; Her, G.; Chiu, W.; Li, C.; Shu, C.; Huang, C.; Liang, C.; Chang, H. Nanoscale in Vivo Imaging of Apoptotic Cells. *Nanoscale* **2015**, *7*,2504–2510.

(38) Zhang, J.; Sun, T.; Niu, A.; Tang, Y.; Deng, S.; Luo, W. Biomaterials Perturbation Effect of Reduced Graphene Oxide Quantum Dots (rGOQDs) on Aryl Hydrocarbon Receptor (AhR) Pathway in Zebra Fi Sh. *Biomaterials* **2018**, *133* (2017), 49–59.

(39) Li, P.; Xu, T.; Wu, S.; Lei, L.; He, D. Chronic Exposure to Graphene-Based Nanomaterials Induces Behavioral Deficits and Neural Damage in Caenorhabditis Elegans. *J. Appl. Toxicol.* **2017**, *37*, 1140–1150.

(40) Zhao, Y.; Wu, Q.; Wang, D. RSC Advances A microRNAs – mRNAs Network Involved in the Control of Graphene Oxide Toxicity in *Caenorhabditis elegans*. RSC *Adv.* **2015**, *5*, 92394–92405.

(41) Hui, L.; Huang, J.; Chen, G.; Zhu, Y.; Yang, L. Antibacterial Property of Graphene Quantum Dots (Both Source Material and Bacterial Shape Matter). *ACS Appl. Mater. Interfaces* **2016**, *8*, 20-25.

(42) Ristic, B. Z.; Milenkovic, M. M.; Dakic, I. R.; Todorovic-markovic, B. M.; Milosavljevic, M. S.; Budimir, M. D.; Paunovic, V. G.; Dramicanin, M. D.; Markovic, Z. M.; Trajkovic, V. S. Biomaterials Photodynamic Antibacterial Effect of Graphene Quantum Dots. *Biomaterials* **2014**, *35* (15), 4428–4435.

(43) Nurunnabi, M.; Khatun, Z.; Huh, K. M.; Park, S. Y.; Lee, D. Y.; Cho, K. J.; Lee, Y. In Vivo Biodistribution and Toxicology of Carboxylated Graphene Quantum. *ACS Nano* **2013**, *7* (8), 6858–6867.

(44) Chong, Y.; Ma, Y.; Shen, H.; Tu, X.; Zhou, X.; Xu, J.; Dai, J.; Fan, S.; Zhang, Z. The in Vitro and in Vivo Toxicity of Graphene Quantum Dots. *Biomaterials* **2014**, *35*, 5041-5048.

(45) Li, J.; Zhang, X.; Jiang, J.; Wang, Y.; Jiang, H.; Zhang, J.; Nie, X.; Liu, B. Systematic Assessment of the Toxicity and Potential Mechanism of Graphene Derivatives In Vitro and In Vivo. Toxicol. Sci. **2018**, doi: 10.1093/toxsci/kfy235.

(46) Halder, A.; Godoy-gallardo, M.; Ashley, J.; Feng, X.; Zhou, T.; Hosta-rigau, L.; Sun, Y. One-Pot Green Synthesis of Biocompatible Graphene Quantum Dots and Their Cell Uptake Studies. *ACS Appl. Bio Mater.* **2018**, *1*, 452–461.

(47) Tian, X.; Xiao, B.; Wu, A.; Yu, L.; Zhou, J.; Wang, Y.; Wang, N.; Guan, H.; Shang, Z. Hydroxylated-graphene Quantum Dots Induce Cell Senescence in Both p53-Dependent and-independent Manner. *Toxicol. Res.*, **2016**, *5*, 1639–1648.

(48) Yuan, X.; Liu, Z.; Guo, Z.; Ji, Y.; Jin, M.; Wang, X. Cellular Distribution and

Cytotoxicity of Graphene Quantum Dots with Different Functional Groups. *Nanoscale Res. Lett.* **2014**, *9*(1), 108.

(49) Wu, C.; Wang, C.; Han, T.; Zhou, X.; Guo, S. Insight into the Cellular Internalization and Cytotoxicity of Graphene Quantum Dots. *Adv. Healthc. Mater.* **2013**, *2*(12)1613–1619.

(50) Markovic, Z. M.; Ristic, B. Z.; Arsikin, K. M.; Klisic, D. G.; Harhaji-trajkovic, L. M.; Todorovic-markovic, B. M.; Kepic, D. P.; Kravic-stevovic, T. K.; Jovanovic, S. P.; Milenkovic, M. M.; et al. Biomaterials Graphene Quantum Dots as Autophagy-Inducing Photodynamic Agents. *Biomaterials* **2012**, *33* (29), 7084–7092.

(51) Wang, X.; Lei, R.; Huang, H.; Wang, N.; Yuan, L.; Xiao, R.; Bai, L.; Li, X.; Li, L.; Yang, X. Nanoscale The Permeability and Transport Mechanism of Graphene Quantum Dots (GQDs) across the Biological Barrier. *Nanoscale*, **2015**, *7*, 2034–2041.

(52) Nasrollahi, F.; Rui, Y.; Chen, P.; Varshosaz, J.; Ali, A. Targeting Graphene Quantum Dots to Epidermal Growth Factor Receptor for Delivery of Cisplatin and Cellular Imaging. *Materials Science & Engineering C*, 2018, 247-257.

(53) Fasbender, S.; Allani, S.; Wimmenauer, C.; Cadeddu, R.; Raba, K.; Fischer, J. C.; Bulat, B.; Luysberg, M.; Seidel, C. A. M.; Haas, R. RSC Advances Uptake Dynamics of Graphene Quantum Dots into Primary Human Blood Cells Following in Vitro Exposure †. *RSC Adv.* **2017**, *7*, 12208–12216.

(54) Wang, T.; Zhu, S.; Jiang, X. Toxicity Mechanism of Graphene Oxide and Nitrogen-Doped Graphene Quantum Dots in RBCs Revealed by Surface-Enhanced

Infrared Absorption.*Toxicol. Res*. **2015**, *4*, 885–894.

(55) Shang, W.; Zhang, X.; Zhang, M.; Fan, Z.; Sun, Y. The Uptake Mechanism and Biocompatibility of Graphene Quantum Dots with Human Neural Stem Cells. *Nanoscale*, **2014**, *6*(11), 5799–5806.

(56) Chong, Y.; Ge, C.; Fang, G.; Tian, X.; Wen, T.; Wamer, W. G.; Chen, C.; Chai, Z.; Yin, J. Crossover between Anti- and Pro-oxidant Activities of Graphene Quantum Dots in the Absence or Presence of Light. *ACS Nano* **2016**, *10*, 8690-8699.

(57) Chanda, A.; Deshpande, S.; Shinde, D. B.; Pillai, V. K.; Singh, N. Mitigating the Cytotoxicity of Graphene Quantum Dots and Enhancing Their Applications in Bioimaging and Drug Delivery. *ACS Macro. Lett.* **2014,** *3*, 1064-1068.

(58) Xu, S.; Ziegler, J.; Nann, T. Rapid Synthesis of Highly Luminescent InP and InP / ZnS Nanocrystals. *J. Mater. Chem.* **2008**, *18*, 2653–2656.

(59) Chibli, H.; Park, S.; Dimitrijevic, N. M.; Nadeau, J. Cytotoxicity of InP / ZnS Quantum Dots Related to Reactive Oxygen Species Generation. *Nanoscale*, **2011**, *3*(6), 2552-2559.

(60) Shen, W.; Tang, H.; Yang, X.; Cao, Z.; Cheng, T.; Wang, X.; Tan, Z.; You, J.; Deng, Z. Synthesis of Highly Fluorescent InP / ZnS Small-core/thick-shell Tetrahedral-shaped Quantum Dots for Blue Light-emitting Diodes . *J. Mater. Chem. C.* **2017**, *5*, 8243–8249.

(61) Liang, X.; Zha, J. Comparative Biochemistry and Physiology , Part D Toxicogenomic Applications of Chinese Rare Minnow (Gobiocypris Rarus) in

Aquatic Toxicology . *Comp. Biochem. Physiol. - Part D Genomics Proteomics* **2016**, *19*, 174–180.

(62) Chen, Y.; Yang, Y.; Ou, F.; Liu, L.; Liu, X.; Wang, Z.; Jin, L. InP / ZnS QDs Exposure Induces Developmental Toxicity in Rare Minnow (Gobiocypris Rarus) Embryos. *Environ. Toxicol. Pharmacol.* **2018**, *60* (December 2017), 28–36.

(63) Brunetti, V.; Chibli, H.; Fiammengo, R.; Galeone, A.; Malvindi, M. A.; Vecchio, G.; Cingolani, R.; Nadeau, J. L.; Pompa, P. P. InP/ZnS as a Safert Alternative to CdSe/ZnS Core/Shell Quantum Dots : In Vitro and in Vivo Toxicity Assessment. Nanoscale, **2013**, *5*(1), 307–317.

(64) Chibli, H.; Carlini, L.; Park, S.; Dimitrijevic, N.; Nadeau, J. L. Indium Phosphide : Cadmium Free Quantum Dots for Cancer Imaging and Therapy. *NSTI-Nanotech* **2011**, *3*, 133–136.

(65) Xie, R.; Chen, K.; Chen, X.; Peng, X. InAs / InP / ZnSe Core / Shell / Shell Quantum Dots as Non-Cadmium Containing , and Biocompatible. *Nano Res.* **2008**, *1*, 457-464.

(66) Lin, G.; D, M.; Ouyang, Q.; S, B.; Hu, R.; Ph, D.; Ding, Z.; S, B.; Tian, J.; M, M.; et al. In Vivo Toxicity Assessment of Non-Cadmium Quantum Dots in BALB / c Mice. *Nanomedicine Nanotechnology, Biol. Med.* **2018**, *11* (2), 341–350.

(67) Yaghini, E.; Turner, H.; Pilling, A.; Naasani, I.; Macrobert, A. J. In Vivo Biodistribution and Toxicology Studies of Cadmium-Free Indium-Based Quantum Dot Nanoparticles in a Rat Model. *Nanomedicine Nanotechnology, Biol. Med.* **2018**, *14* (8), 2644–2655.

(68) Speranskaya, E. S.; Beloglazova, N. V; Aubert, T.; Smet, P. F.; Poelman, D.;

Goryacheva, I. Y.; Saeger, S. De; Hens, Z. Hydrophilic , Bright CuInS 2 Quantum Dots as Cd-Free Fluorescent Labels in Quantitative Immunoassay. *Langmuir*, **2014**, *30* (25), 7567-7575.

(69) Chen, C.; Wu, D.; Chan, Y.; Lin, C. C.; Chung, P.; Hsiao, M.; Liu, R. Evaluations of the Chemical Stability and Cytotoxicity of CuInS 2 and CuInS 2 /ZnS Core/Shell Quantum Dots. *J. Phys. Chem. C* **2015,** *119*(5).

(70) Liu, L.; Xiao, Y.; Ji, Y.; Liu, M.; Chen, Y.; Zeng, Y.; Zhang, Y. CuInS 2 / ZnS QD Exposure Induces Developmental Toxicity , Oxidative Stress and DNA Damage in Rare Minnow (Gobiocypris Rarus) Embryos and Larvae. *Comp. Biochem. Physiol. C Toxicol. Pharmacol.* 2017, *198*, 19-27.

(71) Pons, T.; Pic, E.; Lequeux, N.; Cassette, E.; Bezdetnaya, L.; Dubertret, B. Cadmium-Free CuInS 2 / ZnS Quantum Dots for Sentinel Lymph Node Imaging with Reduced Toxicity. *ACS Nano* **2010**, *4* (5), 2531–2538.

(72) Sun, G.; Xing, W.; Xing, R. E. N.; Cong, L. I. U.; Tong, S. U. N.; Yu, S. Targeting Breast Cancer Cells with a CuInS 2 / ZnS Quantum Dot - Labeled Ki - 67 Bioprobe. *Oncol. Lett.* **2018**, *15*(2), 2471–2476.

(73) Speranskaya, E. S.; Sevrin, C.; Saeger, S. De; Hens, Z.; Goryacheva, I. Y.; Grand, C. Synthesis of Hydrophilic CuInS 2 / ZnS Quantum Dots with Different Polymeric Shells and Study of Their Cytotoxicity and Hemocompatibility. *ACS Appl. Mater. Interfaces* **2016**, *8*(12), 7613-7622.

(74) Wang, H.; He, Y.; Ji, T.; Yan, X. Surface Molecular Imprinting on Mn-Doped ZnS Quantum Dots for Room-Temperature Phosphorescence Optosensing of Pentachlorophenol in Water. *Anal. Chem.* **2009**, *81* (4), 1615–1621.

(75) Yang, Y.; Lan, J.; Xu, Z.; Chen, T.; Zhao, T.; Cheng, T.; Shen, J. Toxicity and Biodistribution of Aqueous Synthesized ZnS and ZnO Quantum Dots in Mice Toxicity and Biodistribution of Aqueous Synthesized ZnS and ZnO Quantum Dots in Mice. *Nanotoxicology* **2013**, *8* (1), 107-116.

(76) Sapra, S.; Prakash, A.; Ghangrekar, A.; Periasamy, N.; Sarma, D. D. Emission Properties of Manganese-Doped ZnS Nanocrystals. *J. Phys. Chem. B* **2005**, *109*(5), 1663–1668.

(77) Williams, D. N.; Pramanik, S.; Brown, R. P.; Zhi, B.; Mcintire, E.; Hudson-smith, N. V; Haynes, C. L.; Rosenzweig, Z. Adverse Interactions of Luminescent Semiconductor Quantum Dots with Liposomes and Shewanella Oneidensis. *ACS Appl. Nano Mater.* **2018**, *1*, 4788–4800.

(78) Bellanger, X.; Billard, P.; Schneider, R.; Balan, L; Merlin, C. Stability and Toxicity of ZnO Quantim Dots: Interplay Between Nanoparticles and Bacteria*J. Hazard. Mater.* 2015, *283*, 110-116.

(79) Jin, T.; Sun, D.; Su, J. Y.; Zhang, H.; Sue, H.-J. Antimicrobial Efficacy of Zinc Oxide Quantum Dots against *Listeria monocytogenes* , *Salmonella enteritidis* , and *Escherichia coli* O157 : H7. *J. Food. Sci.* **2009**, *74* (1), M46-M52..

(80) Chang, S.; Kang, B.; Dai, Y.; Zhang, H.; Chen, D. One-Step Fabrication of Biocompatible Chitosan- Coated ZnS and ZnS : Mn 2 + Quantum Dots via a G - Radiation Route. *Nanoscale Res. Lett.* **2011**, *6* (1), 591.

(81) Mohammad, F.; Al-lohedan, H. A. Toxicity Assessment of Engineered Mn – ZnS Quantum Dots in Vitro. *J. Mater. Sci.* **2016**, *51* (20), 9207–9216.

(82) Zhou, R.; Li, M.; Wang, S.; Wu, P.; Wu, L.; Hou, X. Low-Toxic Mn-Doped ZnSe

@ ZnS Quantum Dots Conjugated with Nano-Hydroxyapatite for Cell Imaging. *Nanoscale* **2014**, *6*(23), 14319–14325.

(83) Yang, Y.; Lv, S.-Y.; Yu, B.; Xu, S.; Shen, J.; Zhao, T.; Zhang, H. Hepatotoxicity Assessment of Mn-Doped ZnS Quantum Dots after Repeated Administration in Mice. *Int. J. Nanomed.* **2015**, *10*(1), 5787–5796.

(84) Wilcoxon, J. P.; Samara, G. A. Tailorable, visible light emission from silicon nanocrystals. *Appl. Phys. Lett.* **1999**, *74*, 3164-3166. (85) Zou, J.; Baldwin, R. K.; Pettigrew, K. A.; Kauzlarich, S. M. Solution Synthesis of Ultrastable Luminescent Siloxane-Coated Silicon Nanoparticles. Nano Lett. **2004,** *4*(7), 1181-1186.

(86) Baldwin, R. K.; Pettigrew, K. A.; Garno, J. C.; Power, P. P.; Liu, G.; Kauzlarich, S. M. Room Temperature Solution Synthesis of Alkyl-Capped Tetrahedral Shaped Silicon Nanocrystals. *J. Am. Chem. Soc.* **2002**, *124*(7), 1150-1151.

(87) Mangolini, L.; Thimsen, E.; Kortshagen, U. High-Yield Plasma Synthesis of Luminescent Silicon Nanocrystals. *Nano Lett.* **2005**, *5* (4), 655–659.

(88) Jurbergs, D.; Rogojina, E.; Mangolini, L.; Kortshagen, U.; Jurbergs, D.; Rogojina, E. Silicon Nanocrystals with Ensemble Quantum Yields Exceeding 60 % Silicon *Appl. Phys. Lett.* **2006**, *88*, 231116..

(89) Li, Q.; He, Y., Chang, J.; Wang, L.; Chen, H.; Tan, Y.-W.; Wang, H.; Shao, Z. Surface-Modified Silicon Nanoparticles with Ultrabright Photoluminescence and Single-Exponential Decay for Nanoscale Fluorescence Lifetime Imaging of Temperature. J. Am. Chem. Soc. **2013**, 135(40), 14924-14927.

(90) Stanca, L.; Petrache, S. N.; Serban, A. I.; Staicu, A. C.; Sima, C.; Munteanu, M.

C.; Otilia, Z.; Dinu, D.; Dinischiotu, A. Interaction of Silicon-Based Quantum Dots with Gibel Carp Liver : Oxidative and Structural Modifications. *Nanoscale Res. Lett.* **2013**, *8*(1), 254.

(91) Filho, D. W. Reactive oxygen species, antioxidants and fish mitochondria *Frontiers in Biosceince*, **2007**, *12*, 1229–1237.

(92) Fan, J.; Vankayala, R.; Chang, C. Preparation , Cytotoxicity and in Vivo Bioimaging of Highly Luminescent Water- Soluble Silicon Quantum Dots. *Nanotechnology*, 2015, *26*(21), 215703.

(93) Kustov, L. M.; Mashkin, P. V; Zakharov, V. N.; Abramenko, N. B.; Krysanov, E. Y. Silicon Nanoparticles: Characterization and Toxicity Studies *Environ. Sci. Nano* **2018**, 10.1039/C8EN00934A.

(94) Stan, M.; Sima, C.; Cinteza, L. O.; Dinischiotu, A. Silicon-Based Quantum Dots Induce Inflammation in Human Lung Cells and Disrupt Extracellular Matrix Homeostasis. *FEBS J.* **2015**, *282*, 2914–2929.

(95) Herynková, K.; Šimáková, P.; Cibulka, O.; Fučíková, A.; Kalbáčová, M. Hydrophilic Luminescent Silicon Nanoparticles in Steric Colloidal Solutions : Their Size , Agglomeration , and Toxicity *Phys Status Solidi*. **2017**, *14*, *1700195*.

(96) Wang, Q.; Bao, Y.; Zhang, X.; Coxon, P. R.; Jayasooriya, U. A. Uptake and Toxicity Studies of Poly-Acrylic Acid Functionalized Silicon Nanoparticles in Cultured Mammalian Cells. *Adv. Healthcare Mater.* **2012**, *1*, 189–198.

(97) Liu, J.; Erogbogbo, F.; Yong, K.; Ye, L.; Liu, J.; Hu, R.; Chen, H.; Hu, Y.; Yang, Y.; Yang, J.; Roy, I.; Karker, N. A.; Swihart, N. T.; Prasad, P. N. Assessing Clinical Prospects of Silicon Quantum Dots : Studies in Mice and Monkeys. *ACS*

Nano **2013**, *7*(8), 7303–7310.

Chapter 2

(1) Kamat, P. V. Quantum dots continue to shine brightly. *J. Phys. Chem. Lett.* **2016**, *7*, 584–585.

(2) Dabbousi, B. O.; Mikulec, F. V.; Heine, J. R.; Mattoussi, H.; Ober, R.; Jensen, K. F.; Bawendi, M. G. (CdSe) ZnS core-shell quantum dots: Synthesis and characterization of a size series of highly luminescent nanocrystallites. *J. Phys. Chem. B.* **1997**, *101*, 9463–9475.

(3) Goldman, E. R.; Mattoussi, H. Quantum dot bioconjugates for imaging, labelling and sensing. *Nat. Mater.* **2005**, *4*, 435–446.

(4) Zorman, B.; Ramakrishna, T.M.V.; Friesner, R. A. Quantum confinement effects in CdSe quantum dots. *J. Phys. Chem.* **1995**, *99*, 7649–7653.

(5) Kim, T.; Cho, C.; Kim, B.; Park, S. Quantum confinement effect in crystalline silicon quantum dots in silicon nitride grown using and quantum confinement effect in crystalline silicon quantum dots in silicon nitride grown using SiH_4 and NH_3. *Appl. Phys. Lett.* **2006**, *88*, 123102-1-3.

(6) Ekimov, A. I.; Onushchenko, A. A. Quantum size effect in three dimensional microscopic semiconductor crystals. *JETP Lett.* **1981**, *34*, 345–349.

(7) Shirasaki, Y.; Supran, G. J.; Bawendi, M. G.; Bulović, V. Emergence of colloidal quantum-dot light-emitting technologies. *Nat. Photonics*. **2013**, *7*, 13-23.

(8) Reiss, P.; Protière, M.; Li, L. Core / shell semiconductor nanocrystals. *Small*. **2009**, *5*, 154-168.

(9) Vasudevan, D.; Gaddam, R. R.; Trinchi, A.; Cole, I. Core-shell quantum dots: properties and applications. *J. Alloys Compd.* **2015**, *636*, 395–404.

(10) Chan, W. C. W.; Maxwell, D. J.; Gao, X.; Bailey, R. E.; Han, M.; Nie, S. Luminescent quantum dots for multiplexed biological detection and imaging. *Curr Opin Biotechnol*. **2002**, *13*, 40-46.

(11) Xu, G.; Zeng, S.; Zhang, B.; Swihart, M. T.; Yong, K.; Prasad, P. N. New generation cadmium-free quantum dots for biophotonics and nanomedicine. *Chem Rev*. **2016**, *116*, 12234-12327.

(12) Bhattacharya, P.; Ghosh, S.; Stiff-Roberts, A. D. Quantum dot opto-electronic devices. *Annu. Rev. Mater. Res*. **2004**, *34*, 1–40.

(13) Yang, Y.; Zheng, Y.; Cao, W.; Titov, A.; Hyvonen, J.; Manders, J. R.; Xue, J.; Holloway, P. H.; Qian, L. High-efficiency light-emitting devices based on quantum dots with tailored nanostructures. *Nat. Photonics*. **2015**, *9*, 259–266.

(14) Rosenthal, S. J.; Chang, J. C.; Kovtun, O.; Mcbride, J. R.; Tomlinson, I. D. Biocompatible quantum dots for biological applications. *Chem. Biol.* **2011**, *18*, 10–24.

(15) Alivisatos, A. P.; Gu, W.; Larabell, C. Quantum dots as cellular probes. *Annu. Rev. Biomed. Eng*. **2005**, *7*, 55–76.

(16) Bimberg, D. Quantum dots for lasers , amplifiers and computing. *J. Phys. D: Appl. Phys.* **2005**, *38*, 2055–2058.

(17) Bourzac, K. Quantum dots go on display. *Nature* **493,** 283(17 January 2013).

(18) Baldé, C. P.; Wang, F.; Kuehr, R.; Huisman, J. **2015**, The global e-waste monitor – 2014, United Nations University, IAS – SCYCLE, Bonn, Germany.

(19) Hardman, R. A toxicologic review of quantum dots : Toxicity depends on physicochemical and environmental factors. *Environ. Health Perspect*. **2006**, *114*, 165–172.

(20) Pelley, J. L.; Daar, A. S.; Saner, M. A. State of academic knowledge on toxicity and biological fate of quantum dots. *Toxicol. Sci*. **2009**, *112*, 276–296.

(21) Chen, N.; He, Y.; Su, Y.; Li, X., Huang, Q.; Wang, H.; Zhang, X.; Tai, R.; Fan, C. The cytotoxicity of cadmium-based quantum dots. *Biomaterials*. **2012**, *33*, 1238–1244.

(22) Ipe, B. I.; Lehnig, M.; Niemeyer, C. M. On the generation of free radical species from quantum dots. *Small*. **2005**, *1*, 706–709.

(23) Green, M.; Howman, E. Semiconductor quantum dots and free radical induced DNA nicking**.** *Chem. Commun*. **2005**, *0*, 121-123.

(24) Lu, Z.; Li, C. M.; Bao, H.; Qiao, Y.; Toh, Y. Mechanism of antimicrobial activity of CdTe quantum dots. *Langmuir*. **2008**, *24*, 5445–5452.

(25) Morelli, E.; Salvadori, E.; Bizzarri, R.; Cioni, P.; Gabellieri, E. Interaction of CdSe / ZnS quantum dots with the marine diatom *Phaeodactylum tricornutum* and the green alga *Dunaliella tertiolecta*: A biophysical approach. *Biophysical Chemistry*. **2013**, *182*, 4–10.

(26) Lopes, T.; Mestre, N. C.; Maria, S.; Sabóia-Morais, T.; João, M. Environmental behaviour and ecotoxicity of quantum dots at various trophic levels : A review. *Environ. Int.* **2017**, *98*, 1–17.

(27) Yong, K. -T.; Law, W. -C.; Hu, R.; Ye, L.; Liu, L.; Swihart, M. T., Prasad, P. N. Nanotoxicity assessment of quantum dots: From cellular to primate studies. *Chem. Soc. Rev.* **2013**, *42*, 1236–1250.

(28) Wu, J. J.; Kondeti, V. S. S. K.; Bruggeman, P. J.; Kortshagen, U. R. Luminescent , water-soluble silicon quantum dots via micro-plasma surface treatment. *J. Phys. D: Appl. Phys*. **2016**, *49*, 08LT02.

(29) Yiu, Y.; Fan, G.; Fermi, A.; Mazzaro, R.; Morandi, V.; Ceroni, P.; Smilgies, D-M.; Korgel, B. A. Size-dependent photoluminescence efficiency of silicon nanocrystal quantum dots. *J. Phys. Chem. C*. **2017**, *121*, 23240-23248.

(30) Stan, M.; Sima, C.; Cinteza, L. O.; Dinischiotu, A. Silicon-based quantum dots induce inflammation in human lung cells and disrupt extracellular matrix homeostasis. *FEBS J*. **2015**, *282*, 2914–2929.

(31) Stanca, L.; Petrache, S. N.; Serban, A. I.; Staicu, A. C.; Sima, C.; Munteanu, M. C.; Otilia, Z.; Dinu, D.; Dinischiotu, A. Interaction of silicon-based quantum dots with Gibel carp liver: Oxidative and structural modifications. *Nanoscale Res. Lett*. **2013**, *8*, 254.

(32) Buchman, J. T.; Rahnamoun, A.; Landy, K. M.; Zhang, X.; Vartanian, A. M.; Jacob, L. M.; Murphy, C. J.; Hernandez, R.; Haynes, C. L. Using an environmentally-relevant panel of Gram-negative bacteria to assess the toxicity of polyallylamine hydrochloride-wrapped gold nanoparticles. *Environ. Sci.: Nano*, **2018**, *5*, 279-288.

(33) Hau, H. H.; Gilbert, A.; Coursolle, D.; Gralnick, J. A. Mechanism and consequences of anaerobic respiration of cobalt by *Shewanella oneidensis* strain MR-1. *Appl. Environ. Microbiol.* **2008**, *74*, 6880-6886.

(34) Wiatrowski, H. A.; Ward, P. M.; Barkay, T. Novel reduction of mercury(II) by mercury-sensitive dissimilatory metal reducing bacteria. *Environ. Sci. Technol.* **2006**, *40*, 6690-6696.

(35) Bencharit, S.; Ward, M. J. Chemotactic responses to metals and anaerobic electron acceptors in *Shewanella oneidensis* MR-1. *J. Bacteriol.* **2005**, *187*, 5049-5043.

(36) Ye, L.; Yong, K. -T.; Liu, L.; Roy, I.; Hu, R.; Zhu, J.; Cai, H.; Law, W. -C.; Liu, J.; Wang, K.; Liu, J.; Liu, Y.; Hu, Y.; Zhang, X.; Swihart, M. T.; Prasad, P. N. A pilot study in non-human primates shows no adverse response to intravenous injection of quantum dots. *Nat. Nanotech.* **2012**, *7*, 453-458.

(37) Liu, J.; Erogbogbo, F.; Yong, K. -T.; Ye, L.; Liu, J.; Hu, R.; Chen, H.; Hu, Y.; Yang, Y.; Yang, J.; Roy, I.; Karker, N. A.; Swihart, M. T.; Prasad, P. N. Assessing clinical prospects of silicon quantum dots: Studies in mice and monkeys. *ACS Nano*. **2013**, *7*, 7303-7310.

(38) Anthony, R. J.; Rowe, D. J.; Stein, M.; Yang, J.; Kortshagen, U. Routes to achieving high quantum yield luminescence from gas-phase-produced silicon nanocrystals. *Adv. Funct. Mater.* **2011**, *21*, 4042–4046.

(39) Hanaor, D.; Michelazzi, M.; Leonelli, C.; Sorrell, C. C. The effects of carboxylic acids on the aqueous dispersion and electrophoretic deposition of ZrO_2. *J. Eur.*

Ceram. Soc. **2012**, *32*, 235–244.

(40) Mangolini, L.; Jurbergs, D.; Rogojina, E.; Kortshagen, U. Synthesis and characterization of strongly luminescing ZnS-capped CdSe nanocrystals. *J. Lumin.* **2006**, *121*, 327-334.

(41) Hines, M. A.; Guyot-Sionnest, P. Photoluminescence intermittency from single quantum dots to organic molecules: Emerging themes. *J. Phys. Chem.* **1996**, *100*, 468–471.

(42) Derfus, A. M.; Chan, W. C. W.; Bhatia, S. N. Probing the cytotoxicity of semiconductor quantum dots. *Nano Lett.* **2004**, *4*, 11-18.

(43) Priester, J. H.; Stoimenov, P. K.; Mielke, R. E.; Webb, S. M.; Ehrhardt, C.; Zhang, J. I. N. P.; Stucky, G. D. Effects of soluble cadmium salts versus CdSe quantum dots on the growth of planktonic *Pseudomonas aeruginosa*. *Environ. Sci. Technol*. **2009**, *43*, 2589–2594.

(44) Yaghini, E.; Pirker, K. F.; Kay, C. W. M.; Seifalian, A. M.; Macrobert, A. J. Quantification of reactive oxygen species generation by photoexcitation of PEGylated quantum dots. *Small*. **2014**, *10*, 5106–5115.

(45) Nagy, A.; Steinbru, A.; Gao, J.; Doggett, N.; Hollingsworth, J. A.; Iyer, R. Comprehensive analysis of the effects of CdSe quantum dot size , surface charge , and functionalization on primary human lung cells. *ACS Nano*. **2012**, *6*, 4748–4762.

(46) Imlay, J. A. The molecular mechanisms and physiological consequences of oxidative stress: lessons from a model bacterium**.** *Nat. Rev. Microbiol.* **2013**, *11*, 443–454.

(47) Yin, J.; Gao, H. Stress responses of Shewanella. *Int. J. Microbiol*. **2011**, *2011*, 863623.

(48) Hartwig, A.; Asmuss, M.; Ehleben, I.; Herzer, U.; Kostelac, D.; Pelzer, A.; Schwerdtle, T.; Bürkle, A. Interference by toxic metal ions with DNA repair processes and cell cycle control : Molecular mechanisms. *Environ Health Perspect.* **2002**, *110*, 797–799.

(49) Smeets, K.; Cuypers, A.; Lambrechts, A.; Semane, B.; Hoet, P. Induction of oxidative stress and antioxidative mechanisms in *Phaseolus vulgaris* after Cd application. *Plant Physiol Biochem.* **2005**, *43*, 437–444.

(50) Nies, D. Resistance to cadmium, cobalt, zinc, and nickel in microbes. *Plasmid*. **1992**, *28*, 17–28.

(51) Feng, Z. V.; Gunsolus, I. L.; Qiu, T. A.; Hurley, K. R.; Nyberg, L. H.; Frew, H.; Johnson, K. P.; Vartanian, A. M.; Jacob, L. M.; Lohse, S. E.; Torelli, M. D.; Hamers, R. J.; Murphy, C. J.; Haynes, C. L. Impacts of gold nanoparticle charge and ligand type on surface binding and toxicity to Gram-negative and Gram-positive bacteria. *Chem. Sci.* **2015**, *6*, 5186–5196.

(52) Schneider, R.; Wolpert, C.; Guilloteau, H.; Balan, L.; Merlin, C. The exposure of bacteria to CdTe-core quantum dots: The importance of surface chemistry on cytotoxicity. *Nanotechnology*. **2009**, *20*, 225101.

(53) Huismant, O.; D'Ari, R.; Gottesmant, S. Cell-division control in *Escherichia coli*: Specific induction of the SOS function SfiA protein is sufficient to block septation. *Proc. Natl. Acad. Sci. U S A.* **1984**, *81*, 4490-4494.

(54) Adjou, M.; Tréguer, P.; Dumousseaud, C.; Corvaisier, R.; Brzezinski, M. A.;

Nelson, D. M. Particulate silica and Si recycling in the surface waters of the Eastern Equatorial Pacific. *Deep-Sea Research II.* **2011**, *58*, 449-461.

(55) Beucher, C.; Tréguer, P.; Hapette, A. -M.; Corvaisier, R.; Metzl, N.; Pichon, J. -J. Intense summer Si-recycling in the surface Southern Ocean. *Geophys. Res. Lett.* **2004**, *31*,10.1029/2003GL018998.

Chapter 3

1. Kamat, P.; Scholes, G. Quantum Dots Continue to Shine Brightly. *J. Phys. Chem. Lett*. **2016**, *7*, 584-585.
2. Liang, X.; Grice, J.; Zhu, Y.; Liu, D.; Sanchez, W.; Li, Z.; Crawford, D.; Le Couteur, D.; Cogger, V.; Liu, X.; Xu, Z.; Roberts, M. Intravital Multiphoton Imaging of the Selective Uptake of Water-Dispersible Quantum Dots into Sinusoidal Liver Cells. *Small* **2015**, *11*, 1711-1720.
3. Xu, G.; Zeng, S.; Zhang, B.; Swihart, M.; Yong, K.; Prasad, P. New Generation Cadmium-Free Quantum Dots for Biophotonics and Nanomedicine. *Chem. Rev.* **2016**, *116*, 12234-12327.
4. Bimberg, D. Quantum Dots for Lasers, Amplifiers and Computing. *J. Phys. D: Appl. Phys.* **2005**, *38*, 2055-2058.
5. Zhao, K.; Pan, Z.; Zhong, X. Charge Recombination Control for High Efficiency Quantum Dot Sensitized Solar Cells. *J. Phys. Chem. Lett.* **2016**, *7*, 406-417.
6. Bang, J.; Park, J.; Lee, J.; Won, N.; Nam, J.; Lim, J.; Chang, B.; Lee, H.; Chon, B.; Shin, J.; Park, J.; Choi, J.; Cho, K.; Park, S.; Joo, T.; Kim, S. ZnTe/ZnSe

(Core/Shell) Type-II Quantum Dots: Their Optical and Photovoltaic Properties. *Chem. Mater.* **2010**, *22*, 233-240.

7. Ji, W.; Jing, P.; Xu, W.; Yuan, X.; Wang, Y.; Zhao, J.; Jen, A. High Color Purity ZnSe/ZnS Core/Shell Quantum Dot Based Blue Light Emitting Diodes with an Inverted Device Structure. *Appl. Phys. Lett.* **2013**, 103.
8. Vasudevan, D.; Gaddam, R.; Trinchi, A.; Cole, I. Core-Shell Quantum Dots: Properties and Applications. *J. Alloys Compd.* **2015**, *636*, 395-404.
9. Reiss, P.; Protiere, M.; Li, L. Core/Shell Semiconductor Nanocrystals. *Small* **2009**, *5*, 154-168.
10. Protesescu, L.; Yakunin, S.; Bodnarchuk, M.; Krieg, F.; Caputo, R.; Hendon, C.; Yang, R.; Walsh, A.; Kovalenko, M. Nanocrystals of Cesium Lead Halide Perovskites (CsPbX3, X = Cl, Br, and I): Novel Optoelectronic Materials Showing Bright Emission with Wide Color Gamut. Nano Lett. **2015**, *15*, 3692-3696.
11. Liu, W.; Zhang, Y.; Ruan, C.; Wang, D.; Zhang, T.; Feng, Y.; Gao, W.; Yin, J.; Wang, Y.; Riley, A.; Hu, M.; Yu, W. ZnCuInS/ZnSe/ZnS Quantum Dot-Based Downconversion Light-Emitting Diodes and Their Thermal Effect. *J. Nanomater*. **2015,** *2015*, Article ID 298614.
12. Fu, P.; Xia, Q.; Hwang, H.; Ray, P.; Yu, H. Mechanisms of Nanotoxicity: Generation of Reactive Oxygen Species. *J. Food Drug Anal.* **2014**, *22*, 64-75.
13. Drobintseva, A. O.; Matyushkin, L. B.; Aleksandrova, O. A.; Drobintsev, P. D.; Kvetnoy, I. M.; Mazing, D. S.; Moshnikov, V. A.; Polyakova, V. O.; Musikhin, S. F. Colloidal CdSe and ZnSe/Mn Quantum Dots: Their Cytotoxicity and Effects on

Cell Morphology. *St. Petersburg Polytechnical University Journal: Physics and Mathematics* **2015**, *1*, 272-277.

14. Ippen, C.; Greco, T.; Kim, Y.; Kim, J.; Oh, M.; Han, C.; Wedel, A. ZnSe/ZnS Quantum Dots as Emitting Material in Blue QD-LEDs with Narrow Emission Peak and Wavelength Tunability. *Org. Electron.* **2014**, *15*, 126-131.
15. Xie, R.; Battaglia, D.; Peng, X., Colloidal InP Nanocrystals as Efficient Emitters Covering Blue to Near-Infrared. *J. Am. Chem. Soc*. **2007**, *129*, 15432-15433.
16. Zhao, Y.; Liu, Q.; Shakoor, S.; Gong, J.; Wang, D., Transgenerational Safety of Nitrogen-doped Graphene Quantum Dots and the Underlying Cellular Mechanism in Caenorhabditis elegans. *Toxicology Research* **2015**, *4*, 270-280.
17. Erogbogbo, F.; Yong, K.; Roy, I.; Xu, G.; Prasad, P.; Swihart, M., Biocompatible Luminescent Silicon Quantum Dots for Imaging of Cancer Cells. *ACS Nano* **2008**, *2*, 873-878.
18. Das, A.; Snee, P. Synthetic Developments of Nontoxic Quantum Dots. *Chemphyschem* **2016**, *17*, 598-617.
19. Maurer-Jones, M.; Gunsolus, I.; Murphy, C.; Haynes, C. Toxicity of Engineered Nanoparticles in the Environment. *Anal. Chem.* **2013**, *85*, 3036-3049.
20. Priester, J.; Stoimenov, P.; Mielke, R.; Webb, S.; Ehrhardt, C.; Zhang, J.; Stucky, G.; Holden, P. Effects of Soluble Cadmium Salts Versus CdSe Quantum Dots on the Growth of Planktonic *Pseudomonas aeruginosa*. *Environ. Sci. Technol.* **2009**, *43*, 2589-2594.
21. Derfus, A.; Chan, W.; Bhatia, S. Probing the Cytotoxicity of Semiconductor Quantum Dots. *Nano Lett.* **2004**, *4*, 11-18.

22. Lai, L.; Li, S.; Feng, J.; Mei, P.; Ren, Z.; Chang, Y.; Liu, Y. Effects of Surface Charges on the Bactericide Activity of CdTe/ZnS Quantum Dots: A Cell Membrane Disruption Perspective. *Langmuir* **2017**, *33*, 2378-2386.
23. Lu, Z.; Li, C.; Bao, H.; Qiao, Y.; Toh, Y.; Yang, X. Mechanism of Antimicrobial Activity of CdTe Quantum Dots. *Langmuir* **2008**, *24*, 5445-5452.
24. Green, M.; Howman, E. Semiconductor Quantum Dots and Free Radical Induced DNA Nicking. *Chem. Comm.* **2005**, *0*, 121-123.
25. Manshian, B.; Soenen, S.; Al-Ali, A.; Brown, A.; Hondow, N.; Wills, J.; Jenkins, G.; Doak, S. Cell Type-Dependent Changes in CdSe/ZnS Quantum Dot Uptake and Toxic Endpoints. *Toxicol. Sci.* **2015**, *144*, 246-258.
26. Hardman, R. A Toxicologic Review of Quantum Dots: Toxicity Depends on Physicochemical and Environmental Factors. *Environ. Health Perspect.* **2006**, *114*, 165-172.
27. Yong, K.; Ding, H.; Roy, I.; Law, W.; Bergey, E.; Maitra, A.; Prasad, P. Imaging Pancreatic Cancer Using Bioconjugated InP Quantum Dots. *ACS Nano* **2009**, *3*, 502-510.
28. Mo, D.; Hu, L.; Zeng, G.; Chen, G.; Wan, J.; Yu, Z.; Huang, Z.; He, K.; Zhang, C.; Cheng, M. Cadmium-Containing Quantum Dots: Properties, Applications, and Toxicity. *Appl. Microbiol. Biotechnol.* **2017**, *101*, 2713-2733.
29. Medintz, I.; Uyeda, H.; Goldman, E.; Mattoussi, H. Quantum Dot Bioconjugates for Imaging, Labelling and Sensing. *Nat. Mater.* **2005**, *4*, 435-446.
30. Mahendra, S.; Zhu, H.; Colvin, V.; Alvarez, P. Quantum Dot Weathering Results in Microbial Toxicity. *Environ. Sci. Technol.* **2008**, *42*, 9424-9430.

31. Heidelberg, J.; Paulsen, I.; Nelson, K.; Gaidos, E.; Nelson, W.; Read, T.; Eisen, J.; Seshadri, R.; Ward, N.; Methe, B.; Clayton, R.; Meyer, T.; Tsapin, A.; Scott, J.; Beanan, M.; Brinkac, L.; Daugherty, S.; DeBoy, R.; Dodson, R.; Durkin, A.; Haft, D.; Kolonay, J.; Madupu, R.; Peterson, J.; Umayam, L.; White, O.; Wolf, A.; Vamathevan, J.; Weidman, J.; Impraim, M.; Lee, K.; Berry, K.; Lee, C.; Mueller, J.; Khouri, H.; Gill, J.; Utterback, T.; McDonald, L.; Feldblyum, T.; Smith, H.; Venter, J.; Nealson, K.; Fraser, C. Genome Sequence of the Dissimilatory Metal Ion-Reducing Bacterium *Shewanella oneidensis*. *Nat. Biotechnol.* **2002**, *20*, 1118-1123.

32. Hang, M.; Gunsolus, I.; Wayland, H.; Melby, E.; Mensch, A.; Hurley, K.; Pedersen, J.; Haynes, C.; Hamers, R. Impact of Nanoscale Lithium Nickel Manganese Cobalt Oxide (NMC) on the Bacterium *Shewanella oneidensis* MR-1. *Chem. Mater.* **2016**, *28*, 1092-1100.

33. Mei, B.; Susumu, K.; Medintz, I.; Mattoussi, H. Polyethylene Glycol-based Bidentate Ligands to Enhance Quantum Dot and Gold Nanoparticle Stability in Biological Media. *Nat. Protoc.* **2009**, *4*, 412-423.

34. Mei, B.; Susumu, K.; Medintz, I.; Delehanty, J.; Mountziaris, T.; Mattoussi, H. Modular Poly(ethylene glycol) Ligands for Biocompatible Semiconductor and Gold Nanocrystals with Extended pH and Ionic Stability. *J. Mater. Chem.* **2008**, *18*, 4949-4958.

35. Jasieniak, J.; Smith, L.; van Embden, J.; Mulvaney, P.; Califano, M. Re-examination of the Size-Dependent Absorption Properties of CdSe Quantum Dots. *J. Phys. Chem. C* **2009**, *113* (45), 19468-19474.

36. Xie, R.; Kolb, U.; Li, J.; Basche, T.; Mews, A. Synthesis and Characterization of Highly Luminescent CdSe-Core CdS/Zn0.5Cd0.5S/ZnS multishell nanocrystals. *J. Am. Chem. Soc.* **2005**, *127*, 7480-7488.

37. Wenger, W.; Bates, F.; Aydile, E. Functionalization of Cadmium Selenide Quantum Dots with Poly(ethylene glycol): Ligand Exchange, Surface Coverage, and Dispersion Stability. *Langmuir* **2017**, *33*, 8239-8245.

38. Zhang, L.; Shen, X.; Liang, H.; Chen, F.; Huang, H. Phosphine-free synthesis of ZnSe:Mn and ZnSe:Mn/ZnS doped quantum dots using new Se and S precursors. *New J. of Chem.* **2014**, *38*, 448-454.

39. Liu, D.; Snee, P. Water-Soluble Semiconductor Nanocrystals Cap Exchanged with Metalated Ligands. *ACS Nano* **2011**, *5*, 546-550.

40. Zheng, Z.; Saar, J.; Zhi, B.; Gallagher, M. J.; Fairbrother, D. H.; Haynes, C. L.; Lienkamp, K.; Rosenzweig, Z. Structure-Property Relationships of Amine-Rich and Membrane-Disruptive Poly(oxonorbornene)-Coated Gold Nanoparticles Langmuir **2018**, *34*, 4614-4625.

41. Fortier, C. Preparation, Characterization, And Application of Liposomes in the Study of Lipid Oxidation Targeting Hydroxyl Radicals. University of New Orleans, University of New Orleans Theses and Dissertations, **2008**.

42. Haldar, S.; Chattopadhyay, A. Application of NBD-labeled Lipids in Membrane and Cell Biology. In Fluorescent Methods to Study Biological Membranes, Springer: Berlin, Heidelberg, **2012**; Vol. 13.

43. Feng, Z.; Gunsolus, I.; Qiu, T.; Hurley, K.; Nyberg, L.; Frew, H.; Johnson, K.; Vartanian, A.; Jacob, L.; Lohse, S.; Torelli, M.; Hamers, R.; Murphy, C.; Haynes,

C. Impacts of Gold Nanoparticle Charge and Ligand Type on Surface Binding and Toxicity to Gram-negative and Gram-positive Bacteria. *Chem. Sci.* **2015**, *6*, 5186-5196.

44. Lyons, T.; Williams, D.; Rosenzweig, Z. Addition of Fluorescence Lifetime Spectroscopy to the Tool Kit Used to Study the Formation and Degradation of Luminescent Quantum Dots in Solution. *Langmuir* **2017**, 33, 3018-3027.
45. Were, L.; Bruce, B.; Davidson, P.; Weiss, J., Size, Stability, and Entrapment Efficiency of Phospholipid Nanocapsules Containing Polypeptide Antimicrobials. *J. Agric. Food Chem.* **2003**, *51*, 8073-8079.
46. Cornelison, G.; Mihic, S. Contaminating Levels of Zinc Found in Commonly-used Labware and Buffers Affect Glycine Receptor Currents. *Brain Res. Bull.* **2014**, *100*, 1-5.
47. Verebes, G. S.; Melchiorre, M.; Garcia-Leis, A.; Ferreri, C.; Marzetti, C.; Torreggiani, A. Hyperspectral Enhanced Dark Field Microscopy for Imaging Blood Cells. *J. Biophotonics* **2013**, *6*, 960-967.
48. Gao, L.; Smith, R. T. Optical Hyperspectral Imaging in Microscopy and Spectroscopy–A Review of Data Acquisition. *J. Biophotonics* **2015**, *8*, 441-456.
49. Zamora-Perez, P.; Tsoutsi, D.; Xu, R.; Rivera_Gil, P., Hyperspectral-Enhanced Dark Field Microscopy for Single and Collective Nanoparticle Characterization in Biological Environments. *Materials* **2018**, *11*, 243.
50. Peña, M. D. P. S.; Gottipati, A.; Tahiliani, S.; Neu-Baker, N. M.; Frame, M. D.; Friedman, A. J.; Brenner, S. A. Hyperspectral Imaging of Nanoparticles in

Biological Samples: Simultaneous Visualization and Elemental Identification. *Microsc. Res. Tech.* **2016**, *79*, 349-358.

51. Gong, K.; Kelley, D. A Predictive Model of Shell Morphology in CdSe/CdS Core/Shell Quantum Dots. *J. of Chem. Phys.* **2014**, 141.
52. Yu, Z.; Guo, L.; Du, H.; Krauss, T.; Silcox, J. Shell Distribution on Colloidal CdSe/ZnS Quantum Dots. *Nano Lett.* **2005**, *5*, 565-570.

Chapter 4

(1) Meneguzzo, F.; Ciriminna, R.; Albanese, L.; Pagliaro, M. The Great Solar Boom : A Global Perspective into the Far Reaching Impact of an Unexpected Energy Revolution. *Eenergy Science & Engineering*, **2015**, 499–509.

(2) Lee, T. D.; Ebong, A. U. A Review of Thin Fi Lm Solar Cell Technologies and Challenges. *Renew. Sustain. Energy Rev.* **2017**, *70* (November 2016), 1286–1297.

(3) Almosni, S.; Delamarre, A.; Jehl, Z.; Suchet, D.; Giteau, M.; Behaghel, B.; Julian, A.; Tatry, L.; Wang, H.; Kubo, T.; et al. Material Challenges for Solar Cells in the Twenty- First Century : Directions in Emerging Technologies. *Sci. Technol. Adv. Mater.* **2018**, *6996*, 1–34.

(4) Adams, W. G.; Day, R. E. IX . The Action of Light on Selenium. *Philosophical Transactions of the Royal Society of London*, **1877**, *167*, 313–349.

(5) Parida, B.; Iniyan, S.; Goic, R. A Review of Solar Photovoltaic Technologies. *Renew. Sustain. Energy Rev.* **2011**, *15* (3), 1625–1636.

(6) O'Regan, B.; Grätzel, M. A low cost high-efficiency solar cell based on dye-sensitized TiO_2 films. *Nature*, **1991**, *353*, 737-740.

(7) Walsh, A.; Chen, S.; Wei, S.; Gong, X. Kesterite Thin-Film Solar Cells : Advances in Materials Modelling of Cu2ZnSnS4. *Adv. Energy Mater.* **2012**, *2*, 400–409.

(8) Oh, J.; Yuan, H.; Branz, H. M.An 18.2%-efficient black-silicon solar cell achieved through control of carrier recombination in nanostructures. *Nat. Naotech.* **2012**, *7* (November), 743–748.

(9) Kumar, M.; Dubey, A.; Adhikari, N. Environmental Science Strategic Review of Secondary Phases , Defects and. *Energy Environ. Sci.* **2015**, *8*, 3134–3159.

(10) Mokkapati, S.; Catchpole, K. R. Nanophotonic Light Trapping in Solar Cells.*Appl. Phys. Rev. — FOCUSED REVIEW* **2016**, *101101* (2012).

(11) Lee, C.; Lee, G.; Zande, A. M. Van Der; Chen, W.; Li, Y.; Han, M.; Cui, X.; Arefe, G.; Nuckolls, C.; Heinz, T. F.; et al. Atomically Thin P – N Junctions with van Der Waals Heterointerfaces. *Nat. Nanotechnol.* **2014**, *9* (9), 676–681.

(12) Mitzi, D. B.; Gunawan, O.; Todorov, T. K.; Barkhouse, D. A. R.; Mitzi, D. B. Prospects and Performance Limitations for Cu – Zn – Sn – S – Se Photovoltaic Technology *Phys. Trans. Royal Soc. A* **2013**, *371* (1996), 20110432

(13) Kazmerski, L. L.; White, F. R.; Morgan, G. K. Thin-Film CuInSe2/CdS Heterojunction Solar Cells. *Appl. Phys. Lett.* **2008**, *29*, 1976..

(14) Anthony, T. C.; Fahrenbruch, A. L.; Peters, M. G.; Bube, R. H.; Anthony, T. C.; Fahrenbruch, A. L.; Peters, M. G.; Bube, R. H. Electrical Properties of CdTe Films

and Junctions *J. Appl. Phys.* **1985**, *57*(2), -400-410.

(15) Nakayama, K.; Tanabe, K.; Atwater, H. A.; Nakayama, K.; Tanabe, K.; Atwater, H. A. Plasmonic Nanoparticle Enhanced Light Absorption in GaAs Solar Cells *Appl.Phys. Lett.***2008**, *93*,121904.

(16) Schock, H.-W.; Noufi, R. CIGS-Based Solar Cells for the Next Millennium. *Prog. Photovoltaics* **2000**, *8*(1).151–160.

(17) Jackson, P.; Hariskos, D.; Lotter, E.; Paetel, S.; Wuerz, R.; Menner, R.; Wischmann, W.; Powalla, M. New World Record Efficiency for Cu (In , Ga) Se 2 Thin-Film Solar Cells beyond 20 %. *Prog. Photovoltaics* **2011**, *19*, 894–897.

(18) Oriya, K. M.; Anaka, K. T.; Chiki, H. U. Brief Communication Fabrication of Cu 2 ZnSnS 4 Thin-Film Solar Cell Prepared by Pulsed Laser Deposition. **2007**, *46* (9), 5780–5781.

(19) Katagiri, H.; Jimbo, K.; Maw, W. S.; Oishi, K.; Yamazaki, M.; Araki, H.; Takeuchi, A. Development of CZTS-Based Thin Fi Lm Solar Cells. *Thin Solid Films* **2009**, *517* (7), 2455–2460.

(20) Shin, B.; Gunawan, O.; Zhu, Y.; Bojarczuk, N. A.; Chey, S. J.; Guha, S. Thin Film Solar Cell with 8 . 4 % Power Conversion Efficiency Using an Earth-Abundant Cu 2 ZnSnS 4 Absorber. *Prog. Photovoltaics*. **2013**, No. November 2011, *21*, 72–76.

(21) Williams, B. A.; Trejo, N. D.; Wu, A.; Holgate, C. S.; Francis, L. F.; Aydil, E. S. Copper − Zinc − Tin − Sulfide Thin Films via Annealing of Ultrasonic Spray Deposited Nanocrystal Coatings. Appl. Mater. Interfaces. **2017**, 9, 18865-18871.

(22) Zhou, H.; Hsu, W.; Duan, H.; Bob, B.; Yang, W. Environmental Science CZTS Nanocrystals : A Promising Approach for next Generation Thin Fi Lm Photovoltaics. *Energy Environ. Sci.* **2013**, *6*, 2822–2838.

(23) Woo, K.; Kim, Y.; Moon, J. A non-toxic, solution-processed, earth abundant absorbing layer for thin-film solar cells. *Energy Environ. Sci.* **2012**, *4*, 5340–5345

(24) Wang, W.; Winkler, M. T.; Gunawan, O.; Gokmen, T.; Todorov, T. K.; Zhu, Y.; Mitzi, D. B. Device Characteristics of CZTSSe Thin-Film Solar Cells with. 12.6% efficiency. *Adv. Energy Mater.* **2014**, *4*, 1301465

(25) Guo, Q.; Hillhouse, H. W.; Agrawal, R. Synthesis of Cu 2 ZnSnS 4 Nanocrystal Ink and Its Use for Solar Cells. *J. Am. Chem. Soc.* **2009**, *131* (33), 11672–11673.

(26) Tanaka, T.; Kawasaki, D.; Nishio, M.; Guo, Q.; Ogawa, H. Fabrication of Cu 2 ZnSnS 4 Thin Films by Co-Evaporation.*Phys. Stat. Solidi.* **2006**, *2847* (8), 2844–2847.

(27) Jeon, M.; Tanaka, Y.; Shimizu, T.; Shingubara, S. Formation and Characterization of Single-Step Electrodeposited Cu 2 ZnSnS 4 Thin Films : Effect of Complexing Agent Volume. *Energy Procedia* **2011**, *10*, 255–260.

(28) Steinhagen, C.; Panthani, M. G.; Akhavan, V.; Goodfellow, B.; Koo, B.; Korgel, B. A. Synthesis of Cu 2 ZnSnS 4 Nanocrystals for Use in Low-Cost Photovoltaics. *J. Am. Chem. Soc.* **2009**, *131* (35), 12554–12555.

(29) Absorber, L.; Todorov, B. T. K.; Reuter, K. B.; Mitzi, D. B. High-Efficiency Solar Cell with Earth-Abundant Liquid-processed Absorber. *Adv. Mater.* **2010**, *22*(20),

156–159.

(30) Kumar, R. S.; Maddirevula, S.; Easwaran, M. Antibacterial Activity of Novel Cu2ZnSnS4 Nanoparticles against Pathogenic Strains. *RSC Adv.* **2015**, *5*, 106400–106405.

(31) Feng, Z. V.; Gunsolus, I. L.; Qiu, T. A.; Hurley, K. R.; Nyberg, L. H.; Frew, H.; Johnson, K. P.; Vartanian, A. M.; Jacob, L. M.; Lohse, S. E.; et al. Impacts of Gold Nanoparticle Charge and Ligand Type on Surface Binding and Toxicity to Gram-Negative and Gram-Positive Bacteria. *Chem. Sci.* **2015**, *6* (9), 5186–5196.

(32) Pramanik, S.; Hill, S. K. E.; Zhi, B.; Hudson-smith, N. V; Wu, J. J.; White, J. N.; Mcintire, E. A.; Kondeti, V. S. S. K.; Lee, A. L.; Bruggeman, P. J.; et al. Environmental Science Nano Quantum Dots and Their Traditional Cd-Based Oneidensis and Bacillus Subtilis. *Environ. Sci Nano* **2018**, *5*,1890–1901.

(33) Tosun, B. S.; Chernomordik, B. D.; Gunawan, A. a; Williams, B.; Mkhoyan, K. A.; Francis, L. F.; Aydil, E. S. Cu_2ZnSnS_4 Nanocrystal Dispersions in Polar Liquids. *Chem. Commun. (Camb).* **2013**, *49* (34), 3549–3551.

(34) Todorov, T. K.; Tang, J.; Bag, S.; Gunawan, O.; Gokmen, T.; Zhu, Y.; Mitzi, D. B. Beyond 11 % Efficiency : Characteristics of State-of-the-Art Cu 2 ZnSn (S , Se) 4 Solar Cells. *Adv. Energy Mater*. **2013**, *3*, 34–38.

(35) Khare, A.; Wills, A. W.; Ammerman, L. M.; Norris, J.; Aydil, E. S. ChemComm Size Control and Quantum Confinement in Cu 2 ZnSnS 4 Nanocrystals . *Chem. Commun.* **2011**, *47*, 11721–11723.

(36) Chernomordik, B. D.; Beland, A. E.; Trejo, N. D.; Gunawan, A. A.; Deng, D. D.; Mkhoyan, K. A.; Aydil, E. S. Rapid facile synthesis of Cu_2ZnSnS_4 nanocrystals. *J. Mater. Chem.* A. **2014**, *2* (27), 10389-10395..

(37) Zhi, B.; Mishra, S.; Hudson-smith, N. V; Kortshagen, U. R.; Haynes, C. L. Toxicity Evaluation of Boron- and Phosphorus-Doped Silicon Nanocrystals toward Shewanella Oneidensis MR-1. *ACS Appl. Nano Mater.* **2018**, *1*, 4884–4893.

(38) Zhang, H.; Pokhrel, S.; Ji, Z.; Meng, H.; Wang, X.; Lin, S.; Chang, C. H.; Li, L.; Li, R.; Sun, B.; Wang, M.; Liao, Y. P; Liu, R.; Xia, T.; Madler, L.; Nel, AE. PdO Doping Tunes Band-Gap Energy Levels as Well as Oxidative Stress Responses to a Co 3 O 4 P - Type Semiconductor in Cells and the Lung. *J. Am. Chem. Soc.* **2014,** *136*(17), 6406-6420.

(39) Kittler, S.; Greulich, C.; Diendorf, J.; Koller, M.; Epple, M. Toxicity of Silver Nanoparticles Increases during Storage Because of Slow Dissolution under Release of Silver Ions. *Chem. Mater.* **2010**, *22*(16), 4548–4554.

(40) Hang, M. N.; Gunsolus, I. L.; Wayland, H.; Melby, E. S.; Mensch, A. C.; Hurley, K. R.; Pedersen, J. A.; Haynes, C. L.; Hamers, R. J. Impact of Nanoscale Lithium Nickel Manganese Cobalt Oxide (NMC) on the Bacterium *Shewanella Oneidensis* MR - 1. Chem. Mater. **2016**, 28(4), 1092-1110.

(41) Abdullah, A. M. Synergistic Effects of Zinc and Copper Ions in a Freshwater Isopod Asellus aquaticus (L .) *J. Basrah. Researches* ,. **2004**, *30*. .

(42) Sengōr, S. S.; Barua, S.; Gikas, P.; Ginn, T.R.; Peyton, B.; Sani, R. K.; Spycher, N. F. Influence of heavy metals on microbial growth kinetics including lag time: Mathematical modeling and experimental verification. *Environ. Toxicol. Sci.* **2009**, *28* (10), 2020–2029.

(43) Ochoa-herrera, V.; León, G.; Banihani, Q.; Field, J. A.; Sierra-alvarez, R. Science of the Total Environment Toxicity of Copper (II) Ions to Microorganisms in Biological Wastewater Treatment Systems. *Sci. Total Environ.* **2011**, *412–413*, 380–385.

(44) Groisman, E. A.; Hollands, K.; Kriner, M. A.; Lee, E.-J.; Park. S. Y.; Pontes, M.H. Bacterial Mg2+ Homeostasis, Transport, and Virulence. *Annu. Rev. Genet.* **2013**, *47*, 625–646.

(45) Klein, N. D.; Hurley, K. R.; Feng, Z. V.; Haynes, C. L. Dark Field Transmission Electron Microscopy as a Tool for Identifying Inorganic Nanoparticles in Biological Matrices. *Anal. Chem.* **2015**, 87(8), 4356-4362.

(46) Nosaka, Y.; Nosaka, A. Y. Generation and Detection of Reactive Oxygen Species in Photocatalysis. *Chem. Rev.* **2017,** *117*(17), 11302-11336..

(47) George, S.; Pokhrel, S.; Ji, Z.; Henderson, B. L.; Xia, T.; Li, L.; Zink, I.; Nel, E.; Lutz, M. Role of Fe Doping in Tuning the Band Gap of TiO 2 for the Photo-Oxidation-Induced Cytotoxicity Paradigm. *J. Am. Chem. Soc.* **2011**,*133*(29), 11270–11278.

(48) Gonzalez-pozos, V. E. M. U. S.; Velumani, S.; Andrea, L. A. Cytotoxicity of Semiconductor Nanoparticles in A549 Cells Is Attributable to Their Intrinsic

Oxidant Activity. *J. Nanoparticle Res.* **2016**, *18* (4), 1–12.

(49) Yin, J.; Gao, H. Stress Responses of Shewanella. *Int. J. Microbiol.* **2011**, *2011*, 863623.

Chapter 5

(1) Litvin, A. P.; Martynenko, I. V.; Purcell-Milton, F.; Baranov, A. V.; Fedorov, A. V.; Gun'ko, Y. K. Colloidal Quantum Dots for Optoelectronics. *J. Mater. Chem.* **2017**, *5*, 13252–13275.

(2) Matea, C. T.; Mocan, T.; Tabaran, F.; Pop, T.; Mosteanu, O.; Puia, C.; Iancu, C.; Mocan, L. Quantum Dots in Imaging , Drug Delivery and Sensor Applications. *Int. J. Nanomedicine.* **2017**, *12*, 5421–5431.

(3) Rzigalinski, B. A.; Strobl, J. S. Cadmium-Containing Nanoparticles : Perspectives on Pharmacology and Toxicology of Quantum Dots I. *Toxicol. Appl. Pharmacol.* **2009**, *238* (3), 280–288.

(4) Williams, D. N.; Pramanik, S.; Brown, R. P.; Zhi, B.; Mcintire, E.; Hudson-smith, N. V; Haynes, C. L.; Rosenzweig, Z. Adverse Interactions of Luminescent Semiconductor Quantum Dots with Liposomes and Shewanella Oneidensis. *ACS Appl. Nano Mater.* **2018**, *1*, 4788–4800.

(5) Kirchner, C.; Liedl, T.; Kudera, S.; Pellegrino, T.; Gaub, H. E.; Sto, S.; Fertig, N.; Parak, W. J. Cytotoxicity of Colloidal CdSe and CdSe / ZnS Nanoparticles. Nano Lett. **2005**, *5*(2), 331-338.

(6) Hoshino, A.; Fujioka, K.; Oku, T.; Suga, M. Physicochemical Properties and Cellular Toxicity of Nanocrystal Quantum Dots Depend on Their Surface Modification. *Nano Lett.,* **2004**, *4*(11), 15–18.

(7) Buchman, J. T.; Rahnamoun, A.; Landy, K. M.; Vartanian, A. M.; Jacob, L. M.; Murphy, C. J. Environmental Science Using an Environmentally-Relevant Panel of Gram-negative bacteria to assess the toxicity of polyallylamine hydrochloride-wrapped gold nanoparticles. *Environ. Sci.: Nano* **2018**, *5*, 279–288.

(8) Berardinis, D.; Durot, M.; Weissenbach, J.; Salanoubat, M. Acinetobacter Baylyi ADP1 as a Model for Metabolic System Biology. *Curr. Opin. Microbiol.* **2009**, *12* (5), 568–576.

(9) Vinogradov, E.; Kubler-Kielb, J.; Korenevsky, A. The structure of the carbohydrate backbone of the LPS from Shewanella spp MR-4. *Carbohydr. Res.* **2008**, *343* (15), 2701–2705.

(10) Klockgether, J.; Munder, A.; Neugebauer, J.; Davenport, C. F.; Stanke, F.; Larbig, K. D.; Heeb, S.; Scho, U.; Pohl, T. M. Genome Diversity of Pseudomonas Aeruginosa PAO1 Laboratory Strains. *J. Bacteriol.* **2010**, *192* (4), 1113–1121.

(11) Jacobson, K. H.; Gunsolus, I. L.; Kuech, T. R.; Troiano, J. M.; Melby, E. S.; Lohse, S. E.; Hu, D.; Chrisler, W. B.; Murphy, C. J.; Orr, G.; et al. Lipopolysaccharide Density and Structure Govern the Extent and Distance of Nanoparticle Interaction with Actual and Model Bacterial Outer Membranes. Environ. Sci. Technol. **2015**, *49* (17), 10642-10650.

(12) Triantafilou, M.; Triantafilou, K.; Fernandez, N. Rough and Smooth Forms of

Fluorescein-Labelled Bacterial Endotoxin Exhibit CD14 / LBP Dependent and Independent Binding That Is Influenced by Endotoxin Concentration. *Eur. J. Biochem.* **2000**, *267 (8)*, 2218–2226.

(13) Pramanik, S.; Hill, S. K. E.; Zhi, B.; Hudson-smith, N. V; Wu, J. J.; White, J. N.; Mcintire, E. A.; Kondeti, V. S. S. K.; Lee, A. L.; Bruggeman, P. J.; et al. Environmental Science Nano Quantum Dots and Their Traditional Cd-Based Oneidensis and Bacillus Subtilis. *Environ. Sci.: Nano* **2018**, 5, 1890–1901.

(14) Jasieniak, J.; Smith, L.; Embden, J. Van; Mulvaney, P. Re-Examination of the Size-Dependent Absorption Properties of CdSe Quantum Dots. *J. Phys. Chem. C* **2009**, *113* (45), 19468–19474.

(15) Xie, R.; Kolb, U.; Li, J.; Basche, T.; Mews, A. Synthesis and Characterization of Highly Luminescent CdSe-Core CdS/Zn0.5Cd0.5S/ZnS Multishell Nanocrystals. *J. Am. Chem. Soc.* **2005**, *127*, 7480–7488.

(16) Wenger, W. N.; Bates, F. S.; Aydil, E. S. Functionalization of Cadmium Selenide Quantum Dots with Poly(ethylene Glycol): Ligand Exchange, Surface Coverage, and Dispersion Stability. *Langmuir*, **2017**, *33* (33), 8239-8245.

(17) Zhang, L.; Shen, X.; Liang, H.; Chen, F. Phosphine-Free Synthesis of ZnSe : Mn and ZnSe : Mn / ZnS Doped Quantum Dots Using New Se and S Precursors. *New J. Chem.* **2014**, *38*, 448–454.

(18) Feng, Z. V.; Gunsolus, I. L.; Qiu, T. A.; Hurley, K. R.; Nyberg, L. H.; Frew, H.; Johnson, K. P.; Vartanian, A. M.; Jacob, L. M.; Lohse, S. E.; et al. Impacts of Gold Nanoparticle Charge and Ligand Type on Surface Binding and Toxicity to Gram-

Negative and Gram-Positive Bacteria. *Chem. Sci.* **2015**, *6* (9), 5186–5196.

(19) Huismant, O.; Arit, R. D.; Gottesmant, S. Cell-Division Control in *Escherichia Coli* : Specific Induction of the SOS Function SfiA Protein Is Sufficient to Block Septation. *Proc. Natl. Acad. Sci. USA* **1984**, *81* (14), 4490–4494.